Testing the application of coastal altimetry in two south-eastern African bights: the relationship between mesoscale features and chlorophyll-*a*

L.ZIEGLER

2018

Testing the application of coastal altimetry in two south-eastern African bights: the relationship between mesoscale features and chlorophyll-*a*

Cyclonic eddies in the Indian Ocean

Author:
Lisa ZIEGLER

Supervisor:
Prof. Michael ROBERTS
Co-supervisors:
Dr. Derek DU PREEZ
Dr. Paolo CIPOLLINI

NELSON MANDELA UNIVERSITY

DEPARTMENT OF OCEANOGRAPHY

Submitted in fulfilment of the requirements for the degree of Biological Oceanography to be awarded at the Nelson Mandela University.

JANUARY 2018

AUTHOR'S DECLARATION

I, Lisa Ziegler (216929601), hereby declare that the reatise/ dissertation/ thesis for the masters degree in Biological Oceanography, to be awarded is my own work and that it has not previously been submitted for assessment or completion of any postgraduate qualification to another University or for another qualification.

SIGNED:  DATE: 13 March 2018

Official use:

In accordance with Rule G5.6.3,

5.6.3 A treatise/dissertation/thesis must be accompanied by a written declaration on the part of the candidate to the effect that it is his/her own work and that it has not previously been submitted for assessment to another University or for another qualification. However, material from publications by the candidate may be embodied in a treatise/dissertation/thesis.

NELSON MANDELA UNIVERSITY

Faculty of Science

Department of Oceanography

Master of Science Degree in Biological Oceanography

Testing the application of coastal altimetry in two south-eastern African bights: the relationship between mesoscale features and chlorophyll-*a*

Lisa ZIEGLER

Abstract

Enhanced coastal altimetry, adaptive Leading-Edge Subwaveform (ALES), was used to study two well known eddies along the southeastern African coast, namely the Delagoa Bight Lee Eddy and the Durban Lee Eddy. I address a two part problem. Firstly, how well does the application of coastal altimetry techniques behave in the coastal region? Secondly, is there a relationship between the eddies' presence and chlorophyll-*a* (chl-*a*). Sea level anomalies (SLA) were computed from the re-tracked ALES data of two satellite missions — Envisat (used for Delagoa Bight eddy) and Jason -2 (for the Durban eddy) with geophysical corrections removed. These datasets were compared with the original satellite, 1 Hz RADS, AND AVISO gridded data. Two regions were selected to see if there was a biophysical link. A centre region of the eddy and an outside region of the eddy were taken. Results indicate that coastal altimetry was successful in delimiting both features. ALES was less noisey and able to recover more data that were missed by the 1 Hz RADS dataset. Hovmöller plots showed the Delagoa Bight eddy to be more of a transient feature than semi-permanent, as had previously been suggested. Results from the linear model indicate a negative correlation between SLA and chl-*a*. This influence could be through facilitation of chl-*a* in the bight or just retaining chl-*a*. This is hard to elucidate without *in situ* data. These results show a promising indication that coastal altimetry will be a useful and reliable product to further biophysical coupling research along the coast.

Keywords: Coastal Altimetry, Remote-sensing, Sea Level Anomaly, Chlorophyll-*a*, Mesoscale eddies, Delagoa Bight Lee Eddy, Durban Lee Eddy, Coastal zone

ACKNOWLEDGMENTS

To my home crew, kitty, and Sylvester :)
Hugs and Kisses

List of abbreviations

AC	Agulhas Current
ADCP	Acoustic Doppler Current Profiler
ALES	Adaptive Leading-Edge Subwaveform
ALtika	A satellite altimeter working in Ka-band, 35 GHz
Aqua	A multi-national NASA scientific research satellite
AVISO	Archiving, Validation, and Interpretation of Satellite Oceanographic Data
BC	Brazil current
CCS	California Current System
COASTALT	Coastal Altimetry community
CGDR	Coastal Geophysical Data Records
chl-*a*	chlorophyll-a
CLA	Chlorophyll Anomaly
CNES	National Centre for Space Studies
CTD	Conductivity, Temperature and Depth Rosette
DAAC	Distributed Active Archive Centre
DBLE	Delagoa Bight Lee Eddy
DLE	Durban Lee Eddy
Duacs	Data Unification and Altimeter Combination System
DTU	Mean Sea Surface computed by Technical University of Denmark
EAC	Eastern Australian Current
Envisat	Environmental Satellite
ERS	European Remote-Sensing
ESA	European Space Agency
GFO	Geosat Follow-on
GMT	Generic Mapping Toolbox
GPS	Global Positioning System
KZN	Kwa-Zulu Natal

MC	Mozambique Current
MSSH	Mean Sea Surface Height
MODIS	Moderate Resolution Imaging Spectroradiometer
NaN	Not a Number
NOC	National Oceanography Centre
OC-CCI	Ocean Colour Climate Change Initiative
OPenDAP	Open-source Project for a Network Data Access Protocol
PISTACH	Processing for Coastal and Hydrology products
RADS	Radar Altimeter Database System
RMS	root-mean-square
RMSD	root mean square difference
ROMS	Regional Ocean Modelling System
SeaWiFS	Sea-viewing Wide Field-of-view Sensor
SGDR	Sensor Geophysical Data Records
SLA	Sea Level Anomaly
SL-CCI	Sea Level Climate Change Initiative
Ssalto	Ssalto multi-mission ground segment
SSH	Sea Surface Height
SST	Sea Surface Temperature
SSW	Sea Surface winds
SWH	Significant Waveform Height

TABLE OF CONTENTS

LIST OF TABLES

TABLE **Page**

LIST OF FIGURES

FIGURE **Page**

CHAPTER 1

INTRODUCTION

This thesis addresses a two-part problem on the east coast of southern Africa. Part one is scientific and stems from an oceanography and ecosystem functioning perspective. It tackles the lack of understanding on the importance of cyclonic eddies along the shoreward boundary of the Agulhas Current — in particular lee-trapped cyclones and their contribution to primary production (phytoplankton). In principle, cold core eddies should promote phytoplankton growth as a result of higher nutrient levels in the eddy core Doney et al. (2003). The dominant eddies of interest in this system are the Delagoa Bight and the Durban lee-trapped eddies. However, despite several *in situ*, ship-based field campaigns, the role of these two features in production has not been determined (Roberts unpubl.) This is because of the hit-and-miss 'momentary snap-shot' nature of this measurement technique to observe a very unremitting and dynamic process, *i.e.* the cyclonic spin of water and uplift-ment of nutrients into the euphotic zone, and the respondent stimulation of phytoplankton growth and biomass.

Quantifying the role of eddies in production is therefore a major challenge. One approach might be the deployment of a string of moorings, but this is very costly in terms of equip-ment and ship time required for deployment, maintenance and recovery. In the open ocean satellite altimetry has cleverly and successfully been used to link eddy presence and intensity with local surface chlorophyll-*a* (chl-*a*), and therefore the role of eddies in ocean production has been determined (Godø et al., 2012). However, the accuracy of sea surface height (SSH) measurements used to identify eddies becomes questionable near coastlines as the returned satellite radar signal is distorted by the effects of land (Passaro et al., 2014). This limitation in recent years has been overcome by the satellite altimetry community who have developed a new product known as *coastal altimetry* or sometimes *enhanced altimetry* (Passaro et al.,

2014). The second part of the problem is of a technical nature, and concerns the question of whether the coastal altimetry product can be reliably used to detect lee-trapped eddies along the east coast of Africa, and therefore, be used in the same way as it has for offshore eddies.

Expansion on this two-part problem follows in the remainder of the chapter together with the scientific motivation, objectives and key questions of this thesis.

1.1 The role of cyclonic eddies in ocean productivity

In the open ocean, mesoscale cyclonic eddies are important drivers for enhancing biological production (Godø et al., 2012). Indeed, it is estimated that they are responsible for 25 % of the total production in the global ocean (Godø et al., 2012). Ocean colour, as observed from space, is often correlated with mesoscale eddies, which have shown strong physical influence controlling phytoplankton dynamics (*e.g.* Doney et al., 2003). According to Doney et al. (2003), this physical control is thought to be linked to mechanisms supplying nutrients to the euphotic zone where they can stimulate growth of phytoplankton. The general idea is that the formation and intensification of cyclonic eddies (cold core) create a decrease in SSH and an upwelling of isopycnal surfaces at depth, drawing the thermocline in their centres towards the sea surface in the northern hemisphere (Fig. 1.1(b)) (Stramma et al., 2013); in anticyclonic eddies (warm core) the opposite is observed (Fig. 1.1(a)) (Stewart, 2008). In the southern hemisphere the same eddy circulation patterns are observed for cold core and warm core eddies, however the rotation changes (cyclonic eddies rotate clockwise and anticyclonic eddies anticlockwise). This mechanism has been identified as 'eddy pumping'(Sarmiento, 2013), which causes the lifting of cold nutrient-rich water into the subsurface layers (Eden and Dietze, 2009; McGillicuddy and Robinson, 1997; Siegel et al., 1999). Chl-*a*, therefore, should be most abundant and dominant in the core of cyclonic eddies.

Primary production at ocean rims is more complicated. On the east coast of South Africa for example, the high volume, fast flowing Agulhas Current brings warm subtropical and oligotrophic water southwards (Lutjeharms, 2006b), (Fig. 1.2(a)) with correspondingly extremely low phytoplankton biomass (Fig. 1.2(b)). A MODIS satellite sea surface temperature (SST) image on 31 July 2006 illustrates this classical western boundary advection (Fig. 1.2(a)). What is not shown in this images, are a number of oceanographic processes that promote the movement of colder, nutrient-rich water from depth into the surface layer. These include cyclonic eddies (Roberts et al., 2016; Guastella and Roberts, 2016; Lutjeharms and Da Silva, 1988; Lutjeharms, 2006a; Jose et al., 2014), river inflow (Dove, 2015; Kyewalyanga et al., 2007), and upwelling events, both at the coast (Roberts et al., 2016) and at the shelf break (Guastella and Roberts, 2016; Roberts et al., 2010; Lutjeharms, 2006a).

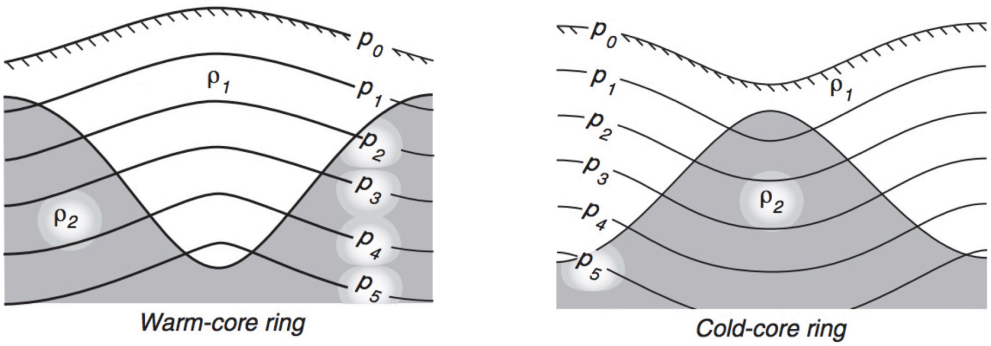

(a) (b)

Figure 1.1: (a) Warm core eddy: clockwise circulation with isobars sloping downwards and isopycnals upwards from the center. (b) Cold core eddy: anti-clockwise circulation; isobars slope upward but isopycnals slope downwards from the center (Stewart, 2008).

Of these, the two cyclonic eddies are of particular interest. The first, being the Delagoa Bight lee eddy (DBLE), located offshore of Maputo (Fig. 1.3). Lutjeharms and Da Silva (1988) as well as Cossa et al. (2016) suggested this eddy to be semi-permanent, but results from Lamont et al. (2010) do not support this, suggesting that this feature is transient. The occurrence of upwelling associated with a cyclonic eddy is expected to introduce cooler, nutrient-rich water into the surface layers, which will result in an increase in phytoplankton abundance (Lamont et al., 2010). Interestingly, Barlow et al. (2008) and Lamont et al. (2010) indicated that increased phytoplankton biomass was coincident with cooler water along the north-eastern limit of the Delagoa Bight.

The second eddy of interest is the Durban lee eddy (DLE), which forms off Durban at the southern limit of the KwaZulu-Natal (KZN) Bight (Fig. 1.3). This eddy too has been recognised as a semi-permanent feature, being highly variable in occurrence and strength. Its formation period is ca. 10 days, after which it then 'breaks away' from its shelf edge bight and heads southwards along the shoreward boundary of the Agulhas Current. Already, in the 1970's, Pearce (1977) noticed the inshore region off Durban as a productive area that has been exploited by mariners for many centuries (Fréon et al., 2010; Roberts et al., 2010). Guastella and Roberts (2016) showed, using satellite-tracked surface drifters released in the eddy, the potential for nutrient-rich eddy water to be advected northwards into the KZN Bight, thus contributing to the functioning of the bight ecosystem. Hewitt (1981) hypothesised that a trapped-lee cyclonic eddy would act to retain a small part of an ecosystem on the shelf, whether this is true for the Delagoa Bight and KZN Bight eddies remains to be confirmed.

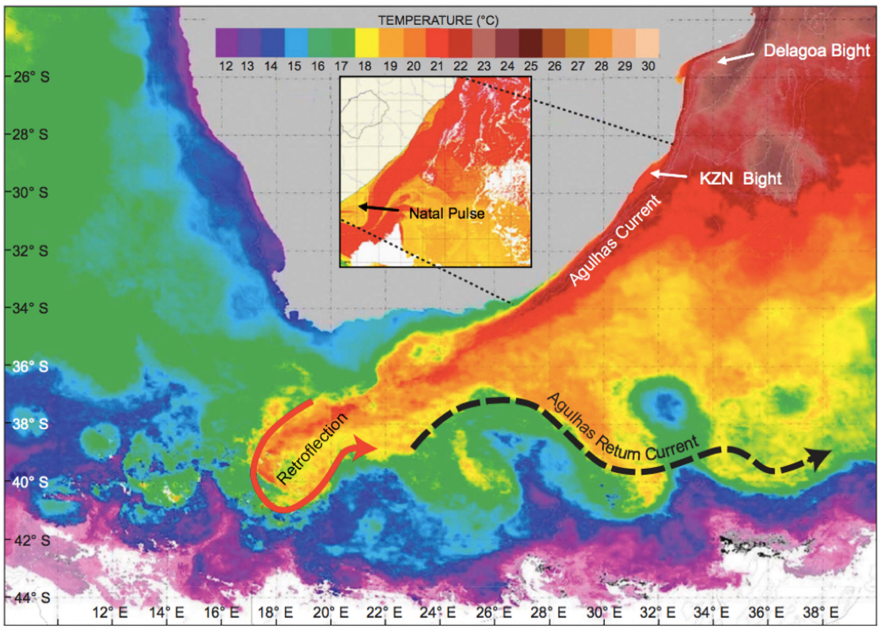

(a)

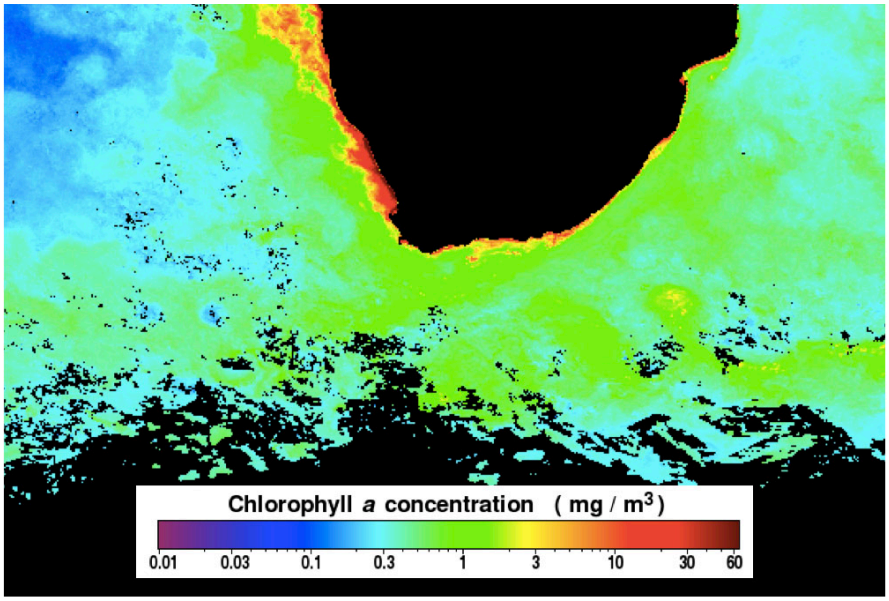

(b)

Figure 1.2: (a) MODIS satellite sea surface temperature image on 31 July 2006 illustrates the warm (red), fast Agulhas Current flowing down the east coast of South Africa, past the KZN Bight. At the southern tip of the continent (Agulhas Bank) the current undergoes retroflection to become the Agulhas Return Current, which flows along the Subtropical Convergence. About 4–6 times a year, a solitary meander (insert), known as a Natal Pulse, moves downstream between the KZN Bight and the Agulhas Bank, at times causing the current to retroflect farther east (Roberts et al., 2010). (b) Aqua MODIS monthly composite for July 2006 (source: oceancolor.gsfc.nasa.gov/cgi/l3).

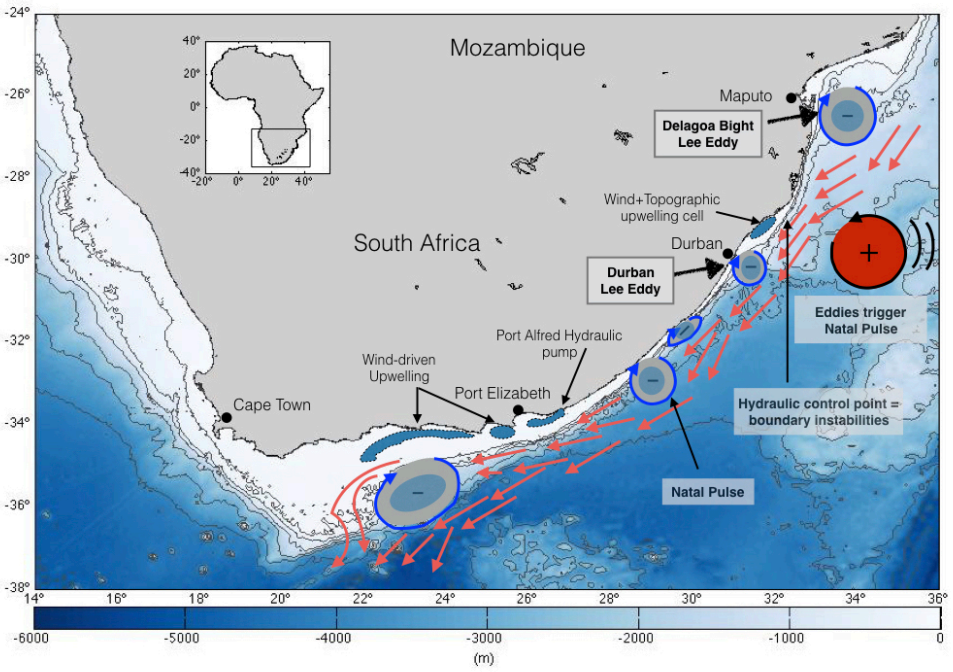

Figure 1.3: Schematic of the main oceanographic features identified along the east coast of South African. The map also includes the bathymetry. White indicates the shelf regions with depths of < 1000 m (adapted from Roberts, pers. comm., 2008).

From a few chl-*a* studies by (O'Reilly, 2012; Kyewalyanga et al., 2007; Dove, 2015), it has been hypothesised that these lee eddies might be facilitating primary production in the region. None of these studies, however, made any attempt to gauge the importance of these features as production centres. Several fundamental questions still remain, and for particular relevance to this thesis are: i) what is their frequency of occurrence, and ii) what is their link to primary production?

1.2 Satellite oceanography: an observational tool for science

As already mentioned, a conventional way of measuring the frequency of occurrence of these quasi-stationary eddies is the use of current meter arrays deployed ideally for at least 12 months to capture seasonality. This however, is extremely costly, both in terms of equipment and ship time necessary for deployment and retrieval. More so, it is not practical to continue such a field campaign over many years to measure inter annual variability.

An alternative method that is smart, readily available and easily accessible, is to use satellite-derived altimetry, which is able to detect the negative SSH in the centre of mesoscale cyclonic eddies. This is because of geostrophic circular flow in the cyclone and the relationships with pressure gradients. The height of the sea surface, ζ, is the height of the sea surface relative

to a particular level surface coincident with the ocean at rest — this surface is the geoid (Vignudelli et al., 2011). Since we can measure the surface topography from satellite altimeters we can calculate the slope of the surface and in turn the surface geostrophic currents. Geostrophy is the balance between rotation (Coriolis force) and the horizontal pressure gradient (Salmon, 1998). The equations (eq. 1.1, 1.2 and 1.3) provided, expand on this point.

The gradient of SSH is related to the geostrophic flow as follows: in Cartesian coordinates (*i.e.*, x and y), the geostrophic balance is:

$$u = -\frac{1}{fg}\frac{\partial \zeta}{\partial y} \tag{1.1}$$

$$v = \frac{1}{fg}\frac{\partial \zeta}{\partial x} \tag{1.2}$$

where: u = zonal component, v = meridional component, g = gravity, f = Coriolis force, ∂x = longitude, ∂y = latitude, $\partial \zeta$ = dynamic height.

In other words, this says that the acceleration due to the Coriolis force (u in eq. 1.1 and v in eq. 1.2) balances the change in SSH in zonal and meridional directions. Water 'wants' to flow 'downhill' from high to low pressure, but is deflected to the right (left) in the Northern (Southern) Hemisphere by the Coriolis force. When the pressure gradient force and the Coriolis force come into balance, water then moves along isobars with high pressure to the right (left) in the Northern (Southern) Hemisphere. Now imagine we are in the Southern Hemisphere. Here, $f < 0$. Imagine a Gaussian mountain in the middle of the ocean, which is anticyclonic. If the SSH increases as x increases (that is, if $\frac{\partial \zeta}{\partial x}$ is > 0), then v must be < 0. If SSH increases as y increases (that is, if $\frac{\partial \zeta}{\partial y}$ is > 0), then u must be positive. Thus, at the western (southern) side of an anticyclonic eddy, the flow is directed south or $v < 0$ (east or $u > 0$). The opposite is true for a cyclonic eddy.

Pressure gradients can be caused by differences in SSH, where ρ is a density ($kg/(m)^3$) and dynamic height ($\partial \zeta$) is in units of metres (m). The dynamic height is usually measured as the difference, or the anomaly from a reference value (Vignudelli et al., 2011). Typically it has a range of a couple of metres:

$$p = \rho g \partial \zeta \tag{1.3}$$

Whilst satellite altimetry is indispensable as a reliable measurement of SSH in the open ocean, its accuracy becomes questionable near coastlines as the returned radar signal becomes distorted due to the effects induced by land, both in the satellite measurement and in

the modeling of some of the geophysical corrections applied to the measurements (Fenoglio-Marc et al., 2010; Vignudelli et al., 2011; Cipollini et al., 2008). Commonly used signal processing algorithms are incapable of rectifying this and signals are thus flagged as 'contaminated'. Note that as a general rule, data collected < 50 km from a landmass should be of concern (Fig. 1.4) (refer to Section 2.4 for more detail).

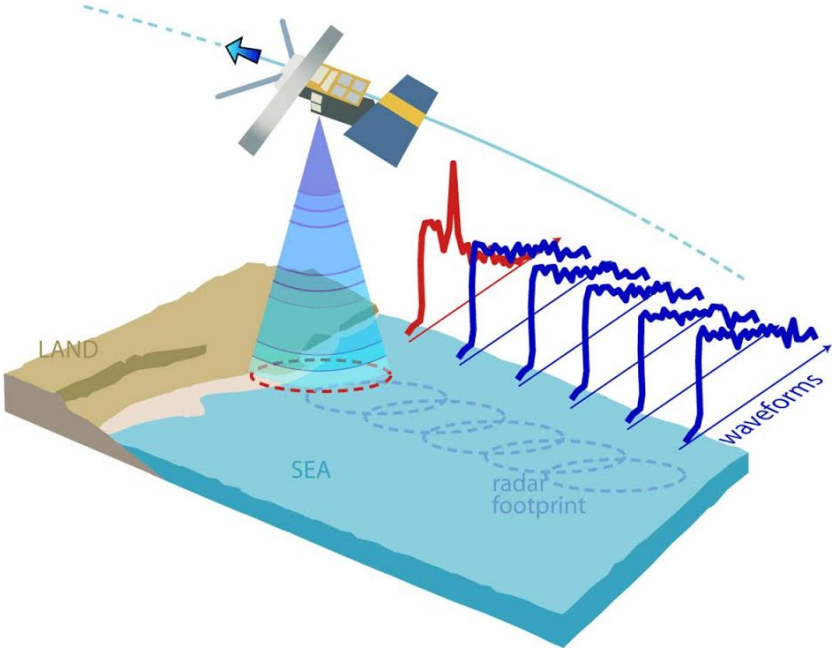

Figure 1.4: Depiction of the corruption of waveforms when the altimetric footprints approach the coast (P. Cipollini, NOC, 2015).

This problem has over the last 10 years attracted much attention, as shelf and open ocean interactions are one of the most important aspects of oceanography that have great social benefits. A few algorithms (*e.g.* Passaro et al., 2014; Roblou et al., 2007) have recently been developed in an attempt to recover SSH from the distorted returned radar signals, and have led to a new form of altimetry referred to as *coastal altimetry*. This has allowed the reprocessing of existing datasets, and has at times extended the reliability of SSH data to within a few kilometers from the coast (Bouffard et al., 2011). While coastal altimetry has become a very useful tool for coastal oceanography, it is limited by the position of satellite mission ground tracks.

1.3 Motivation for this study

The east coast of South Africa is far less productive compared with the west coast, where large-scale upwelling occurs due to the persistent southerly winds. The extent of the upwelling on the west coast ranges from Cape Agulhas on the western Agulhas Bank, around the Cape Peninsula, up to the Namibia-Angolan border — a distance of some 3,300 km. The

intensity of the upwelling is such that it produces one of the largest production (phytoplankton and zooplankton) zones in the global ocean, with the only other western boundary currents such as East Australian, Brazilian, Kuroshio, and California Current upwelling systems being comparable. This production supports large commercial fisheries including sardines, pilchards, hake, and mackerel Roberts et al. (2010).

The Agulhas Bank at the southern tip of the African continent, provides an intermediate region of production, with much of it produced at the intense thermocline that characterises this shelf, and wind-driven coastal upwelling off interspersed prominent capes along the southern coastline. Many commercially utilised species use the Agulhas Bank as a spawning ground, taking advantage of the mix between warm Agulhas Current water on the outer shelf (good for egg incubation) and the cooler more productive (good for larval survival and growth) inshore waters (Roberts et al., 2016).

By comparison, the east coast of South Africa has a very narrow shelf that is swept by the warm, fast flowing Agulhas Current . While upwelling winds do blow along this region of South Africa's coast, they are far less effective in drawing cool, nutrient-rich water to the surface owing to the presence of the dominant Agulhas Current that descends to a depth of some 1,500 m. Satellite images of surface chl-*a* commonly portray primary production along the inshore boundary of the current, often associated with mesoscale turbulence such as eddies and filaments. This primary production is far less extensive in terms of spatial extent. Satellite-determined levels show it to be not too dissimilar from that on the Agulhas Bank. Presumably, this supports the rich biodiversity and important line fisheries found on the east of South Africa. Hutchings et al. (2002) have suggested that the KZN Bight, positioned mid-way on the east coast, plays a major role in spawning and recruitment for many species along this coast in that it offers a refuge from the Agulhas Current. Combined with the inshore boundary production of the Agulhas Current, this implies the fulfillment of all three of the 'Bakun' requirements for good recruitment: retention, concentration and enrichment (Bakun, 2006)

Another similar situation is found north of the KZN Bight in the Delagoa Bight (Fig. 1.5). This is the largest coastal offset on the east African coast and is situated at the beginning of the Agulhas Current. As already indicated, the DBLE is commonly observed here, and is thought to be a major source of ocean primary production, similarly providing a conducive recruitment environment for many species including the commercially important ones. The Delagoa Bight is the second most important fisheries region for Mozambique after the Sofala Bank found farther north off the Zambezi River delta (Dove, 2015)..

Roberts (pers. comm., 2008) has suggested that the Delagoa Bight and the KZN Bight could provide a coupled-recruitment system conducive for fish egg retention and larval growth

covering a substantial area. Primary production to sustain this would likely come from turbulence generated by the Agulhas Current and the eddies.

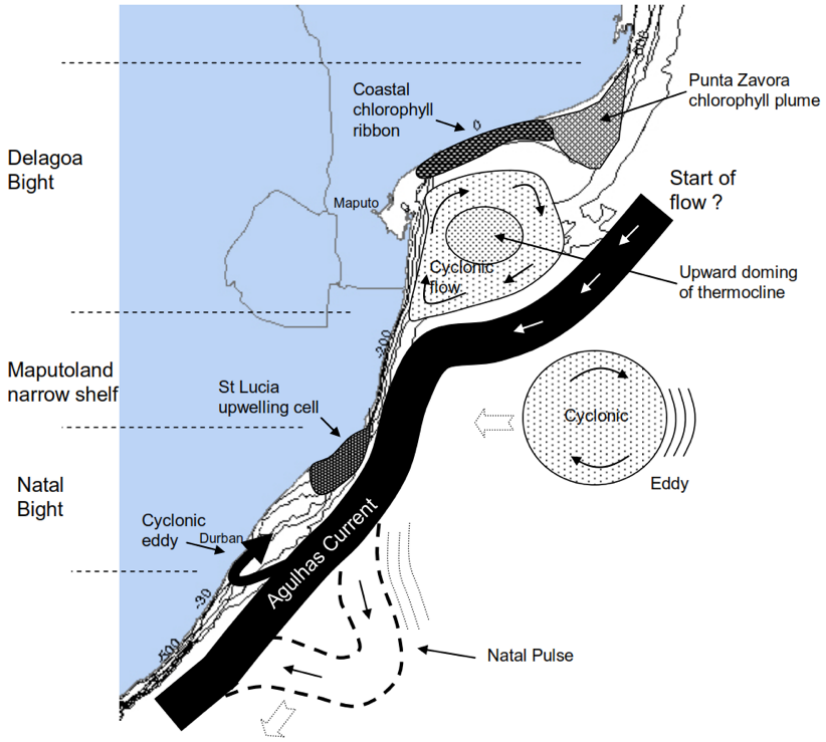

Figure 1.5: Schematic diagram showing the prominent known features of the Natal Bight-Delagoa Bight system (Roberts, pers. comm.).

1.4 Research aims and objectives

This study aims to begin an investigation into the coupled KZN Bight-Delagoa Bight system. Specifically, I will determine whether coastal altimetry can be used to reliably detect the DBLE (which typically has a dimension of approximately 100 km) (Cossa et al., 2016) and the DLE (which typically has a shelf dimension of approximately 40 km) Guastella and Roberts (2016). Secondly — if the first aim is successful — it will investigate whether satellite-derived surface chl-*a* is associated with these eddies. Given this association and the large amount of literature on eddy pumping and chl-*a* production, I will make the very reasonable assumption that cyclonic eddies are important centres for the generation of production in the boundary ocean, and in this case are important elements of the coupled KZN Bight-Delagoa Bight recruitment system. This association will be shown through observational data processing and correlation analyses using coastal altimetry, sea level anomalies (SLA) (standard product) and chl-*a*. Both assessments are tested using the following case studies: the Delagoa Bight as Case Study 1 and Durban lee eddy as Case Study 2.

1.5 Research questions

The key questions below help guide technical and scientific parts of this study.

Part 1: A technical assessment of coastal altimetry

1. Can coastal altimetry be used to detect the larger (~100 km) Delagoa Bight lee eddy?
2. If so, how close to the coast are the SSH data reliable?
3. How does the coastal altimetry product compare with the standard along-track and modeled AVISO product?
4. Can coastal altimetry be used to detect the semi-permanent smaller (~40 km) Durban lee eddy, and likewise, answer Question 3?

Part 2: Identifying the association between SLA of eddy and chl-*a*

1. Is the occurrence of the eddy correlated with enhanced surface chl-*a*?

1.6 Outline of dissertation

Chapter 2 provides a literature review on mesoscale eddies in the global ocean, and greater detail on the Delagoa Bight and the Durban eddy (Cases studies 1 and 2 respectively). This chapter also serves to provide an overview of the conceptual aspect of the use of satellite remote-sensing, coastal altimetry and ocean colour products. Chapter 3 discusses the protocols used to process the data and address each of the aims identified in Chapter 1. Chapter 4 presents the research outcomes pertaining to Part 1 and 2 of this study. In Chapter 5, the results are discussed in context with literature. Lastly, in Chapter 6, a summarised conclusion of the main outcomes are provided.

CHAPTER 2

LITERATURE REVIEW

The purpose of this chapter is to introduce eddies, addressing their formation, structure and their contributive role in the global ocean. In addition, a detailed review of current literature available on the two case studies (as mentioned in Section 1.4) is discussed, followed by an overview of how measurements are derived from satellites, and the recent advances made in the altimetry community (*i.e.* coastal altimetry).

2.1 Mesoscale eddies

The use of satellite altimetry in biophysical studies of the ocean has been demonstrated to be a powerful tool to study mesoscale eddies (Fu et al., 2010). Eddies can be defined simply as circular motions of water particles, circulating either in a clockwise or anti-clockwise direction. Eddies are common in the ocean, and range in diametre from centimetres to hundreds of kilometres (Adcroft et al., 2016; WHOI, 2015). At the ocean's surface and beneath, currents, gyres and eddies play a crucial role in the transport of water, salt and heat for long distances, thus helping promote large-scale mixing of the ocean (Liang and Thurnherr, 2012). Simultaneously, nutrients and inorganic carbon resulting from natural and human activities are transported, facilitating the regulation and perturbation of the planet's weather, climate and marine ecosystems (Liang and Thurnherr, 2012; Dove, 2015). These features are important components of Earth's global ocean circulation that move water mainly horizontally. Eddies being a primary foci of this study, are associated with another important component of water transport (Owen, 1981), *i.e.* vertical fluxes, which bring nutrients up from deeper levels in the water column.

Eddies that form off the coast carry local nutrient-rich waters far offshore into regions with

low ambient nutrient levels (Kyewalyanga et al., 2007; Lamont et al., 2010) (this is very important along the east coast of South Africa, which is generally very oligotrophic). As eddies transport recently advected seawater and nutrients into the regions, they provide nourishment for the phytoplankton and higher trophic positions (*viz.* zooplankton/larvae, which then provide food for larger marine species, for example fish) (Hewitt, 1981; Srokosz, 2000). Their effects can also extend down for kilometres, in some places reaching the ocean bottom. Eddies can form in almost any part of a current, but are more energetic in western boundary current regions. Eddies are usually comprised of water masses that are different from those outside of the eddy. That is, the water within an eddy usually has different temperature (Fig. 2.1(a)) and salinity (Fig. 2.1(b)) characteristics compared to the water outside of the eddy (Lutjeharms and Da Silva, 1988; Lutjeharms, 2006a), resulting in the variability of nutrients across the length of the feature. These swirling features are surrounded by currents, which flow in a roughly circular motion around the centre of the eddy (Pond and Pickard, 2013). The rotation of these currents may either be cyclonic or anticyclonic. There is a direct link between the water mass properties of an eddy and its rotation. Warm eddies rotate anticyclonically, while cold eddies rotate cyclonically (Pond and Pickard, 2013). Cyclonic eddies also known as cold-core eddies, cause cool, nutrient-rich waters to be upwelled (move vertically) from the deeper waters. Whereas anticyclonic eddies are also known as warm-core eddies, and cause warmer, nutrient-poor waters to be downwelled (Simpson et al., 1984).

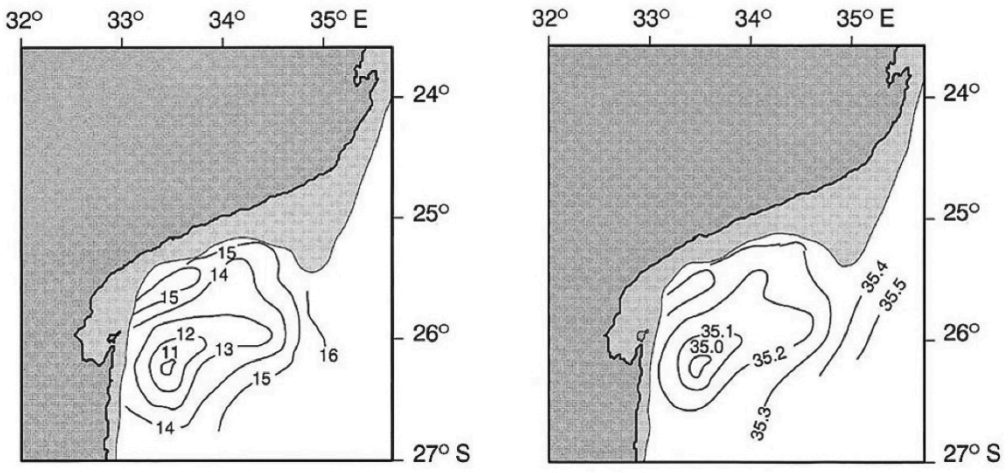

(a) (b)

Figure 2.1: Horizontal profiles of (a) temperature and (b) salinity of water upwelled from 900–1000 m in the core of Delagoa Bight cyclonic eddy at 200 m (Lutjeharms and Da Silva, 1988; Lutjeharms, 2006a).

On a much broader scale, shelf-edge upwelling and cyclonic eddies are also known to occur along the shelf edge of other warm western boundary currents such as the Brazil Current (Campos et al., 2000; Lima et al., 1996), East Australian Current (Oke and Griffin, 2011;

Roughan and Middleton, 2002), Gulf Stream (Lee et al., 1981, 1991) and Kuroshio Current in the East China Sea (Ito et al., 1995). A few examples will be discussed in some detail.

The SÃčo TomÃl' semi-permanent eddy is one of the main mesoscale features observed in the Southeast Brazilian region. The Southeast Brazilian coast has direct influence of the oligotrophic waters from the Brazil Current (BC) (Peterson and Stramma, 1991; Stramma and England, 1999). Waters from BC are saline, warm and oligotrophic (Brandini et al., 1997). Primary production and phytoplankton biomass tend therefore to be low, but they can be altered by oceanographic processes that promote injections of nutrients from subsurface waters to the euphotic zone. A study by Ciotti and Kampel (2001) was carried out to illustrate the impact of the eddy (21–22°S) on the estimations of surface chl-*a*. Preliminary results from the six day continuous observation found that at the centre of the eddy chl-*a* remained relatively low. Areas of high chl-*a* (~0.4–0.5 $mg.m^{-3}$) associated with this eddy were located at the edges in the offshore side of the eddy. Part of this high chlorophyll segment is visible in the centre of the eddy over time, which is suggested to be associated with the entrapment of cold shelf waters by the eddy than to upwelling in the central core of the eddy.

Another example includes the California Current System (CCS), an eastern boundary current of the North Pacific Ocean off the USA and Mexico west coasts (Castelao et al., 2006). This extends between the North Pacific Current in the north and Baja California in the south. This system is located in a rich eddy field (Castelao et al., 2006). A study carried out by Hewitt (1981) aimed to determine the importance of cyclonic eddies and its connection to the biological production in Punta Eugenia, Baja California. At Point Conception and Punta Eugenia, at the south of these two headlands, semi-permanent eddies are apparent, which cause the offshore divergence of surface flow of the California Current (Reid et al., 1958). Specifically, in Punta Eugenia these eddies are evident at both the north and south ends. Their findings suggest that these eddies play a role in the recruitment of pelagic larvae in these areas. Limited connectivity between the eddies suggest a speciation mechanism that would be most effective on populations that time their spawning to coincide with strong eddy formation (Hewitt, 1981). Also on the west coast of the USA a semi-permanent cyclonic eddy found in the Southern California Bight, between Point conception and San Diego reaches its maximum strength in summer, with its weaker intensity in winter. The location and stability of this eddy appears to be determined by the coastline geography. These semi-permanent eddies are found to be of importance in the Bight, in terms of its influence on the biological ecosystems.

The Eastern Australian Current (forms between 10 and 15°S), supplies the western boundary of the South Pacific Gyre with warm nutrient poor water (Speich et al., 2002). It flows, along the Australian coastal boundary to the south, following its separation into a northeastward

(Subtropical Counter Current), eastward (Tasman Front) and residual southward (EAC Extension) components at around 31°S resulting in the formation of semi-permanent eddies. These eddies are 200–300 km in diameter with 2–3 eddies generated annually and have lifetimes often exceeding a year (Nilsson and Cresswell, 1980). They follow complex southward trajectories, but are generally constrained within the Pacific deep basin. The main biological influence of the eddies are to increase the vertical mixing within the upper ocean in the western Tasman Sea, extending the effective mixed layer depth and thus suppressing the winter phytoplankton and zooplankton populations due to light-limited conditions for phytoplankton growth (Condie and Dunn, 2006). These conditions result in spring and autumn blooms of chl-*a*, with lower summer concentrations because of stratification and nutrient depletion.

Moreover, upwelling associated with eddies supplies more nutrients to the surface layer once the bloom has begun, delaying the depletion of nutrients and prolonging the duration of the blooms (Tilburg et al., 2001). The EAC and its eddies frequently move onto the continental shelf and close inshore and influence in local circulation patterns. At prominent coastal features such as Cape Byron, Sugarloaf Point and Port Stephens, the EAC moves away from the coast, driving divergent upwelling, which draws nutrient-rich water from a depth of 200 m or more (Oke and Middleton, 2000, 2001). However, while the EAC may drive nutrient-rich water onto the shelf, upwelling-favourable winds (northerly) are required to bring the water to the surface (Church and Craig, 1998).

In the vicinity of the Agulhas Current, large indentations in the coastline of east Africa have resulted in abrupt downstream broadening of the continental shelf and terrace at two locations (i) in the Delagoa Bight south of 20°S and (ii) adjacent to Richards Bay (29°S) to the south (Lutjeharms and Da Silva, 1988). Richards Bay is characterised by its strong inshore reversal currents. Malan and Schumann (1979), assumed that these inshore current reversals were linked to lee eddies driven by the adjacent Agulhas Current. These eddies were further suggested (Lutjeharms, 1981; Lutjeharms and Connell, 1989) as the source of large downstream meanders in the Agulhas Current (AC). Eddies of this nature either appear to be topographically induced (Smith et al., 1984) or trapped by a southward flowing coastal current (Bowman, 1985) further north. Several studies have documented the existence of cyclonic circulation in the Delagoa Bight (Harris, 1972; Lutjeharms, 1976, 1981; Martin, 1981a,b; Michaelis, 1923; Sætre and Da Silva, 1984). Results have implied the possibility of a similar lee eddy (such as the Durban lee eddy) present in this bight.

2.2 Case study 1: Delagoa Bight lee eddy

The Delagoa Bight is influenced by oceanic features travelling through the Mozambique Channel (MC), as well as those coming from the southern tip of Madagascar (Lutjeharms,

2006b). It is one of the largest coastal indentations in the south-west Indian Ocean (Lamont et al., 2010; Lutjeharms and Da Silva, 1988) and is located right offshore of the Mozambican capital, Maputo. The Delagoa Bight is one of the main fishing grounds on the Mozambican Shelf, hosting high biodiversity, including commercial fisheries species such as scad, mackerel and shallow water prawn (*Penaeus indicus* and *Metapenaeus monoceros*) which yield important food and foreign revenue for the Mozambican economy (Hoguane, 2007).

In addition, the bight hosts the largest supposedly semi-fixed eddy on the southeast coast of Africa, commonly referred to as the Delagoa Bight lee eddy (DBLE) (Cossa et al., 2016). Water masses in this eddy have temperature-salinity characteristics suggestive of substantial upwelling in the core of the eddy from depths of at least 900 m (Lutjeharms, 2007). Hence there should be nutrient enrichment of the surface layers and thus increases in the chl-*a* content. To date this has not been observed, except intermittently at the north-eastern point of the Delagoa Bight (Quartly and Srokosz, 2004) in the form of offshore southward orientated plumes. This sporadic increase in primary productivity may be the result of current-induced upwelling as predicted by Gill and Schumann (1979). If driven by passing eddies, such intermittent upwelling would be expected. No evidence for such major increases in either phytoplankton or zooplankton have to date been found in the center of the Delagoa Bight eddy (Lutjeharms, 2007).

Four studies by Lutjeharms and Da Silva (1988), Lamont et al. (2010), Dove (2015), and Cossa et al. (2016), have aimed to understand and define the dynamics of the eddy in terms of its nature and frequency, impacts of passing eddies on the eddy, and chlorophyll variability in the region (further on in this study will be referred to as DBLE).

In 1988, Lutjeharms and da Silva attempted to determine the nature and frequency of occurrence of the DBLE using twenty-five years' of detailed hydrographic data coupled with ten years' of thermal infra-red imagery. Their analysis pointed to the presence of a quasi-permanent eddy in the Delagoa Bight, and particularly dominant below 100 m depth. Interestingly, sediment patterns also supported the concept of a quasi-permanent topographically trapped eddy (Lutjeharms and Da Silva, 1988; Martin, 1981a,b). Conclusions made by Lujeharms and da Silva, suggested this feature was present in the bight most, if not, all the time. The geographical stability of its core lead to the belief that this topographically induced eddy was driven by a well-mixed Equatorial surface Mozambique Current. It was also noted that at depth the temperature and salinity of the eddy had characteristics of Antarctic Intermediate water (Lutjeharms and Da Silva, 1988), suggesting upwelling from 900 m to 400 m on the shelf (Lamont et al., 2010).

Lamont et al. (2010) questioned whether this was in fact a semi-permanent feature. They used four sets of hydrographic data, surface drifters and satellite imagery to investigate the

persistence of the cyclonic lee eddy in the Delagoa Bight. They also noted the influence of passing eddies from the Mozambique Channel on the circulation in the bight. The hydrographic and satellite data illustrated the eddy was present twice, (i) the first observation indicated the eddy, centered at 26°S, 34.25°E, during May 2004 lasted for six weeks, and (ii) the second observation during August 2004 when the core of the eddy was located south of the Bight (27.5°S, 34.5°E). No cyclonic eddy was observed during April 2005 and 2006 leading Lamont et al. (2010) to concluded that the eddy was not a semi-permanent feature as proposed by Lutjeharms and Da Silva (1988), and dependent on the movement of eddies in the adjacent waters of the Mozambique Channel. The only permanent feature observed was the inshore, northward coastal current (25–30 $cm.s^{-1}$), occurring subsurface on the shelf. Upwelling was frequently observed at various locations in the Bight, depending on the distance and interaction of eddies with the topography of the shelf and slope. Increase in phytoplankton biomass was found to be coincident with cooler water along the north-eastern limit of the Delagoa Bight (Barlow et al., 2008; Lamont et al., 2010). Kyewalyanga et al. (2007) concluded that hydrographic conditions were the primary control of the variations in phytoplankton biomass and primary production in the bight during August 2004. Lamont et al. (2010) acknowledges that using sea surface temperature (SST) and chl-*a* in identifying and investigating the eddies was limited.

In 2015, Dove (2015) analysed ten years' (2003–2012) of multi-satellite (MODIS/Aqua) monthly data, which aimed to describe the seasonal and interannual variability of chl-*a* and its relationship with SST, sea surface winds and sea level anomalies (SLA) in the Delagoa Bight. Distinct patterns of variability were found. At a seasonal level chl-*a* concentration increased from June through September (late autumn–late winter) and decreased from December to May (late spring–mid autumn). In addition, a strong seasonal horizontal structure was identified in the averaged chl-*a* concentrations and SST. The lowest maximum in monthly chl-*a* concentration occurred in December (0.13 $mg.m^{-3}$) and August (0.54 $mg.m^{-3}$). Increased chl-*a* concentrations were observed, which were consistent with cooler SSTs. Cooler SSTs (upwelling) associated with cyclonic eddies were expected introducing cooler, nutrient-rich water into the surface layers, which would result in an increase in phytoplankton abundance and primary production (Lamont et al., 2010). In particular increased phytoplankton biomass was found to be coincident with cooler water along the north-eastern limit of the Delagoa Bight (Barlow et al., 2008; Lamont et al., 2010). In addition, five years (2006–2011) of in situ SST confirmed a seasonal signal with amplitude of about 6.5°C. Cool coastal water events were found mostly in summer and spring, with a maximum amplitude of 6°C. The timing of these cool events at the northern Delagoa Bight at Ponta Zavora (24.48°S, 35.24°E) was irregular. Results also suggest episodic influences of both cyclonic and anticyclonic features at the eastern perimeter of the Delagoa Bight, although

the SLA amplitude was extremely low. A ROMS model by Jose et al. (2014) has revealed results quite contradictory to previous work by Lutjeharms and Da Silva (1988), showing that several cyclonic eddies were found with low concentrations of chlorophyll at their cores. This also contrasts previous studies in the open ocean (McGillicuddy and Robinson, 1997; Longhurst, 2001).

In fact, several anticyclonic eddies in the biogeochemical model were found with high concentrations of chlorophyll at their cores. It would seem that phytoplankton growth within these mesoscale features (both cyclonic and anticyclonic eddies) occurred in response to nutrient injection by horizontal advection, and subsequent retention of surrounding nutrient-rich waters within eddies. Offshore nutrient distributions depended strongly on lateral advection of nutrient-rich water from the coastal regions, induced by eddy interactions with the shelf. The environmental conditions at the locations where eddies were generated had an important effect on nutrient concentrations within these structures. On the other hand O'Reilly (2012) indicates that chl-*a* concentration in surface water of the cyclonic eddies was significantly higher than in surface waters within the anticyclonic eddy.

Following Lamont et al. (2010) and Cossa et al. (2016) configured a ROMS model in the Delagoa Bight region which indicated the existence of a semi-permanent eddy. This was also apparent in gridded maps of merged altimetry (Ssalto/Daucs) obtained from AVISO. This finding supports the conclusion of Lutjeharms and Da Silva (1988) who suggested that the eddy is a semi-permanent eddy. From the model, the Delagoa Bight lee eddy was shown to occur about 25 % of the time with no clear seasonal occurrence. The diameter of the eddy core varied between 61 and 147 km (lower than the previous estimate of 180 km from Lutjeharms and Da Silva, 1988). The average life time exceeded 20 days which points to a feature that forms, moves away, then forms again. The model analysis revealed the systematic presence of negative vorticity in the Bight that can organise and form a DBLE depending on the intensity of an intermittent southward flow along the southern part of the bight and the spatial distribution of surrounding mesoscale features (Cossa et al., 2016). Cossa et al. (2016) also found (i) the model solution showing other cyclonic eddies generated near Inhambane and eventually traveling through the Bight; and (ii) the only permanent feature observed with or without DBLE is the presence of a northward, surface intensified, coastal counter-current along the Maputaland shelf (between Sodwana and Inhambane).

2.3 Case study 2: Durban lee eddy

The second largest coastal indentation after the Delagoa Bight, is the KwaZulu-Natal Bight (hereafter referred to as the Natal bight). It is a broad shelf; an offset in the coastline on the east coast of South Africa (Fennessy et al., 2016) bounded by the Agulhas Current that flows

southwestward alongside the shelf edge as it narrows (Gründlingh, 1983; Gründlingh and Pearce, 1990). The Natal Bight at its widest point is 45 km (Martin and Flemming, 1988). Earlier description (Martin, 1984) of this indentation suggests that this offset, and associated expansion in shelf width, was caused by a change in the tectonic origin of the continental shelf margin, from a sheared to a short-rifted section , and is approximately 160 km long between Durban and Richards Bay. This shelf widening is in sharp contrast to the remainder of KZN where the average position of the continental slope break is 11 km from the coast (Schumann, 1988). The bightâĂŹs seaward boundary can be considered to be broadly delimited by the shelf break at about 100 m depth (Martin and Flemming, 1988).

The Durban lee eddy (DLE), is a semi-permanent mesoscale cyclonic feature that exists at the southern end of the Natal Bight. The eddy spins up south of Durban, inshore of the southward flowing Agulhas Current and in the lee of the Bight. After some 10 days, it detaches from this position, and migrates southward to flatten inshore of the Current on the Transkei shelf and dissipates. Average values of nitrates in the Durban eddy have been measured around 3.33 μmol.l, but maximum values have reached 16.79 μmol.l, demonstrating the effect of the eddyâĂŹs presence at times (Lutjeharms, 2006a). However, they noted that these higher nutrient concentrations did not always translate into higher chl-*a* levels. Guastella and Roberts (2016), observed that as the DLE migrated further south along the coast, an elevation in chl-*a* was noted. This suggests that there is a strong biological response to the Durban Eddy on occasion. There is however, evidence of higher zooplankton biomass here, but only intermittently. Phytoplankton production rates are below 1 g C.m^2.day (Burchall, 1968). There has been a greater density of fish larvae off Durban on occasion (Beckley and Van Ballegooyen, 1992), but not consistently (Beckley and Hewitson, 1994). A hydrographic cruise covering the whole Natal Bight has clearly demonstrated (Lutjeharms et al., 2000; Meyer et al., 2002) the vertical structure of this eddy compared to the waters over the rest of the shelf. Interestingly, the upwelling of nutrient-rich water did not enhance chl-*a* values on that occasion either.

Lutjeharms (2006b), noted that while the cyclonic lee eddy is a recurrent part of the shelf circulation directly off Durban, it is not always present and seems to have limited any local biological impact. Clearly productivity will vary according to the eddy's occurrence, intensity, longevity, degree of uplift of nutrients, recirculation characteristics and residence time of the water within the eddy. CTD survey data by Guastella and Roberts (2016) have shown that even once the eddy has migrated out of the Durban area, chlorophyll concentrations (indicated by fluorescence) can remain relatively high off Durban, but are more coastal as a result of the upward sloping water column structure induced by the dynamics of the Agulhas Current. Guastella and Roberts (2016) also shows that, while the Durban Eddy is present off Durban some 55 % of the time, its variability in occurrence, intensity, strength and size mean that contributions to primary productivity are in turn variable and inconsistent.

Lutjeharms (2006b), suggested that the DLE is topographically induced and that it may be one of the supplies of nutrients to the Natal bight through northward advection of upwelled eddy water inshore (Meyer et al., 2002), although there was little material evidence for this. Guastella and Roberts (2016) tried to discern the latter using surface drifter buoys and ADCP current measurements, however their results were inconclusive, due to limited sampling in space and time.

While the Natal Pulse (a larger feature associated with meanders in the Agulhas Current) has been the subject of previous oceanographic modeling studies (*e.g.* Tsugawa and Hasumi, 2010), no known dedicated oceanographic modeling has been done on the DLE. A Regional Ocean Modelling System (ROMS) configured by Guastella (unpubl.) uses a parent configuration with a spatial resolution of $1/8°$ simulates the circulation off eastern South Africa, while a first online zoom at $1/24°$ details the dynamics of the Natal Bight and a second embedded zoom at $1/72°$ focuses on the DLE. Results indicate that the ROMS model replicates the circulation of the Natal Bight well in the child domain and reproduces the Durban Eddy spatio-temporal dynamics in the grandchild domain. The destination of eddy water was investigated with a Lagrangian floats trajectory analysis, disseminated at various positions/levels in the model. Preliminary results indicate that it is possible for Durban Eddy water to advect northward at depth, lending support to the theory by Meyer et al. (2002).

In summary, Lutjeharms (2006b) notes that a cyclonic lee eddy is a recurrent, but not ever-present part of the circulation on the shelf directly off Durban, but seems to have hardly any local biological impact. Observations of ocean colour imagery however, seems to indicate otherwise. Other studies suggested that this cyclonic eddy was linked to the incipient Natal Pulses (Lutjeharms and Connell, 1989). When a Natal Pulse forms, due to the interaction of an offshore eddy or otherwise — it seems to carry the Durban lee eddy with it (Lutjeharms et al., 2003) all the way to the southern tip of the continent, intensifying the cyclonic motion in the eddy in its downstream journey. This would imply that inshore currents from Durban downstream would experience a sudden, but short-lived, reversal. As mentioned before, such a reversal has actually been observed (Lutjeharms and Connell, 1989) and directly related to a passing Natal Pulse. This incorporation of the Durban eddy in Natal Pulses also means that a part of the shelf fauna of the Natal Bight will intermittently be carried away. The effect of such a mechanism on the shelf biota is unknown.

2.4 Coastal altimetry: improving accuracy in coastal data

In the last 25 years, satellite-borne radar sensors such as TOPEX/Poseidon (which was launched in 1992), ERS-1 and -2, Envisat, Geosat Follow-On (GFO) and Jason-1 and -2 have been providing reliable datasets that have contributed to the advancement in marine

and climate research, and which have supported operational oceanography (Cipollini and Snaith, 2015). Efforts are naturally being made to use it also in the coastal zone. Altimetry has been used to observe global ocean surface topography and its changes with unprecedented accuracy of about 2 cm root-mean-square (RMS) in SSH and resolutions (up to 50 km spatial scale and weekly temporal sampling) (Chelton et al., 2001; Shum et al., 2003). The basic equation by which the fundamental measurement taken by a radar altimeter, (*i.e.* a measurement of range from the instrument to the sea surface) is converted into an accurate measurement of the surface height:

$$SSH = orbital\_altitude - (range + corrections) \tag{2.1}$$

Where *orbital_altitude* is the height of the satellite center of mass with respect to a reference surface (typically a reference ellipsoid) which is normally modeled to an accuracy of 2–3 cm by using a combination of GPS positioning, laser ranging and radio positioning using ground stations (Cipollini et al., 2017). The *SSH* obtained contains the geoid variations as well as the oceanographic signal; subtraction of a mean sea surface [1] removes the time-invariant geoid and the mean of the dynamic topography and yields the SLA (provided also the tidal signal and the atmospheric signals are corrected for) (Cipollini et al., 2017).

The observation principle of pulse-limited satellite radar altimetry is conceptually straightforward. It transmits an electromagnetic pulse to the sea surface and measures its two-way travel time when the return reflected from the instantaneous sea surface is received (Fig. 2.2). The altimeter measures the range using an on-board tracker, which provides a time series of the received power distribution of the reflected pulse called the altimeter waveform. The two-way travel time represents the time for the midpoint of the pulse to return from the sea surface at nadir (Lee et al., 2010). Therefore, the altimeter determines the two-way travel time by identifying the half-power point on the leading edge of the waveform. The on-board tracker design is based on a Brown (1977) model of the return waveform, to align the return spectral waveform so that the half-power point of the leading edge is at a specified frequency. A key strength of satellite observations is the global and frequent coverage, allowing the sampling of large scale variability (biological and physical) over a wide range of time scales (Fua and Le Traon, 2006; Roblou et al., 2007; Jordi and Basterretxea, 2012).

[1] A mean sea surface height (MSSH) is the level of the sea due to all those contributions that can be assumed constant in time and can be computed as the temporal mean of sufficiently long time series. More accurate MSSH models (for instance DTU15) are built from combinations of multiple altimetric and gravimetric missions. The choice of a specific MSSH over another is critical in the coastal zone, and there may be biases between datasets if they are referred to different mean SSH.

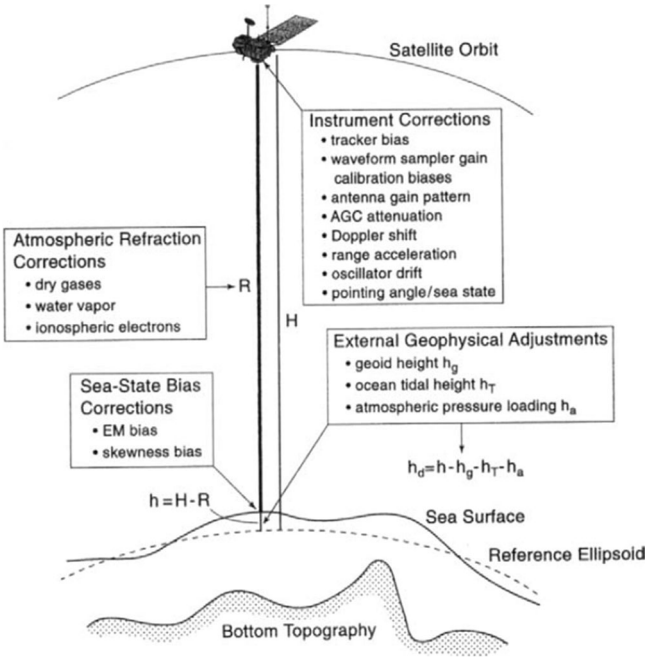

Figure 2.2: Schematic of the satellite radar altimetry system, and the corrections that needs to be applied to the altimeter range measurement R and the relations between R, the orbit height H and the sea surface height h relative to an ellipsoidal approximation of the equipotential of the sea surface from the combined effects of the earth's gravity and the geoid (Chelton et al., 2001).

With continuous technological advancement, remote-sensing data from Earth-orbiting satellites has allowed science to successfully study the ocean making it one of the most successful observational platforms (Roblou et al., 2007; Jordi and Basterretxea, 2012). Most marine applications of satellite altimetry begin with sea surface heights (SSH) (Hwang et al., 2006). Over the deep oceans without land interference, the waveforms [2] created by the returning altimeter pulse generally follow the ocean model of Brown (1977), and the corresponding range can be properly determined using the result from an onboard tracker. Near coasts however, as mentioned in 1.2, the consequent rejection of possible valid data (SSH measurements) become corrupted due to effects induced by land, both in the satellite measurement and in the modeling of some of the geophysical corrections applied to the measurements. The noisier radar returns (Hwang et al., 2006) from the generally rougher coastal sea states and simultaneous returns from reflective land and shallow water (Lee et al., 2010; Brooks et al., 1997; Deng and Featherstone, 2006) limit the application of satellite altimetry in coastal regions. For example, such corruptions of waveforms in ERS and Envisat altimetry over global coastal zones have been presented by Mathers et al. (2004).

[2] Waveforms are a series of powers at altimeter gates generated by a returning pulse from the sea.

Two classes of problems have been encountered when trying to recover meaningful estimates of geophysical parameters (sea level, significant wave height and wind speed) from altimeter data in the coastal zone (Cipollini et al., 2012; Cipollini and Co-Authors, 2010). First, there are problems due to the modification of the altimetric echoes (waveforms) when land enters the footprint of the instrument (Fig. 1.4). Then there are problems due to the unavailability or inaccuracy of some of the corrections that need to be applied to the raw altimetric measurements to account for instrumental, atmospheric or other geophysical effects (for instance tides). Both these classes of problems are described below. The first class of problems impact on the shape of the waveforms and affect the retrieval of parameters which is normally carried out by fitting a waveform model to the waveforms, a process known as retracking. The impact of land on waveforms will not only depend on crude 'distance from coast' but also on the coastal topography; in the coastal zone waveforms will normally suffer an attenuation due to missing ocean surface elements in the altimetric footprint (as land returns are normally weaker then those from the ocean), but their shape is also modified by returns from land elements close to the coastline at an elevation different from zero. Brooks et al. (1997) found that the land return influences TOPEX waveforms within distances of 4.1–34.8 km from coasts with the maximum near the East China Sea. Deng et al. (2002) observed that the waveforms from ERS-2 and Poseidon can be affected up to a maximum distance of 22 km off the Australian coast. Waveforms reflected from these affected coastal oceans do not conform to those over open oceans so that the on-board satellite tracking algorithm cannot accurately compute the range between the satellite and nadir surface, thus producing poorly estimated SSH measurements. Therefore, if to be used the altimeter range measurements over the coastal ocean must be corrected for the deviation of the midpoint of the leading edge from the tracking gate of the on-board tracker.

The second problem pertains to unavailability of some corrections. The most critical corrections in the coastal zone are ocean tides, water vapour, and the sea state bias (SSB) (Cipollini and Co-Authors, 2010). The SSB, *i.e.* the bias on the range estimate dependent on the sea state and due to the shape of the sea surface not being perfectly sinusoidal, is in need of further investigation to migrate from the actual empirical correction models towards physically-based ones — a difficult task even over the open ocean, let alone in the coastal zone. However the largest uncertainty in the coastal altimetry data comes from inaccurate removal of the tides. The global tidal models improve at every new release but still do not perform well in many coastal and shelf locations and from the inaccurate correction of the path delay due to water vapour, known as 'wet tropospheric correction'. The wet tropospheric correction is normally estimated from a multi-channel passive microwave radiometer on the same platform as the altimeter, but this estimate gets quickly corrupted as soon as land enters the radiometer footprint, *i.e.* 20–50 km from the coast. According to Cipollini et al. (2012), as far

as tides are concerned, the obvious solution is to develop accurate local tidal models, which then need to be merged with the global models.

Altimetry is a powerful tool. However, the largest uncertainty in the coastal altimetry data near the coast have limited coastal oceanographic research. Over the last few years' progress in overcoming these problems have been made. Such advances have given rise to a new discipline referred to as coastal altimetry (Jordi and Basterretxea, 2012; Vignudelli et al., 2011). The coastal altimetry community has coalesced in the last few years, and have already developed techniques to recover useful measurements of sea level and significant wave height in the coastal strip. The recent development of coastal altimetry implements re-tracking algorithms and various correction steps during the reprocessing of data (Cipollini et al., 2008). The major space agencies are strongly supporting this new field with initiatives like ESA's COASTALT (for Envisat) and CNES' PISTACH (for Jason-2). In the coastal zone, in addition to the refinement of the statistical techniques for screening and filtering various data and corrections (such as in X-TRACK; case study by Roblou et al., 2007), there are two complementary courses of actions for improving the quality of the retrieved data: (i) applying specialised retracking (*i.e.* improving the estimation of the range term in 2.1) and (ii) applying improved corrections for the atmospheric, surface or geophysical effects (*i.e.* improving the corrections term) (Cipollini et al., 2017).

A solution recently proposed to improve the retrieval of sea level, SWH and wind in the coastal zone is the Adaptive Leading-Edge Subwaveform (ALES) algorithm (Passaro et al., 2014). ALES is a two-pass retracking algorithm, based on the Brown model, where the second-pass subwaveform window is selected based on the first-pass estimates of SWH, in a way that minimizes the performance degradation with regards to an ideal, uncorrupted full-waveform case. This algorithm has been validated for sea level and SWH and used for different altimeters in number of case studies (Passaro et al., 2014, 2015a,b, 2016; Gómez-Enri et al., 2016).

CHAPTER 3

METHODS

In this chapter a brief description of the study regions are given. In addition, remote sensing datasets and protocols used to achieve the aims set out in this research are discussed in detail.

3.1 Areas of focus

The Delagoa Bight study domain comprised of 24–29°S, 32–36°E (~4°×4°) (Fig. 3.1). Data collected over 9 years from February 2002 to September 2010 of high resolution CGDR [1] and SGDR [2] from Envisat (18 Hz), gridded OC-CCI chl-*a* (1/4 degree) and AVISO SLA (1/4 degree) products were analysed. For the Natal Bight, this study domain consisted of 29–36°S, 30.5–31.5°E (~3°×3°) (Fig. 3.2). Data collected over 8 years from April 2008 to September 2015 of CDGR and SGDR from Jason-2 (20 Hz), and gridded OC-CCI chl-*a* (1/4 degree) and AVISO SLA (1/4 degree) products.

The DBLE was used to validate the application of coastal altimetry, as it is easier to detect due to its large size. However, it should be noted that this eddy is normally located 100 km offshore and therefore spans the coastal and offshore domains. Since the algorithm applied to coastal data is only applied within up to 50 km from the coastline, it was decided to test the application on a smaller feature (Durban eddy) inshore, on the basis that the application of coastal altimetry was successfully validated in the Delagoa Bight region.

[1] Coastal Geophysical Data Records, which are essentially copies of the original SGDR with the addition of outputs from the ALES retracker

[2] Sensor Geophysical Data Records, which are the original outputs from the satellite

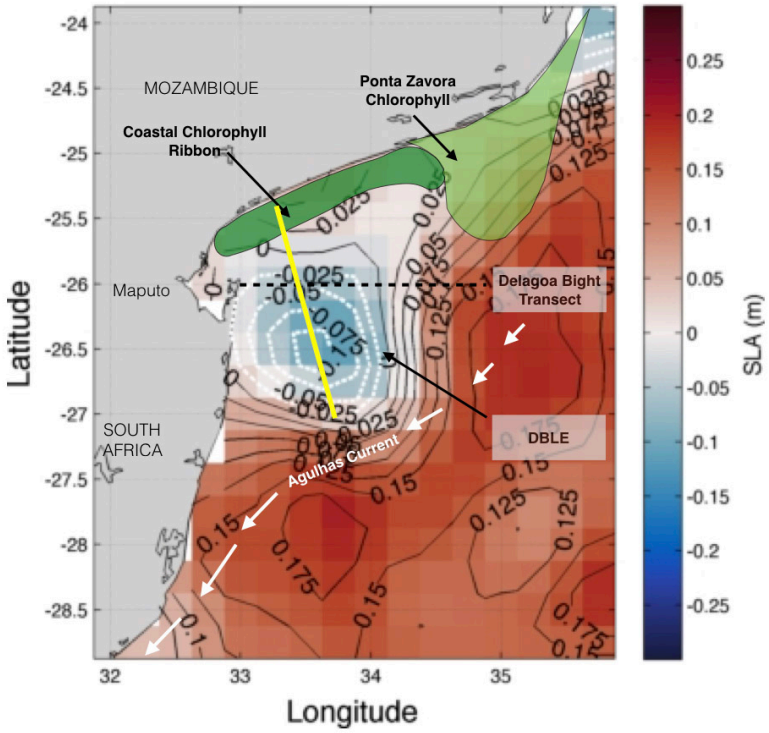

Figure 3.1: An AVISO SLA image on 4 July, 2008. The main oceanographic features in the Delagoa Bight (Adapted from Roberts, pers. comm., 2008) are shown — the local min. ssh indicates the core of the Delagoa Bight Lee Eddy. Included is the location of the DB transect dashed line; used by Lamont et al. (2010). Bold yellow line indicates the Envisat track (0371) analysed in this study.

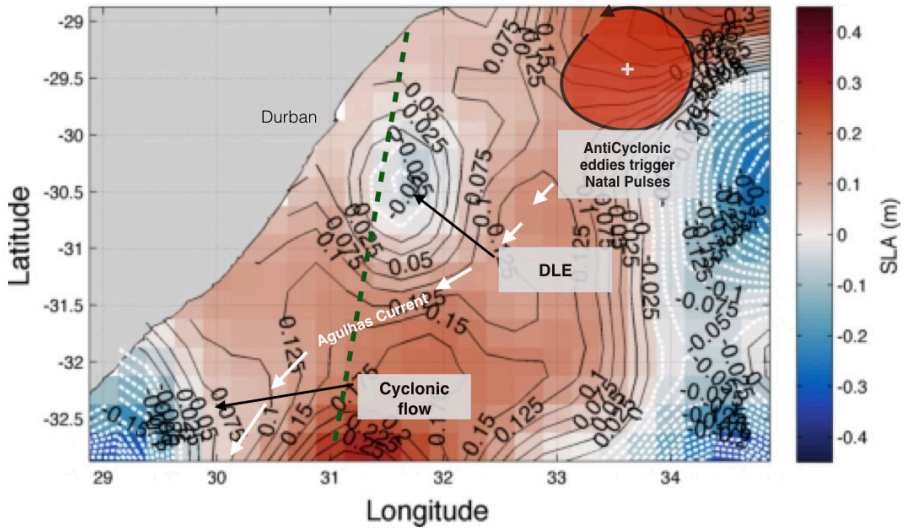

Figure 3.2: An AVISO SLA image on 27 July, 2008. The main feature focused on in this study is the Durban lee eddy highlighted by the negative SSH. Bold dashed line (dark green) indicates the Jason-2 track (0005) analysed in this study.

3.2 Data acquisition and processing

3.2.1 Coastal altimetry data: altimetry data re-tracked by ALES

Remote sensing is seen as an important tool for mapping oceanic properties on both small and large scales. However, it has also brought about a limitation to the reliability and accuracy of data moving closer to the coast. Over the years, advances in satellite altimetry have been made which has resulted in a new form of remote sensing, known as coastal altimetry, which makes use of an algorithm designed to retrack waveforms that other processors such as X-TRACK do not do. This improves quality and quantity of coastal altimetry measurements through improved geophysical corrections and land effects, aiding in the recovery of more data near the coast that was previously disregarded as contaminated.

Along-track datasets are in the form of CGDR, which have been reprocessed by the UK National Oceanography Centre, using the ALES algorithm (Passaro et al., 2014). These measurements are distributed by the JPL Physical Oceanography DAAC and accessible from the COASTALT website (http://www.coastalt.eu). CGDR are copies of the original SGDR (20 Hz) — containing the entire global dataset. The L2 estimates of the geophysical parameters from a Brown re-tracker are retained, along with the addition of ALES variables related to the estimation of range, significant wave height (SWH) and backscatter (sigma-0) (refer to ALES Handbook. Accessible from http://www.coastalt.eu). The limitation of the dataset is that the approach taken by the NOC only regards data points within the coastal strip to be recovered. However, for this study the algorithm was applied up to 1000 km from the coastline. Note, that data were also included up to 5 km inland to account for coastline inaccuracies and variations.

Concerning the reprocessing algorithms it should be remembered that “ALES selects part of each returned echo and models it with a classic open ocean Brown functional form, by means of least square estimation whose convergence is found through the Nelder-Mead non-linear optimization technique. By avoiding echoes from bright targets along the trailing edge, it is capable of retrieving the majority of coastal waveform up to 2 to 3 km from the coasts. By adapting the estimation window to the significant wave height, it preserves the precision of the standard open ocean data. ALES is currently adapted for Envisat, Jason-1, -2 and AltiKa missions.” Full details are in Passaro et al. (2014).

SSH along-track datasets from Envisat and Jason-2 satellites were obtained from UK National Oceanography Centre. These datasets had already been reprocessed by the ALES algorithm. SSH data from Envisat was used for the Delagoa Bight and Jason-2 for the Durban region. It is important to note that Envisat operates on a 35-day repeat cycle and consists of 94 passes (refer to Envisat Handbook). This mission ran from 26 May 2002 to 26 September 2010. In

terms of Jason-2, data are available from 2008 till 2015 and operates on a 10-day repeat cycle consisting of 254 passes (refer to Jason-2 Handbook). The preferred dataset would liked to have been Jason-2 for use in the Delagoa Bight region because measurements are collected much more frequently than Envisat, which would have allowed us to catch the formation of the DBLE, unfortunately the tracks for Jason-2 were not located the right location for the eddy to be caught. Thus the reason for using Envisat.

Two approaches were used to achieve the outcomes of this study. The first was along-track SLA data, which provided a very good one-dimensional spatial sampling. In association with the first approach images derived from gridded products provided a synoptic view of the mesoscale features allowing for a better visualisation and understanding of eddy dynamics.

3.2.2 Computing SLA from ALES datasets

ALES datasets were used to compute the SLA product, which was used to compare to the original dataset and a low resolution dataset. This enabled the evaluation of whether the same features (*i.e.* the DBLE and DLE) were observed and if the same pattern was reflected across all three Hovmöller plots produced. This provided an indication of whether coastal altimetry is accurate and if it could be used to detect these features, and how well it can do this. The same method is used to compute SLA in both study regions, however variable names are defined differently for Jason-2 datasets (Refer to Appendix A.1). The following computational steps were taken to derive SLA:

Along-track data were analysed in MATLAB (v.2013a). Measurements were extracted using a code called read_Ales.m (by Lisa Ziegler), which allows the user to extract variables from the NOC server, compute SLA product, and inserting selected variables into one matrix.

The SLA measurement was calculated using *e.q.* 3.1. The inputs required to perform this calculation are the range, orbit, sea surface height anomaly (SSHA) correction, mean sea surface height (MSSH), and the reference ellipsoid height (see Appendix A.1 for variables required).

$$SLA = orbit - (range + ssha\_correction)mssh + \Delta\_h; \tag{3.1}$$

The following pieces of code were used to calculate the SSHA correction input variable in eq. 3.1— these corrections are applied to correct for the altimeter signal near the coast.

```
% This equation is used to calculate the sea surface height anomaly correction
ssha_correction = ionosphere + dry_troposphere + wet_troposphere +...
           + sea_state_bias + solid_earth_tide + ocean_tide +...
```

```
        + pole_tide + dynamic_atmosphere +...
        + inverted_barometer;
```

DTU10 Ocean wide mean ssh (MSSH) (relative to the Ellipsoid) (Andersen, 2010); was extracted from the DTU Space server accessibleviawww.space.dtu.dk. Data were extracted using the `read_mssh` function (created by P. Cipollini, NOC).

```
% Calculate the mean sea surface (mssh)
MSSH = read_mssh(lon,lat,'dtu10');
```

This ten year global MSSH along the track was then subtracted from the SSH for each cycle to obtain the SLA. It is important to note that Envisat and DTU10 MSSH model makes reference to different ellipsoids [3] (Envisat — WGS84 ellipsoid and DTU10 MSSH — Topex ellipsoid). To solve this problem and eliminate any bias, the reference ellipsoid was corrected to that of the satellite's reference ellipsoid. This was done by calculating the difference in height of both reference ellipsoids (`Δ_h`) using the `dh_ellips` function, allowing the switch from one ellipsoid to another.

```
% Calculating dh_ellips
Δ_h = dh_ellips(lat); % latitude being the area of focus
```

Delta_h was added to eq. 3.1 — only added to the equation when working with Envisat data. Jason-2 reference ellipsoid and DTU10 MSSH makes reference to the same ellipsoid.

3.2.2.1 Testing the suitability of CGDR on a regional scale

The data were filtered before plotting. This was done using a 3 standard deviation filter. Not only does the eliminate outliers, but also their adjoining neighbors that often contain erroneous values. Hovmöller plots of SLA were then produced for each Case Study region. This enabled a comprehensive visualization of the Coastal Altimetry data along side hovmöller plots 1 Hz RADS (Radar Altimetry) (obtained from http://rads.tudelft.nl/rads/rads.shtml) and the original Envisat SGDR. These plots were used to validate, identify eddy propagation and the estimate the number of occurrences.

A time series of SLA at various latitudinal points were taken along the track (Fig. 3.3(a) and 3.3(b)). This was done by extracting SLA data points from ALES, SGDR, RADS and AVISO gridded product at the same latitude point over time, and plotting them on the same plot.

[3] Reference ellipsoid — a mathematically defined surface that approximates the geoid, the truer figure of the Earth. Used as a preferred surface on which geodetic network computations are performed and point coordinates such as longitude, latitude and elevation are defined

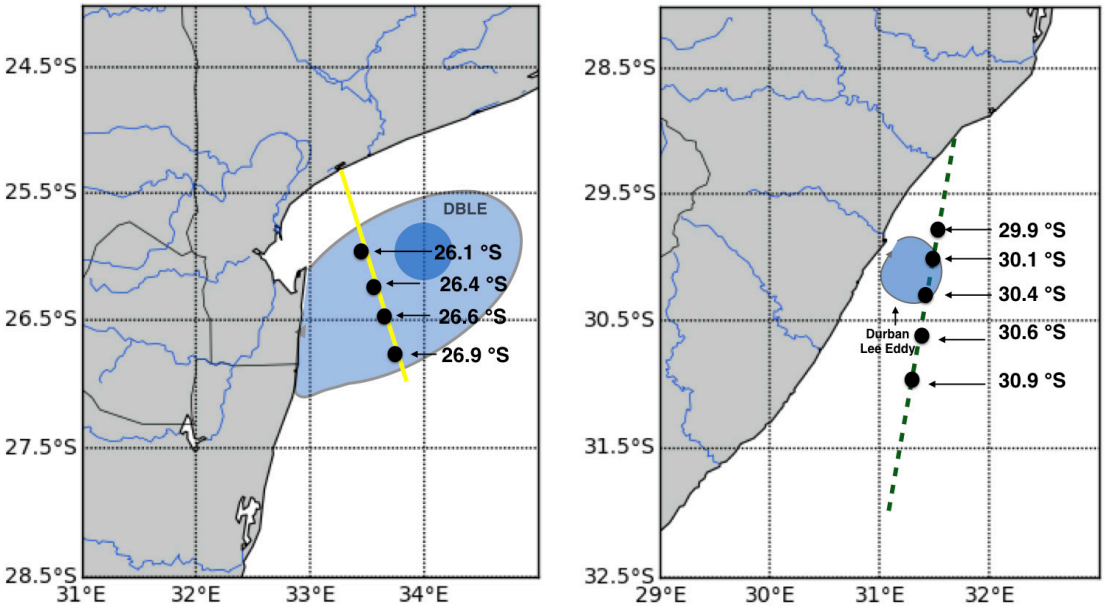

(a) (b)

Figure 3.3: Diagram showing the latitudinal positioning of the point profiles created for (a) DBLE and (b) DLE of SLA.

This comparison between the gridded product and along-track datasets, aimed at (1) identifying how well each dataset(s) performed in accurately reflecting SLA patterns and eddy features and (2) providing confidence in the AVISO gridded product. Identified features were validated using the following case studies: of (Lamont et al., 2010; Cossa et al., 2016) for the Delagoa Bight and (Guastella and Roberts, 2016) for the Durban/ Natal Bight. To get an idea of eddy formation and flow within each region, a random year was selected and composites of SLA images were computed. This was also done to verify the coastal altimetry product for the Durban eddy as RADS data were not available. At the same time the gridded product was also verified in terms of accuracy.

3.3 Linking negative SLA and chl-*a* events

Gridded SLA and chl-*a* datasets were used to investigate the link between the SLA in the Bight and chl-*a* levels. The results will also allow for the accuracy and confidence of the gridded product to be assessed. The following datasets were used:

1. 4 km resolution ESA OCI-CCI MERGED-8-DAY DAILY gridded product using the latest version v3.1 was used (obtained from http://www.esa-oceancolour-cci.org.

2. 1/4 degree optimally interpolated DT all-sat-merged daily Global Ocean Gridded SSALTO/DUACS Sea Surface Height L4 product, (obtained from http://marine.copernicus.eu/).

To compare between SLA and chl-*a* two regions of interest — the centre of the eddy (A), and a reference region outside of the eddy(boxes 1–3). Chl-*a* and SLA data points were extracted within the specified latitude and longitude box. For the DBLE, measurements were extracted from a 1/2°×1/2°boxes for both domains (Fig. 3.4(a)) and for the DLE data were limited by a 1/4°×1/4°block for both domains (Fig. 3.4(b)). Box A takes into consideration the size of the eddy and tries to isolate as much of each center of the eddies as possible. Boxes 1–3 are taken further from the coast, seeing as data become more unreliable closer to the coast line. The reason for having three sampling reference boxes in different places are for validating whether the link between the eddies and chl-*a* are true.

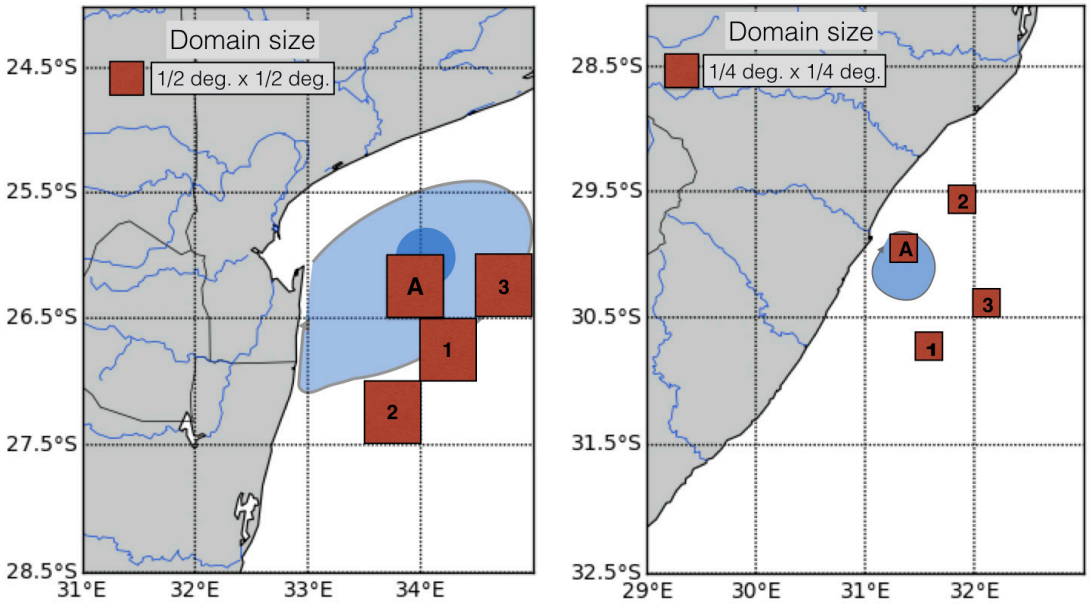

(a) (b)

Figure 3.4: Diagram showing domain 1 and 2 from which SLA and chl-*a* data are extract from for (a) the Delagoa Bight and (b) Durban region.

The following steps were taken to discern the association between SLA and chl-*a* for the DBLE and DLE:

The first step was to extract chl-*a* and SLA data from boxes A and reference SLA data outside of the eddy from boxes 1–3. Data extraction was taken during 2002–2010 for the DBLE and from 2008–2016 for the DLE. An 8-day daily mean of SLA was then computed to match the availability of chl-*a* data that had been averaged over 8 days. This was done by creating an index of time for chl-*a*, which was then used as an index for SLA. Thus, extracting those data only at times that matched chl-*a*.

SLA was linearly interpolated onto the same time frame as chl-*a* as time steps appeared to be different. The seasonal signal was removed. The detrended data were used to compile a

mean for each box at each time step. The mean difference value was obtained by subtracting chl-*a* anD SLA in box A (centre of eddy) by each reference box (outside of eddy) for SLA. It was noted that the data were not centered around zero when plotted. This was solved by standardising the data before calculating the mean difference between box A and the reference box — taking the mean of the detrended data and subtracting it from each value.

To see if there was a potential relationship between SLA and chl-*a* scatter plots were first made. Data was noted to be fairly normally distributed. A linear regression model was fitted to the data. A linear model was used to predict the value of an outcome variable which in this case was chl-*a* based on one or more input predictor variables which were the three reference SLA boxes. To see how SLA from different regions influence chl-*a* within the eddy. Before fitting a linear model, a Pearson's product-moment correlation test was done to determine the level of linear dependence between two the variables and to investigate the relationships that may exist between variables. The linear model tests the hypothesis which states that when the cyclonic eddy is present there will be an increases in chl-*a*. Scatter plots were used to provide a general illustration of the relationship between the two variables and then fitting a linear regression line. The descriptive statistical outputs of the linear model were recorded and tabulated.

CHAPTER 4

RESULTS

This chapter is structured into two main sections: Section 4.1 — assesses the application of coastal altimetry in the Delagoa Bight and inshore region off Durban, at the same time using along-track data to provide confidence in the AVISO gridded data. The SLA results presented are mainly based on the analysis of Hovmöller plots and time series plots of SLA taken at specific latitudes. These slice profiles were also used to assess the reliability and accuracy of the AVISO gridded to produce the same trends as observed in the along-track dataset.

Section 4.2 — two tests were conducted to gain a much stronger understanding of the relationship between SLA and chl-*a*. These results are based on the linear model outputs of mean difference chl-*a* and scatter plots. From superimposed line plots (in Appendix A) it was noticed that not all events matched. To show this, examples of two pairs of matching events and mismatch of events selected at random are provided. What the cause of this mismatch is remains unanswered. This gives a visual idea of when the occurrence of an event and the flow within the region actually coincides with one another. For brevity, SLA maps highlighting the behaviour of the Delagoa Bight and Durban lee eddy have been put into Appendices A.6–A.15.

4.1 Application of coastal altimetry: validation

Using satellite altimetry to study mesoscale features in coastal regions is often noted to be unreliable. A high resolution coastal altimetry product used in this study is retracked by ALES

(designed to increase data retrieval performance in nearshore environments). The performance of this product in recovering more data in the coastal region and its ability to properly resolve the DBLE and DLE are tested. Low resolution along-track RADS and AVISO gridded products are used for comparison and validation. The following results were obtained from analysing SLA in both the Delagoa Bight and Durban region.

4.1.1 *Case Study 1: Delagoa Bight Lee Eddy*

Hovmöller plots were produced to provide a visual representation of SLA along the track in space and time, in order to test the products ability to sufficiently resolve the DBLE. Plots shown in Figure 4.1 indicate a consistency in the SLA pattern obtained from ALES and RADS along-track data over time. This indicates a very clear improvement in spatial resolution and coverage between ALES and RADS. There is seem to be very little discrepences between ALES and SGDR data (Figure 4.3). ALES seem to recover more detail than RADS closer to the coast at 25°S (Fig. 4.1). Better altimetry data are recovered nearshore compared to the standard 1 Hz RADS product. The lower SLAs indicate frequent formation of cyclonic eddies in the bight. The DBLE, which is said to form at 26.4°S, 34°E, is rarely found at the point of origin (reason for this result could be due to infrequent sampling by satellite), but found moving along the track at times spanning the entire bight (Fig. 4.1). Observations show another cyclonic eddy besides the DBLE present in the bight. From the Hovmöller plot the 'semi-fixed' DBLE appeared a total of 12 times over the 9-year period.

The SLA images from 2008 show a substantial cyclone moving into the bight on 1 January–17 January directly from east, which then slips southwards about midway on the 25 January–10 February and does not move past the 26°S, 34°E (DBLE point of origin, which is indicated by the blue dot) (Appendix A.6). This is seen in Figure 4.2, the only date available that best coincides with this observation by the altimeter for this period is on the 20 January (cycle 65), which catches the eddy when it is midway (26.5°S) and moving southwards. Another deep cyclonic eddy similarly moves into the bight during 18 February–29 March (Appendix A.6). Throughout April (Appendix A.7), a cyclone is observed to evolve in the northeast part of the bight. This cyclone moves diagonally across the bight in a southwesterly direction and reaches a little closer into the bight. A significant cyclone is observed during June–July, coming from the Mozambique Channel, which moves diagonally across the channel (Appendices A.7 and A.8). This is not resolved in the altimeter field shown in Figure 3.1. However, on 8 June (cycle 69) a cyclonic eddy appears to pass over the 26°S position and on 13 July (cycle 70) it passes to the southwest of the bight. These signals are not in the gridded product (Fig. A.5(a) and A.5(b)). A smaller-amplitude, less intense cyclone very similar to the one observed in April 2008, moves over the DBLE's known point of origin in the bight, at 26°S (Appendix A.8(a)–A.8(d)). The period from October–November sees an anticyclonic eddy move

diagonally through the bight. This turns out to be a positive part of an eddy dipole. This is observed on the 26 October (cycle 73) in Figure 3.1 at the south end of the bight, identified by the light blue colour indicating the depth to be shallow. Summarising these observations made from the 2008 SLA images, indicate that the cyclonic eddy, which has been reported on from *in situ* observations (Lutjeharms and Da Silva, 1988; Lamont et al., 2010), has two origins: (1) cyclones that come from offshore, either from the Mozambique Channel or Madagascar, and (2) cyclones that are spun up in the bight. A common trait is that they all move in a southwesterly direction.

Times, series of SLA at specific latitudes for the along-track and gridded dataset are plotted to better identify the DBLE cyclonic eddy and evaluate trends in SLA over time between datasets. The fact that the data are so similar provides some confidence in the gridded product. Results from Figure 4.3 shows RADS matching more with the ALES dataset than the gridded product, which seems to be inconsistent with the patterns of the along-track data. The ALES dataset appears to be less noisy than the gridded product. The SLA patterns observed are more strongly represented by the along-track data than the gridded product. The intensity and frequency of cyclonic eddies in Figure 4.3 at the 26.1°S from 2008–2010 are shown to decrease as well as become smaller in size. Lamont et al. (2010) and Cossa et al. (2016) identify the DBLE's point of origin to be at 26.4°S, 34°E. Results from the latitude point profile at 26.4°S (Fig. 4.3 in the DBLE center, shows the spin up of the cyclonic eddy at depths between 0 and 2 m. Lamont et al. (2010) validate the identification of the DBLE on 30 May 2004 in Figure 3.1, which was observed to be present between 8 May and 20 June 2004 by Lamont et al. (2010). There seems to be other low SSH occurring constantly throughout. Dipole eddies appear frequently passing into the bight; these eddies are represented by large spikes that are equal to or less than -2 m and more than 2 m.

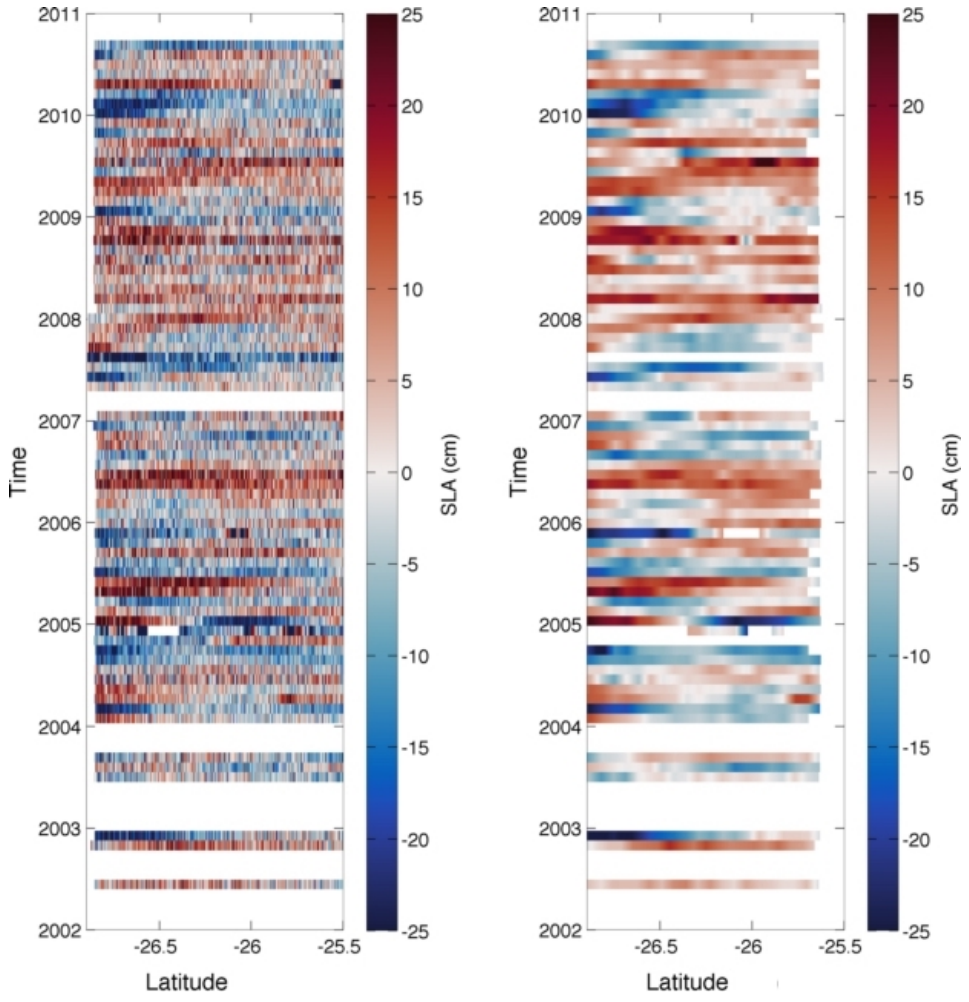

Figure 4.1: Hovmöller plots depict time versus latitude of SLA extracted from high resolution along-track data processed by Envisat every 35 days for (a) retracked ALES (18 Hz) and (b) RADS (1 Hz) data. Showing clear pattern uniformity across both plots for the Delagoa Bight over a period of 9 years from 2002–2010.

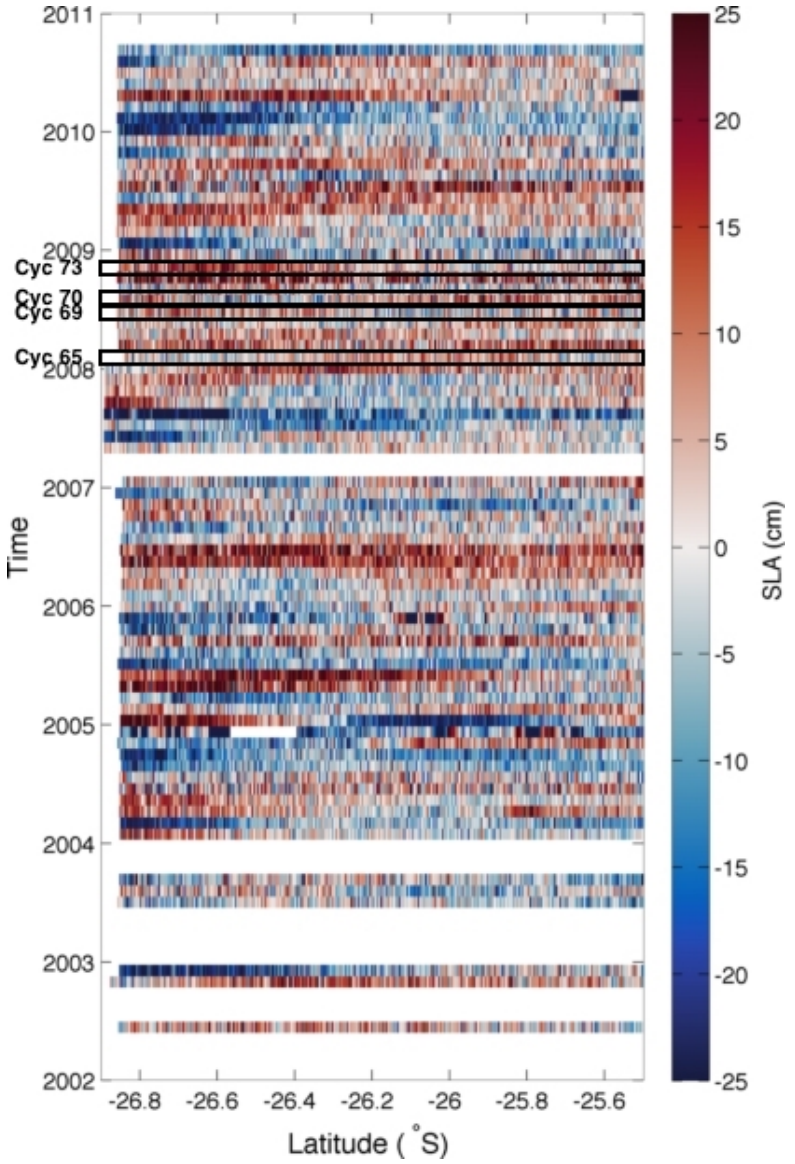

Figure 4.2: Time-Latitude digram of SLA (ALES) within the Delagoa Bight. The black boxes highlight those cycles indentifies in 2008 amd described in the text (refer to Section 4.1.1).

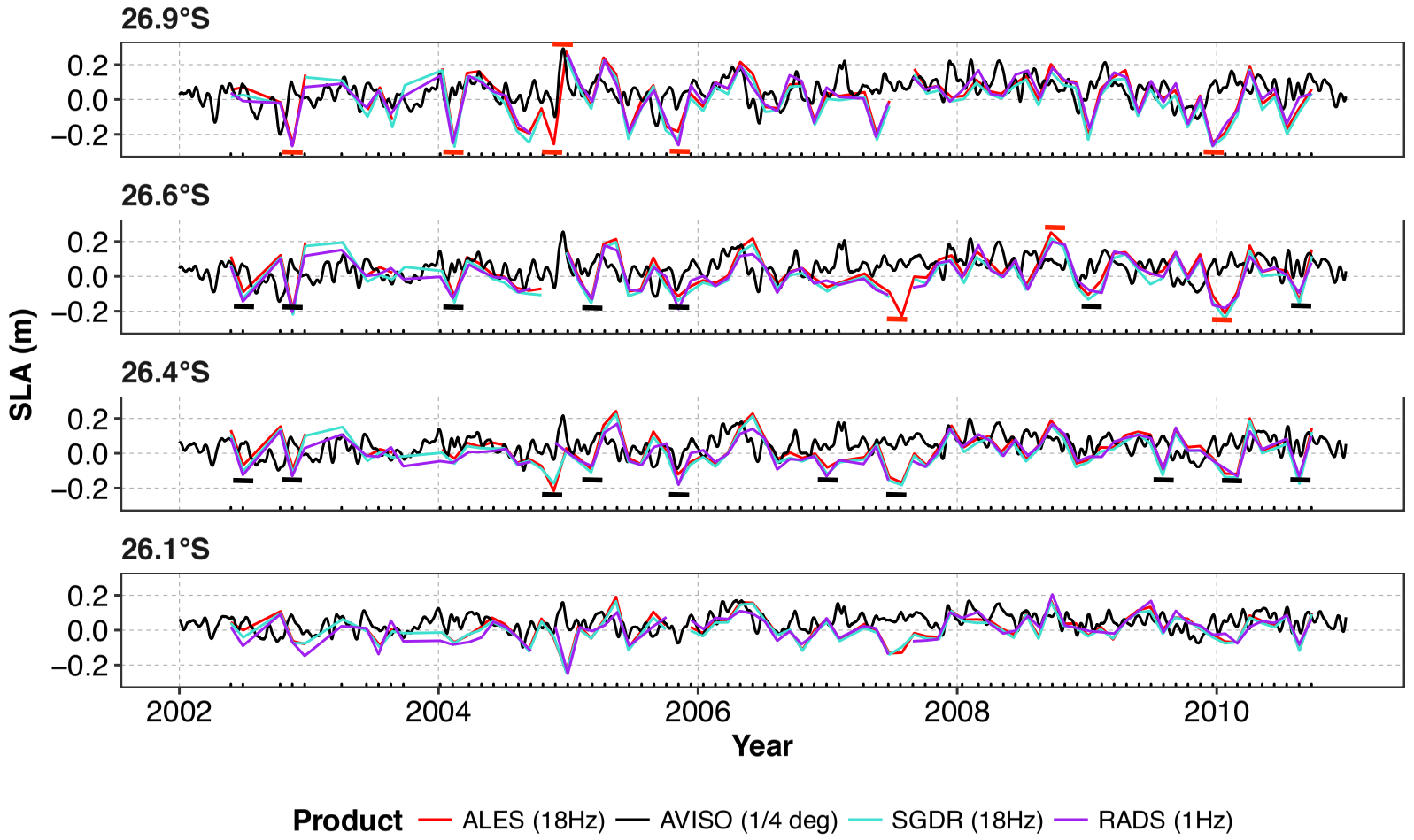

Figure 4.3: Along-track point profiles at specific latitudes for the DBLE show the computed SLA from ALES (18 Hz), SGDR (18 Hz), RADS (1 Hz) along-track and daily AVISO (1/4 degree) gridded datasets over time. Dots indicate where ALES data are available. Red solid bars indicate intense anti-cyclonic and cyclonic eddies (dipoles) and black solid bars indicate the presence of the DBLE. Black bars only inserted at latitudes where the eddy originates.

4.1.2 *Case Study 2: Durban Lee Eddy*

Hovmöller plots were produced to provide a visual representation of SLA along the track in space and time, in an effort to test the products ability to catch the Durban lee Eddy. Observations made from these plots shown in Figure 4.1 also indicate a consistency in the SLA pattern obtained from ALES and RADS along-track data over time, as shown in the DBLE Hovmöller plots. ALES data seem to recover more data points and are less noisy than the SGDR data especially at 29.9°S (Fig. 4.1 and 4.5). Near the coast, between 29.6°S–31°S, one observes two cyclonic eddies forming. The SLA values indicate the existence of small-amplitude at depths between 0 m and -0.15 m, and slightly stronger cyclonic eddies at depths between -0.15 m and greater than -2 m, forming in the Natal Bight off Durban. Due to it being difficult to distinguish between the DLE, break-away eddy, and Natal pulse, the SLA images from 2008 were used. The SLA images reveal a semi-permanent presence within the Natal Bight and further offshore of Durban. There appears to be frequent occurrences of stronger negative SLAs, suggesting that it could be the Natal Pulses passing by, with the smaller-amplitude negative SLA values indicating the formation and breakaway of the Durban lee eddy at 29.81°S, which has also been identified as the point of origin by Guastella and Roberts (2016).

The SLA images from 2008 (see Appendices A.10, A.11, A.12, A.13, A.14, A.15) show the DLE to be present 14 times in that year within the Natal Bight (lasting up to 8 days) before breaking away; these breakaway eddies were observed four out of those 14 occurrences (9 January, 6 April, 16 November, and 26 December). The Natal Pulses can be seen and were identified 12 times during the year at around 31.5°S, 30°E, before moving south. The most prominent features are the Natal Pulse and Durban eddy, as well as large anticyclonic eddies passing by. Focusing on the latitude slice profile at 30.1°S (Fig. 4.5, see Fig. 3.3(b) for latitude position), two types of cyclonic eddies: small-amplitude eddies and slight more intense eddies. One reaching an amplitude of approximately - 0.25 m, (Natal Pulse) and the rest between 0– -0.2 m (DLE). Guastella and Roberts (2016) validates the identification of the anomaly patterns of Figure 4.4 between Durban and Sezela (30°S–32°S).

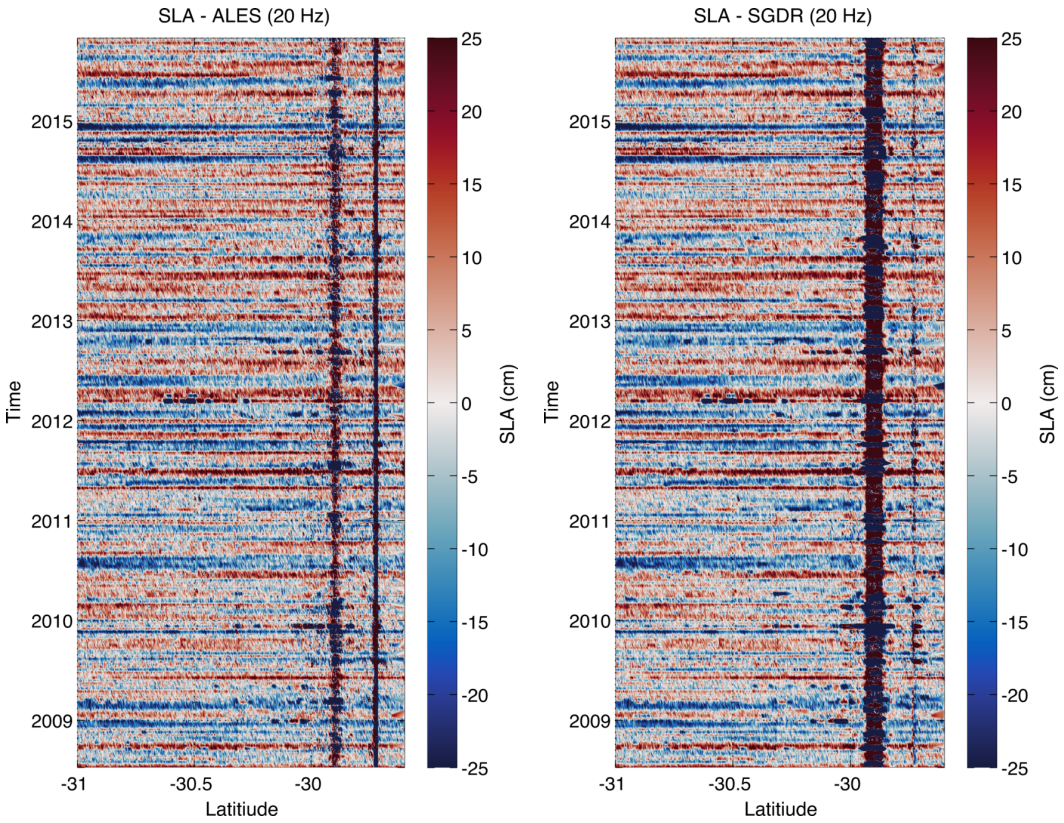

Figure 4.4: Hovmöller plots depict time versus latitude of SLA extracted from high resolution along-track data processed by Jason-2 every ten days for (a) retracked ALES data and (b) the original SGDR. The plots show clear uniform patterns accross the the Natal Bight and offshore of Durban over a period of 8 years from 2008–2015. The reason for the vertical stripes is suggested to be as a result of the white noise/backscatter caused by the topography at the coastline of Durban as the satellite moves along that point.

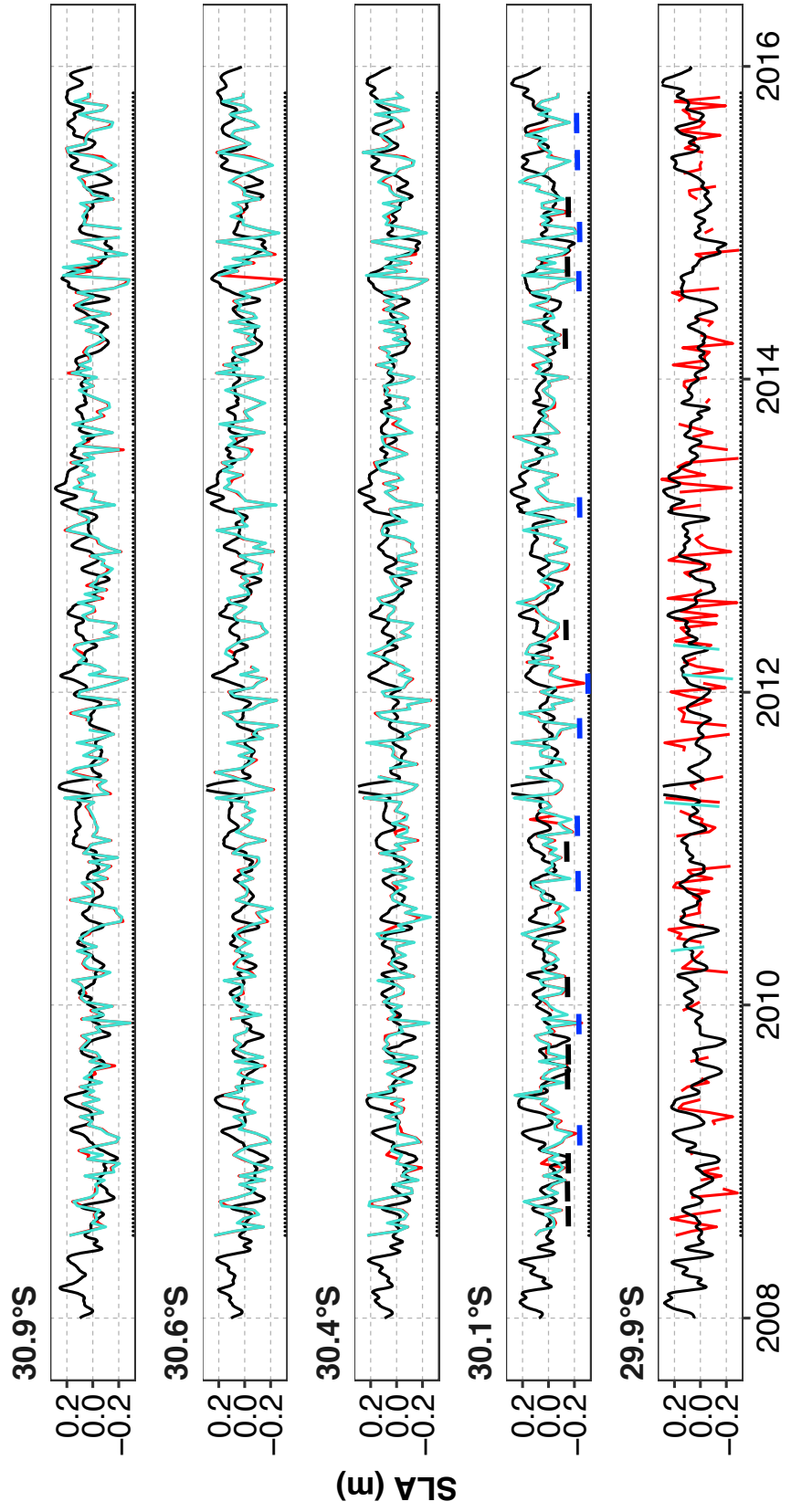

Figure 4.5: Along-track slice profiles at specific latitudes for the DLE show the computed SLA from ALES (20 Hz), SGDR (20 Hz), and AVISO (1/4 degree) gridded product. Data from the RADS database are not available due to data being flagged and thus rejected near the coast. Dots indicate where ALES data are available. Black solid bars indicate the presence of DLE. Black bars only inserted at latitudes where the eddy originates. The blue solid lines indicate the presence of the Natal Pulse.

4.2 Relationship between SLA of eddy and chl-*a*

Remotely sensed ocean colour data were used because they provide more comprehensive coverage to identify the possible relationship between the eddy and chl-*a* for both Case studies. A linear model was fitted to the data to discern the relationship that may exist between the eddy and chl-*a*. Scatters plots were constructed to display this correlation between variables. The mean difference was calculated between the chl-*a* in the center and outside of the eddy and SLA in the center and outside of the eddy. Three reference boxes were taken outside of the eddy to see the influence it had on the chl-*a* within the eddy. Results from the correlation indicated that an inverse relationship, whereby a decrease in SLA results in an increase in chl-*a*; in these cases, stronger correlations between chl-*a* and SLA tend towards -1. However, this correlation was a weak correlation. The results from the linear regression indicate that relationship between chl-*a* in the center of the eddy and SLA outside of the eddy in box 2 show the strongest association and is more linear than box 1 and 3 for both the DBLE (R^2 = 0.1637) shown in Figure 4.6(b), with an estimate of -0.304 mg Chl-*a*/m^3 (Table 4.1) and DLE (R^2 = 0.1375) shown in Figure 4.7(b), with an estimate of -1.661 mg Chl-*a*/m^3 (Table 4.1). The scatter plots (Fig. 4.6 and 4.7) show the eddies' effects being clear across all three boxes, as there is a relationship between the two SLA data sets and chl-*a* within the eddy (*i.e.* in the presence of a cyclonic eddy there is an increase in chl-*a*). However, it was also clear from those figures that not all the events match, as identified by the grey dots which indicate no overlap between SLA and chl-*a*. From the chl-*a* images chosen at random (to avoid any bias) for the Delagoa Bight, the mismatch of events is observed in Figures 4.10 and 4.11, and in others the opposite was observed (Fig. 4.8 and 4.9). For the DLE the same was observed where there was this mismatch in SLA and chl-*a* events (Fig. 4.14 and 4.15), while at other times an good match (Fig. 4.12 and 4.13). These images have been identified in Appendices A.3(a) and A.4(a). Estimates of chl-*a* in Table 4.1 seem to be relatively similar and higher, associated with the DBLE compared to the DLE where chl-*a* estimates are lower and extremely variable. It appears that these eddies might not be the only contributors to primary production near the coast due to the correlations being so small.

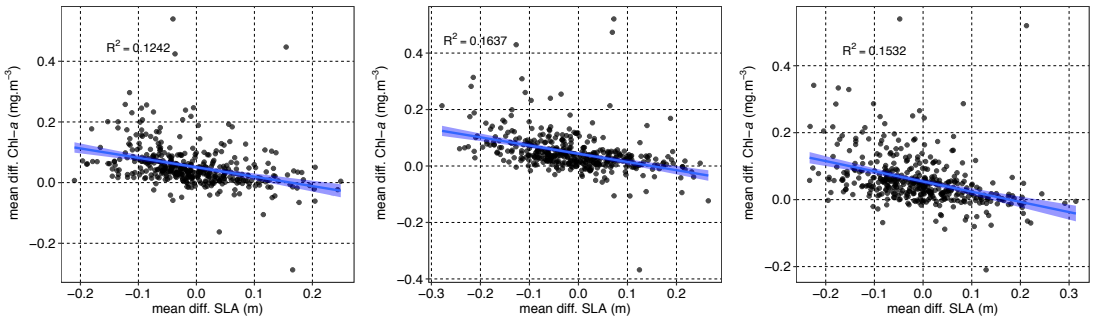

(a) (b) (c)

Figure 4.6: Regression plots showing the relationship between chl-*a* and SLA in the eddy center (A) and SLA outside of the eddy which makes reference to (a) box 1, (b) box 2 and (c) box 3 (Fig. 3.4(a)) in the Delagoa Bight. A linear regression line is fitted to the data (blue line) ± the standard error (blue shading). Black dots indicate overlapping of chl-*a* and SLA points. OC-CCIchl-*a* and AVISO SLA products were used in this analysis.

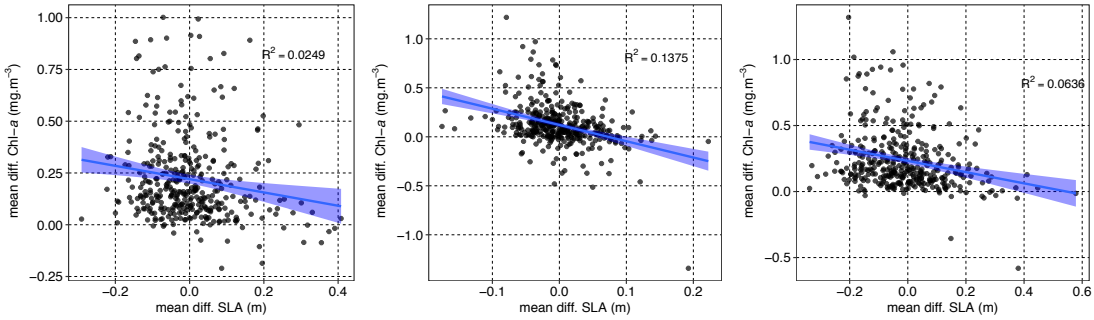

(a) (b) (c)

Figure 4.7: Regression plots showing the relationship between chl-*a* and SLA in the eddy center (A) and SLA outside of the eddy which makes reference to (a) box 1, (b) box 2 and (c) box 3 (Fig. 3.4(b)) in the Durban region. A linear regression line is fitted to the data (blue line) ± the standard error (blue shading). Black dots indicate overlapping of chl-*a* and SLA points. OC-CCIchl-*a* and AVISO SLA products were used in this analysis.

Table 4.1: Linear model results summary for the DBLE and DLE: outputs for the mean differences of chl-*a* and SLA between the eddy centre (A) and SLA outside of the eddy (boxes 1–3) (Fig. 3.4(a) and 3.4(b)). DF values are not all equal as obs. were deleted due to missingness.

	Chl-*a* vs SLA	**adj. R^2**	**estimate ($mg.m^3/m$)**	**SE**	**DF**	***p*-value**
DBLE	1	0.1242	-0.310	0.04	408	$<0.001^{***}$
	2	0.1637	-0.291	0.032	408	$<0.001^{***}$
	3	0.1532	-0.304	0.035	408	$<0.001^{***}$
DLE	1	0.0249	-0.321	0.101	355	0.0016^{**}
	2	0.1375	-1.661	0.217	359	$<0.001^{***}$
	3	0.0636	-0.0424	0.084	357	$<0.001^{***}$

Signif. codes: 0^{***} 0.001^{**}

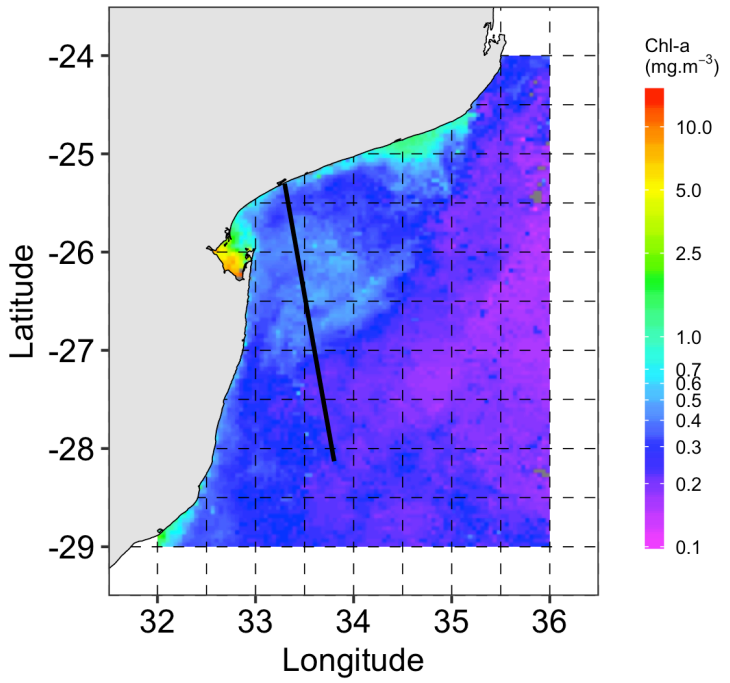

(a)

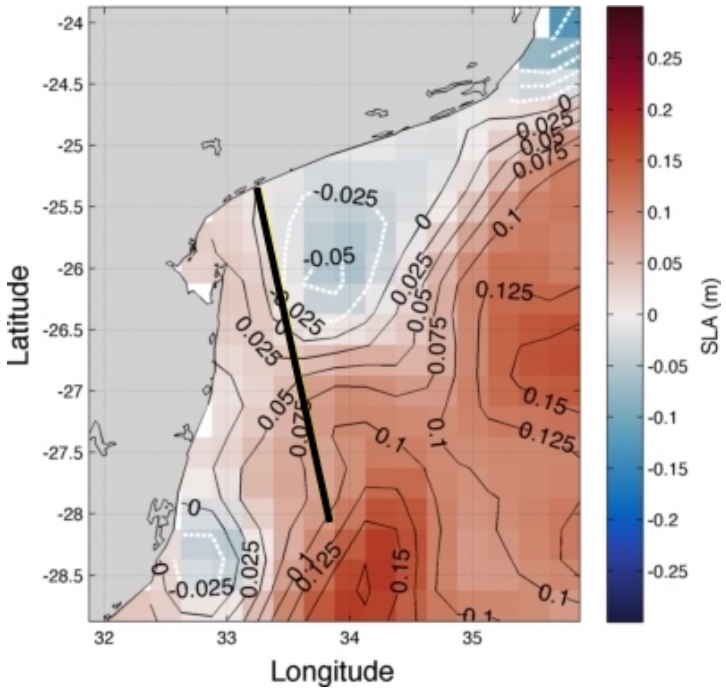

(b)

Figure 4.8: Delagoa Bight: Examples of matching SLA and chl-*a* events on 26 June, 2002. Solid black line indicates the Envisat track (0371) analysed in this study.

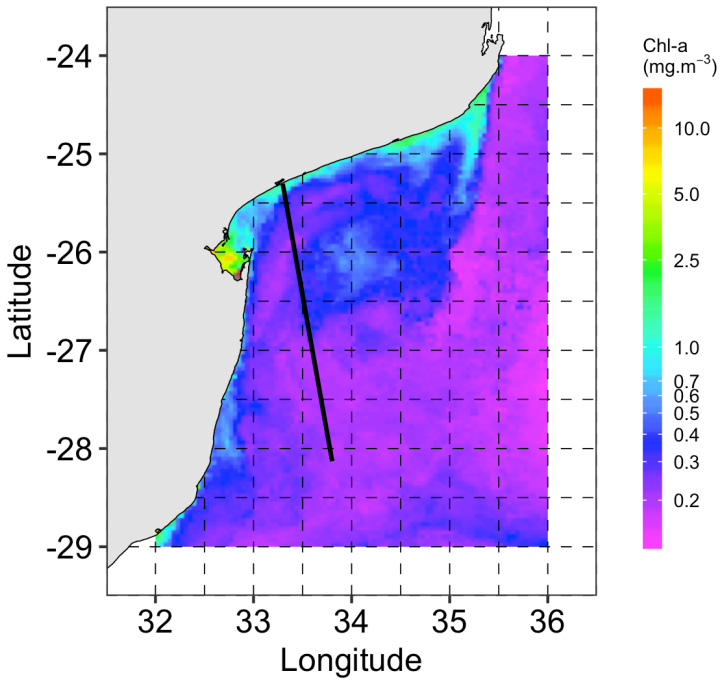

(a)

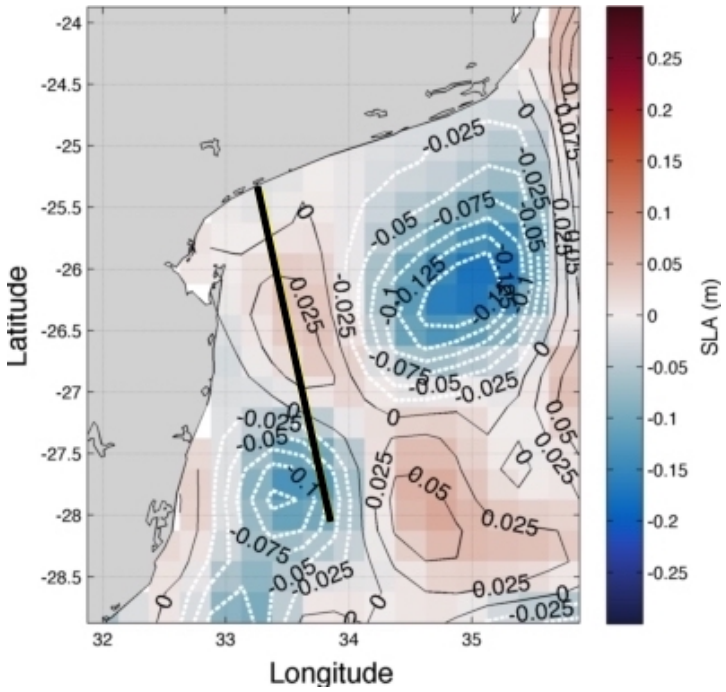

(b)

Figure 4.9: Delagoa Bight: Examples of matching SLA and chl-*a* events on 29 August, 2002. Solid black line indicates the Envisat track (0371) analysed in this study. Grey patches indicate where no data are available.

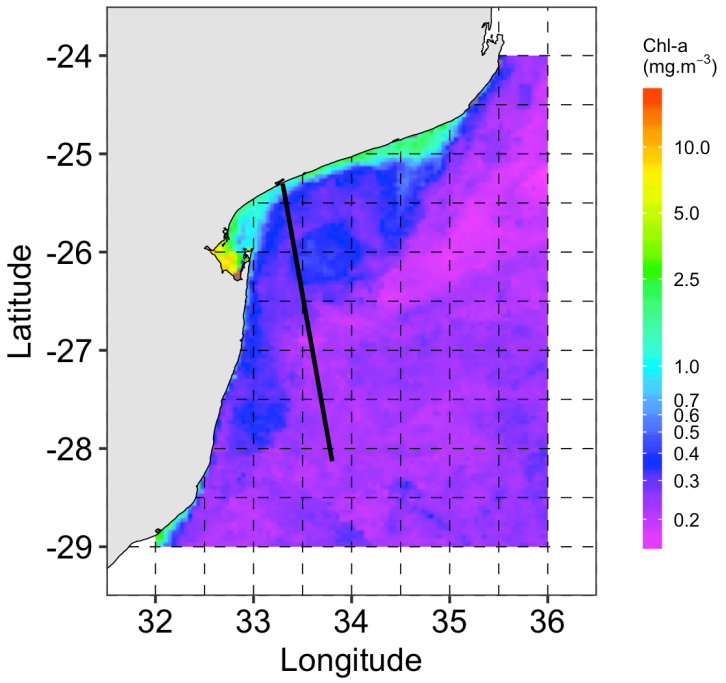

(a)

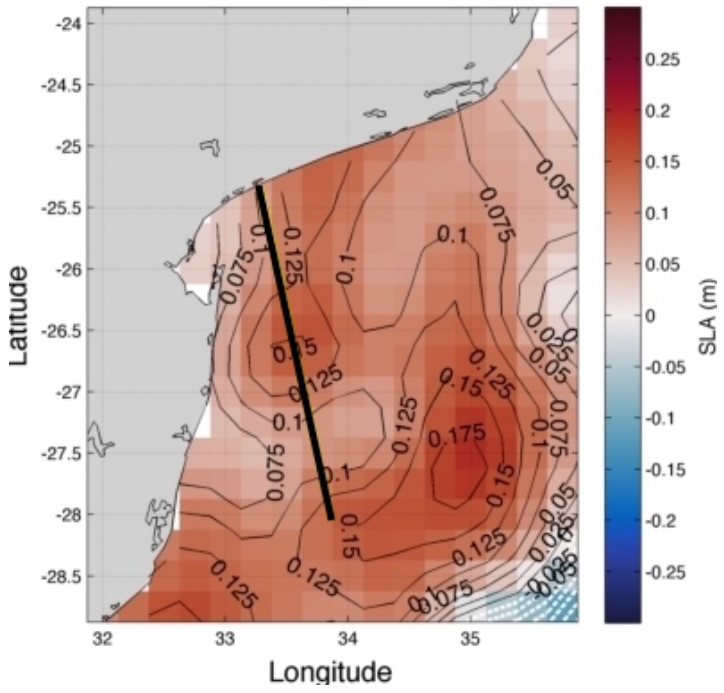

(b)

Figure 4.10: Delagoa Bight: Examples of mismatching SLA and chl-*a* events on 21 September, 2008. Solid black line indicates the Envisat track (0371) analysed in this study

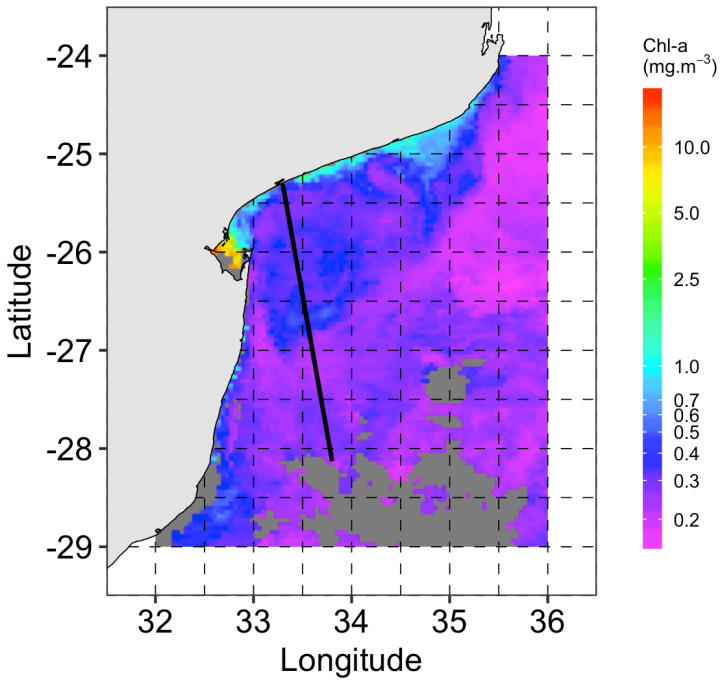

(a)

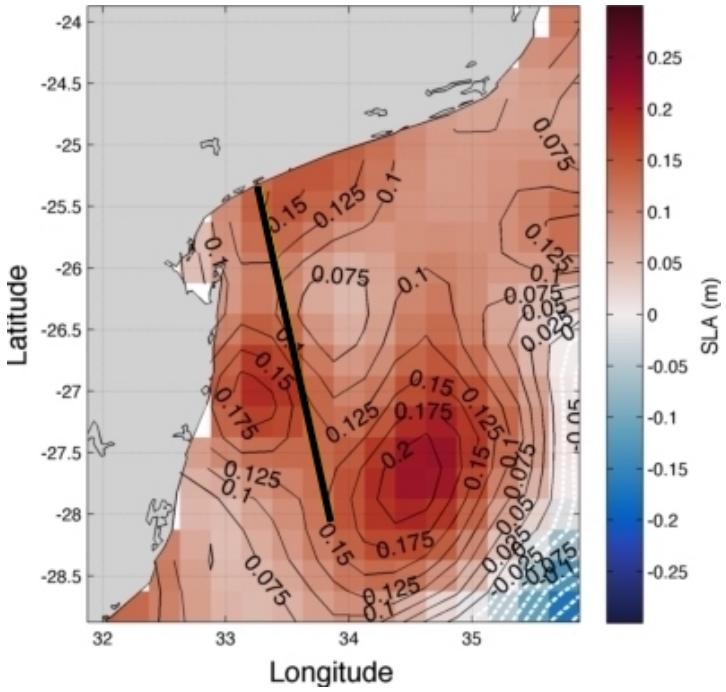

(b)

Figure 4.11: Delagoa Bight: Examples of mismatching SLA and chl-*a* events on 29 September, 2008. Solid black line indicates the Envisat track (0371) analysed in this study. Grey patches indicate where no data are available.

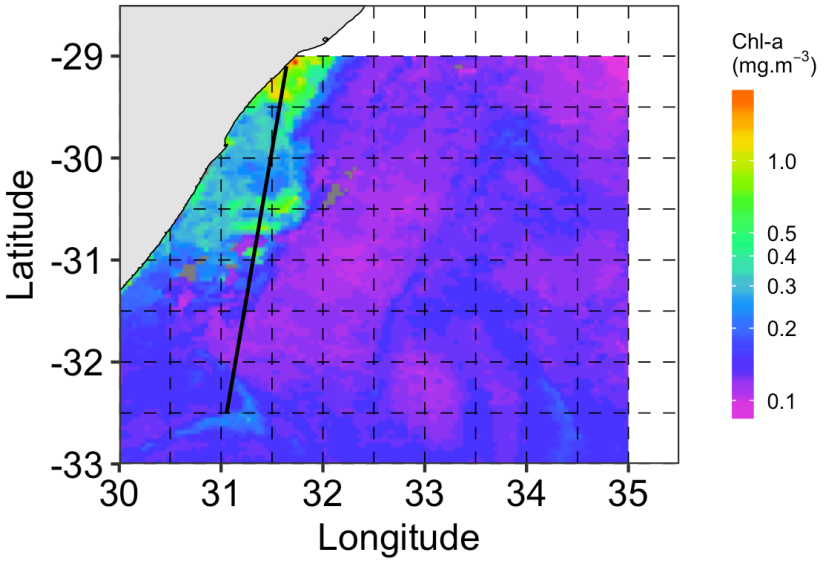

(a)

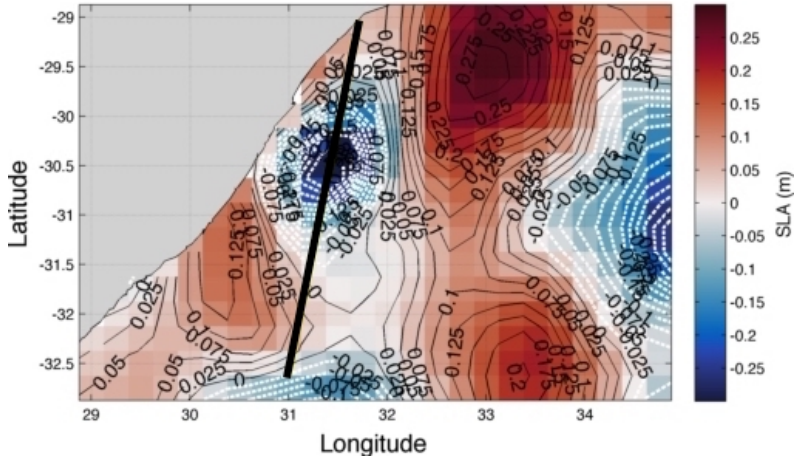

(b)

Figure 4.12: Natal Bight: Examples of matching SLA and chl-*a* events on 3 December, 2010. Solid black line indicates the Jason-2 track (0005) analysed in this study.

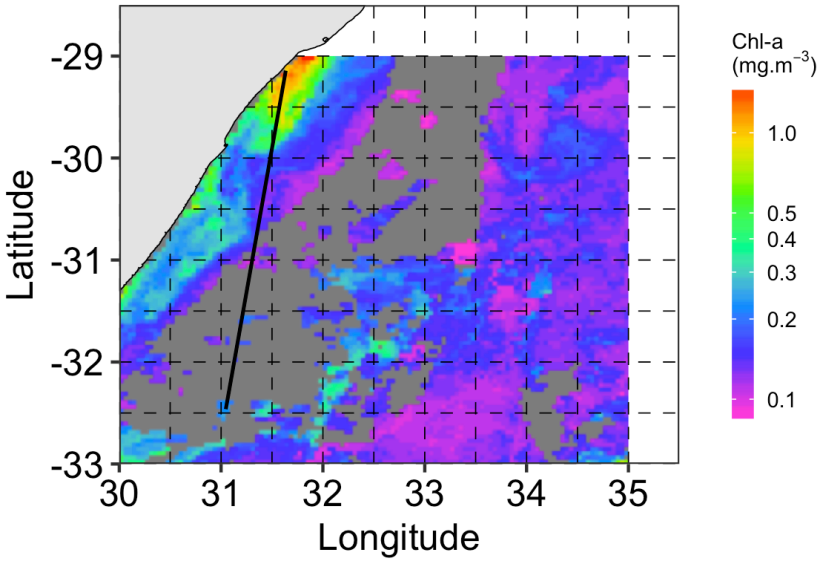

(a)

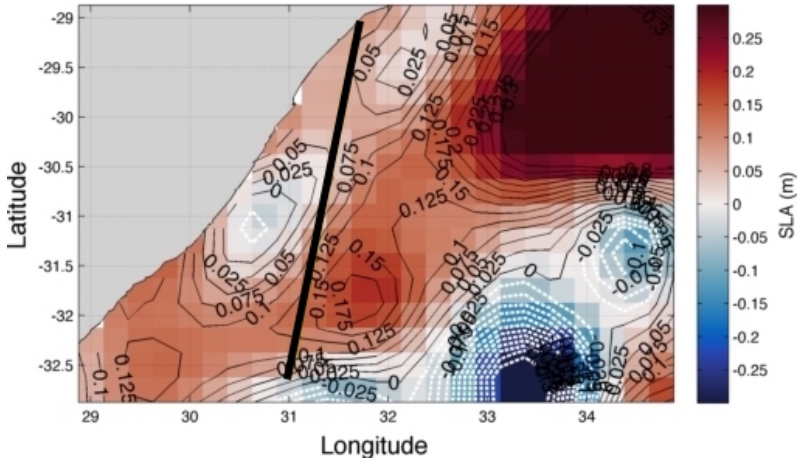

(b)

Figure 4.13: Natal Bight: Examples of matching SLA and chl-*a* events on 25 November, 2015. Solid black line indicates the Jason-2 track (0005) analysed in this study. Grey patches indicate where no data are available.

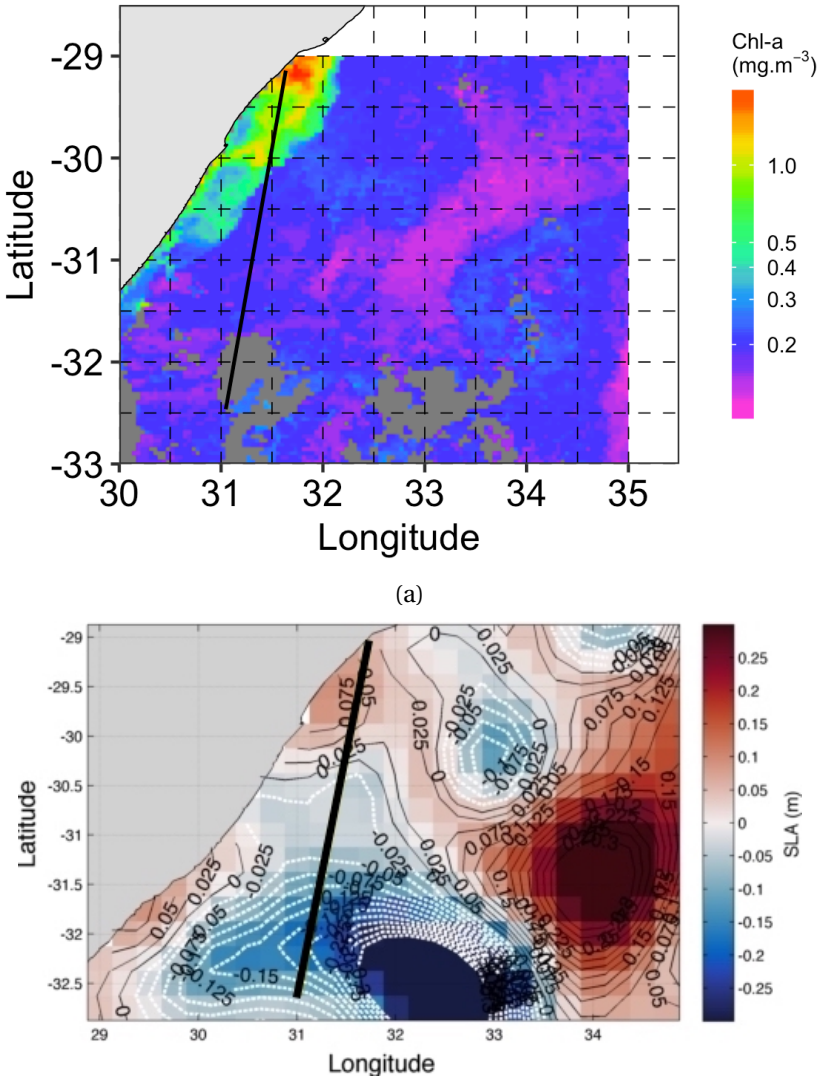

(a)

(b)

Figure 4.14: Natal Bight: Examples of mismatching SLA and chl-*a* events on 8 May, 2012. Solid black line indicates the Jason-2 track (0005) analysed in this study. Grey patches indicate where no data are available.

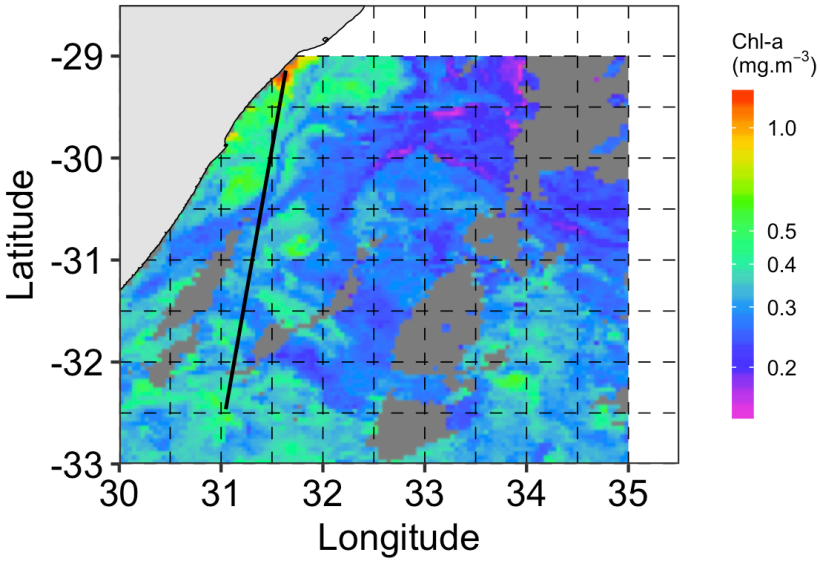

(a)

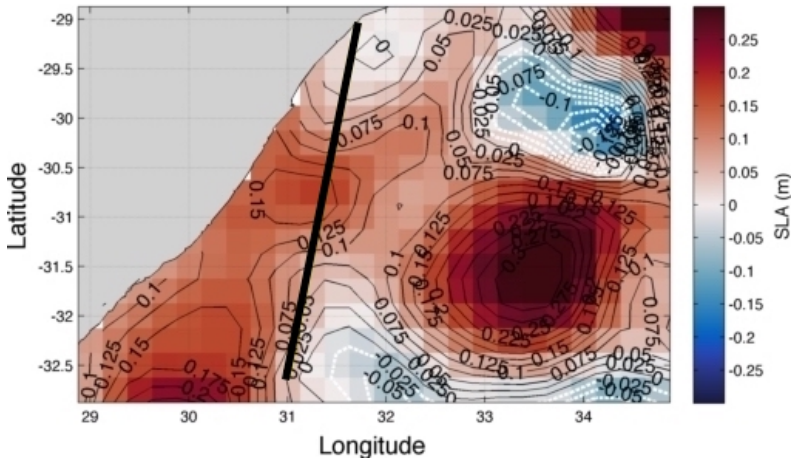

(b)

Figure 4.15: Natal Bight: Examples of mismatching SLA and chl-*a* events on 12 September, 2015. Solid black line indicates the Jason-2 track (0005) analysed in this study. Grey patches indicate where no data are available.

CHAPTER 5

DISCUSSION

5.1 Application of coastal altimetry

Satellite altimetry has been regarded as one of the most successful applications of remote sensing for Earth science and climate studies. In particular, the use of satellite altimetry in biophysical studies, has been demonstrated to be a powerful tool to study the role of mesoscale eddies in enhancing primary production (Fu et al., 2010). Whilst satellite altimetry is indispensable as a reliable measurement of SSH in the open ocean, its accuracy has been questioned near the coastline. This study has made use of coastal altimetry, which has promised the improved retrieval of data near the coast by applying a specialised retracking algorithm (ALES) and improved corrections. So far, the practicality of using coastal altimetry has been highlighted, but the successful use of this application in detecting the DBLE and DLE in my study has not been discussed.

The results from this study indicate increased confidence in the coastal altimetry product. The Hovmöller plots for both Envisat track 0371 in the Delagoa Bight, and Jason-2 track 0005 for the Natal Bight and further south of Durban provides an overall visualisation of the SLA product computed using the ALES dataset alongside the comparative 1 Hz RADS dataset. The overall trend of the data is consistent with that of both the SGDR and RADS along-track datasets, confirming and providing confidence in the ALES products. ALES data appear less noisy in comparison to the SGDR, RADS, and AVISO gridded product. Passaro et al. (2015a) support these findings, illustrating the suitability of the application of coastal altimetry in the North Sea/Baltic Sea transition area. Their findings indicate that the ALES dataset, using geophysical corrections, is able to accurately estimate the annual cycle of SSH up to

the coast. Only ALES-based amplitude estimates of the annual cycle are in agreement with tide gauges within 1 cm in every sub-basin. Secondly, the ALES product is able to detect a slope in the amplitude that follows the bathymetry of the Skagerrak Sea and corresponds to the narrow Norwegian coastal current, which is not well represented in the Sea Level Climate Change Initiative (SL cci) estimates. In Appendix A.1, a comparison between ALES and Envisat SL cci datasets is shown by Passaro et al. (2015a), indicating that ALES is able to increase the quantity of 1 Hz along-track data while improving the quality. In order to be consistent, the standard deviation of the sea surface height anomaly is expected to vary smoothly with no abrupt changes between consecutive 1 Hz points. This supports the observations made showing that ALES is able to successfully retrieve more signal than its comparative along-track dataset (RADS). Passaro et al. (2014), also found that ALES is able to provide more reliable 20 Hz data for all three missions in areas where even 1 Hz averages are flagged as unreliable in standard products. Application of the ALES retracker led to roughly half of the analysed tracks showing a marked improvement in correlation with the tide gauge records, with the root mean square difference (RMSD) being reduced by a factor of 1.5 for Jason-1 and -2 and over 4 for Envisat in the Adriatic Sea (at the closest point to the tide gauge).

The dark blue line running through time at latitude 29.8 °S, is white noise bounced back from the satellite as it passes the tip of Durban. However, ALES is still able to retrieve small scales features where as the ability of SGDR data to retrieve data becomes contaminated. It furthermore suggests that ALES estimates are much less affected by the proximity of the topography of Durban, because of the applied ALES algorithm. My findings also provide much confidence in the low resolution along-track dataset, and less in the gridded product which appears to be inconsistently acceptable. The low resolution data is acceptable to use as an alternative to study the DBLE/or other large mesoscale features, meaning that there is no increased benefit from using the ALES data over the SGDR or RADS when working further offshore. The DBLE is located 100 km offshore and is much larger in magnitude, so using coastal altimetry is not more useful further offshore, except when trying to identify submesoscale structures within the eddy (as coastal altimetry is able to resolve small scale features). That being said, coastal altimetry was a successful tool to identifying the eddy.

The ALES algorithm has been validated for sea level and SWH and has been used for different altimeters in number of case studies (Passaro et al., 2015b, 2016; Gómez-Enri et al., 2016). Appendix A.2, shows an overpass of Jason-2 tangent to the coast of Elba Island in the Mediterranean Sea, where standard retracking algorithms yield unrealistic meter-level variations of the sea level while the adoption of ALES visually improves the height profile. This kind of qualitative assessment of course needs to be followed up by a quantitative validation of the

data, whose scope and methods depend to some extent on the intended application. The latest comparison between ALES data and tide gauges around the coast of the UK carried out by Cipollini et al. (2017), found a very good agreement between coastal altimetry and tide gauge observations, with RMSDs as low as 4 cm at many stations. This has provided confidence to use the combination of altimetry and tide gauges to characterize the annual cycle of sea level along the UK coasts. They also examined the evolution of sea level trend from the open to the coastal ocean along the western coast of Africa, comparing standard and coastally improved products, and observed that different products gave different answers regarding the coastward evolution of the sea level trend; therefore, coastal altimetry cannot yet be used to robustly deduce the quantitative evolution of sea level trend from the open to the coastal ocean.

The limitation when working in the coastal region of Durban is that the eddy is further inshore than the Delagoa Bight eddy. Data seem to be more noisey inshore than offshore. So, distinguishing between noise and the eddy's made it slightly difficult due to its small size. However, having access to SLA images helped to validate the eddy. The problems with using RADS data are that there are no data close to the coast. The available data for the requested period and area were rejected by the quality flag settings, and could not be accessed. Since the area Durban region selected is very close to the coast, the measurements were all flagged to be affected by land in the footprint of the altimeter and/or radiometer. So gaining certainty in the coastal altimetry nearshore was not possible, but the fact that rads data confirmed patterns about 50 km offshore was reassuring enough that I could go ahead and use the dataset inshore. Thus, unless not using hydrographic data and *in situ* data, it is tricky to accurately pin point the eddy. Overall, the use of coastal altimetry as an application in the coastal region was successful, not only were smaller features such as the DLE were detected, but larger upwelling cells such as the Natal Pulse and Durban break-away eddies too. Another limitation with using along-track data, especially in the Delagoa Bight, was the track coverage. In conclusion, data retrieved from the Jason mission would be the most ideal to use when studying mesoscale features as it retrieves data every 10 days; however, there were no ideal tracks that would detect the DBLE, hence the reason for using Envisat. The limitation of using Envisat is that it retrieves data every 35 days, which was is not ideal as it may have lead to the eddy not being caught, or resulted in detecting the eddy as it was forming or dissipating.

5.2 Relationship between SLA and chl-*a*

A study by Laiolo et al. (2016) examined the seasonal plankton dynamics associated with averaged cyclonic and anticyclonic eddies (CE and ACE, respectively) off eastern Australia. Using the CE and ACE seasonal climatologies, they assimilated the surface chl-*a* data into a

multi-phytoplankton class (EMS) biogeochemical model to investigate the level of complexity required to simulate the phytoplankton chl-*a*. Their results from the model simulations indicate that the CE is not solely characterised by having a higher chl-*a* concentration compared to ACE, but also by an increased concentration of large phytoplankton (*i.e.*, diatoms) as a result of its shallow mixed layer. According to their modeled simulations identify the two eddy types to be characterised by different zooplankton communities. Condie and Condie (2016), aimed at estimating eddy retention time-scales across a range of oceanic environments and larval behaviours, with implications for both distributions and future changes in plankton communities. Their results indicate that ocean eddies have the potential to retain and support planktonic communities for many generations and could potentially aid in the survival rate of larvae for many invertebrate and pelagic fish species. Differences in retention with depth suggest that anti-cyclonic and cyclonic eddies will support differing plankton communities.

My findings indicate a significant negative relationship between the Delagoa Bight eddy and chl-*a*. The negative means that the variables move in opposite directions, *i.e.* when SLA decreases chl-*a* increases (vice versa), suggesting that when the eddy is present there is a relationship between SLA and chl-*a* in both bights. Although there is a weak correlation it does provide some indication of the promotion of nutrients in the coastal region, or it indicates the entrainment of the chl-*a* in the eddy. These results support the previously hypothesised relationship between chl-*a* and SLA in the Delagoa Bight and Durban region/Natal Bight. Findings by Dove (2015) support this. Doves findings suggest that although SLA amplitude appeared to be low, cyclonic eddies were still able to influence primary production. This small contribution could also indicate that there are other major contributors to the enhanced primary production in the respective bights. A study carried out in the Kuroshio front by Kasai et al. (2002) revealed that the entrainment process to be important for fish recruitment in the sense that they can remain in the coastal nursery area. The chl-*a* blooms in the Delagoa Bight are mainly due to river inflow and floods; however, the presence of the eddy still represents an important mechanism for phytoplankton production. Dove (2015) and Kahru et al. (2010) both indicate that the upliftment of the cold and nutrient rich waters from the subsurface to the euphotic zone, where light is mostly available, represents an important mechanism for the phytoplankton growth. The phytoplankton abundance in Delagoa Bight is associated with an upwelling cell along the northern shore (Lutjeharms and Da Silva, 1988; Quartly and Srokosz, 2004; Lamont et al., 2010). SLA variation seem to be high for the Delagoa Bight (-30 cm and 30 cm), which was not coherent with the findings of Dove (2015), where SLA variation was observed to be low (-0.5 to 0.5 cm). Their findings suggest both cyclonic and anticyclonic-like structures are sporadically apparent from the eastern limit of the study domain.

Cossa et al. (2016) documented the circulation around the Delagoa Bight region. A ROMS model produced a general circulation of the region as well as indicating the existence of a semi-permanent eddy, which was also apparent in gridded maps of merged altimetry (Ssalto/Daucs) obtained from AVISO. This finding supports the conclusion of Lutjeharms and Da Silva (1988) who suggested that the eddy is semi-permanent. The Delagoa Bight lee eddy was shown to occur about 25 % of the time, with no clear seasonal occurrence. The diameter of the eddy core varied between 61 and 147 km (lower than the previous estimate of 180 km from Lutjeharms and Da Silva, 1988). The average life time exceeded 20 days (which points to a feature that forms, moves away, then forms again). Additional model analyses revealed the systematic presence of negative vorticity in the Bight that can organise and form a DBLE depending on the intensity of an intermittent southward flow along the shore and the spatial distribution of surrounding mesoscale features (Cossa et al., 2016). The following observations derived from Cossa et al. (2016) confirm the same observations made by Lamont et al. (2010): (i) the model solution shows other cyclonic eddies generated near Inhambane and eventually travelling through the Delagoa Bight; and (ii) the only permanent feature observed with or without DBLE is the presence of a northward, surface intensified, coastal counter-current in the former. In addition, my results indicate two cores forming inside the bight and outside, suggesting that the eddy doesn't always originate from the bight, but is formed elsewhere and is advected in.

My results indicate that the Durban Eddy was also found to have a significant correlation with chl-*a*, although much weaker than the Delagoa Bight. A permanent upwelling cell within the bight was also observed from the SLA images. Nutrient analysis done by Meyer et al. (2002) in the Natal Bight indicates that at the surface, the insertion of nutrients is accompanied by an increase in chl-*a*. Intermittent inflows of surface water from the Agulhas Current, particularly over the southern part of the bight, diminish the nutrient content of the waters there. A recurrent lee eddy off the southern termination of the Natal Bight upwells nutrients in its core. A simple model conducted demonstrates that primary productivity may be sustained along the shelf edge by upwelling and that the southward flow of nutrients is affected by considerable mixing (Meyer et al., 2002). Guastella and Roberts (2016) suggest this result indicates that the Agulhas Current controls the nutrient distribution over the largest part of the bight. It does this predominantly by forcing upwelling at its northern end in a site-specific upwelling cell between Richards Bay and Cape St. Lucia. It has previously been shown by Lutjeharms et al. (2000) and Lutjeharms and Connell (1989) that this upwelling is largely wind-independent and a function of the local shelf/current configuration. This St. Lucia upwelling cell is the main source of nutrients for the whole bight. From here, nutrients are moved south-westward with an attendant increase in primary productivity. Injections of higher nutrient concentrations may occasionally be advected downstream at the shoreward

edge of the current. The Agulhas Current has also been suggested to control the nutrient distribution at the southern extremity of the Natal Bight according to Lutjeharms et al. (2000) and Lutjeharms and Connell (1989). It does this by the creation of a lee eddy at Durban that forces nutrient-poor surface water from the Agulhas Current onto the shelf. Guastella and Roberts (2016) suggest that the eddy off Durban is also subject to high levels of variability. Its presence is known to be extremely intermittent and its intensity very variable. This was also evident in the Hovmöller plot (Fig. 4.4). This may have implications for the movement of nutrient-poor surface water from the Agulhas Current onto the Natal Bight according to Guastella and Roberts (2016).

Break-away eddies were also observed from the SLA images, which is consistent with findings by Guastella and Roberts (2016); this indicates that these break-eddies are the DLE, that go through three phases a (1) spin-up phase, (2) a maturation phase and then (3) a dissipative phase when it breaks away from the Durban area and propagates downstream in the inshore edge of the Agulhas Current, losing energy and eventually dissipating as a lateral wave. The Natal Pulse was also present and found further offshore, as observed by Guastella and Roberts (2016). Guastella and Roberts (2016) also indicate that the variability in eddy occurrence, intensity and duration result in variability in the available nutrients and chl-*a*in the water column with each eddy event and between eddy events, and would suggest that primary productivity should similarly be quite variable. This supports the observations of Meyer et al. (2002) and Guastella and Roberts (2016) who found the eddy off Durban to be subject to high levels of variability in terms of presence and intensity. Lamont and Barlow (2015) found that at the Durban site higher biomass and primary production were the result of the development of the cyclonic Durban lee eddy, and the initiation of the DLE was evident by the marked uplift of the subsurface thermohaline structure and increased nutrient supply into the euphotic zone over the study period of 2–6 February 2010, with satellite SST and chl-*a* illustrating a fully formed eddy on 6 February 2010. Similar observations of this cyclonic eddy have been made by Pearce (1977) and Lutjeharms and Machu (2000), and the upliftment of nutrients into the euphotic zone by the Durban Eddy.

The use of satellite remote sensing has been pertaining to my study regions seemed to be limited. In terms of chl-*a*, it is noted that generally remotely sensed chl-*a* concentration for the Case 2 waters, such as in the Delagoa Bight, is overestimated due to the influence of the suspended sediments and dissolved organic matter (Morel and Prieur, 1977; Yoder and Kennelly, 2006) and satellite data provide information only for the topmost layer of the water column. In addition to the inaccuracy of the altimetry data in the shallow coastal areas, the SST data can be affected by clouds and this has been reported to occur in the Mozambican Channel and adjacent waters (Malauene et al., 2014). Another study also confirms the

gross inaccuracy of standard satellite altimetry data (Roberts unpubl.). However results from another study suggests that altimetry sea surface observations can be provide useful information on subsurface currents and their variability through the study of the propagation of deep mesoscale eddies in semi-enclosed seas (Escudier et al., 2016).

CHAPTER 6

CONCLUSION

In this study I analysed two datasets for two regions: (1) nine years (2002–2010) of high resolution coastal altimetry data (CDGR and SGDR) from Envisat (18 Hz), gridded chl-a (1/4 degree) and SLA (1/4 degree)satellite derived products were analysed for the Delagoa Bight, 24–29°S, 32–36°E (~4°x 4°); and (2) eight years of (2008-2015) CDGR and SGDR from Jason-2, satellite-derived chl-a and SLA data for the Natal Bight and south of Durban, 29–36°S, 30.5–31.5°E (~3°x 3°) (Fig. 3.2). The results presented provide more validation and insight into the use of coastal altimetry techniques to understand and quantify mesoscale features. This study also provides more confirmation to the relationship between the DBLE and DLE, and their influence on chl-*a* concentrations. This correlation has not been shown in other studies. I am confident with the quality of my research, but will acknowledge that the data on which it is based should be analysised with caution as there are limitations, especially in the coastal shallow waters as discussed earlier in this study.

1. ALES improved the quantity and the quality of coastal altimetry data without adding significant further noise to the estimation. There was very little discrepencies between ALES and SGDR, however ALES was able to recover data nearshore better than SGDR. The gridded product appears to be consistent with the patterns detected by ALES and RADS data at times and then highly inconsistent. The application of coastal altimetry was successfully validated by along-track RADS data, with data being realible up to 10 m near the coast. These results provide one of many contributions to the increased confidence and validation and in the product. ALES data was successful at detecting the DBLE, but identifying the Durban eddy at times was difficult. Although satellite altimetry is considered appropriate for detecting bigger features in the Delagoa Bight

and Natal Bight; when it comes to detecting smaller features such as the, DLE satellite altimetry data are not ideal without *in situ* measurements for validation.

2. Although I did not manage to quantify the frequency of occurrence of these features, the DBLE was more transient than semi-permanent than previously thought. Two points of origin were identified for the DBLE. These two cores were observed forming (i) within the bight and (ii) outside of the bight, which was being advected into the bight. A common trait observed is that these eddies move in a southwesterly direction. Further studies would need to be carried out to identify which eddy is the DBLE. From the Hovmöller plot, the DLE was found to occur more frequently, the residence time is not clear. Future work is needed using an eddy detecting algorithm that makes use of coastal altimetry to determine the pathways of these eddies to accurately quantify the frequency of occurence.

3. Identifying the role and importance of the eddies in both bights still remains unanswered. Results from the regression analysis indicates a small relationship between the eddy and chl-*a*. This result provides confirmation in the hypothesis put forward in several literature sources (Dove, 2015; Cossa et al., 2016; Guastella and Roberts, 2016; Meyer et al., 2002) that cold-core cyclonic features upwell nutrients to subsurface thus promoting the increase in chl-*a*. This weak relationship might suggest that other processes play a larger role in contributing to the increase chl-*a*. For example, winds, seeing as the east coast is strongly wind driven. However, analysis needs to be conducted to confirm this.

Apart from the described limitations, satellite altimetry has also been shown to be reliable offshore, providing information of the variation in chl-*a* and SLA in the Delagoa Bight and Natal Bight, which would be difficult to get by using *in situ* data. This study provides information that can improve the understanding on the chl-*a* variability and its relationship with the physical drivers in the Delagoa Bight ecosystem. In order to ground truth the data to study these features and any coastal features, more in situ data are needed, but with the advances in altimetry we hope to achieve the same result. There is no doubt that the new coastal altimetry products will constitute a crucial input for coastal observing systems, so that the multi-decadal record is not only continued, but also improved in quality and the quantity of data expanded, and thereby bringing measurements closer to the coast. Certainty in the data can only be made once validated with *in situ* data and not only by satellite data.

APPENDIX A

APPENDIX

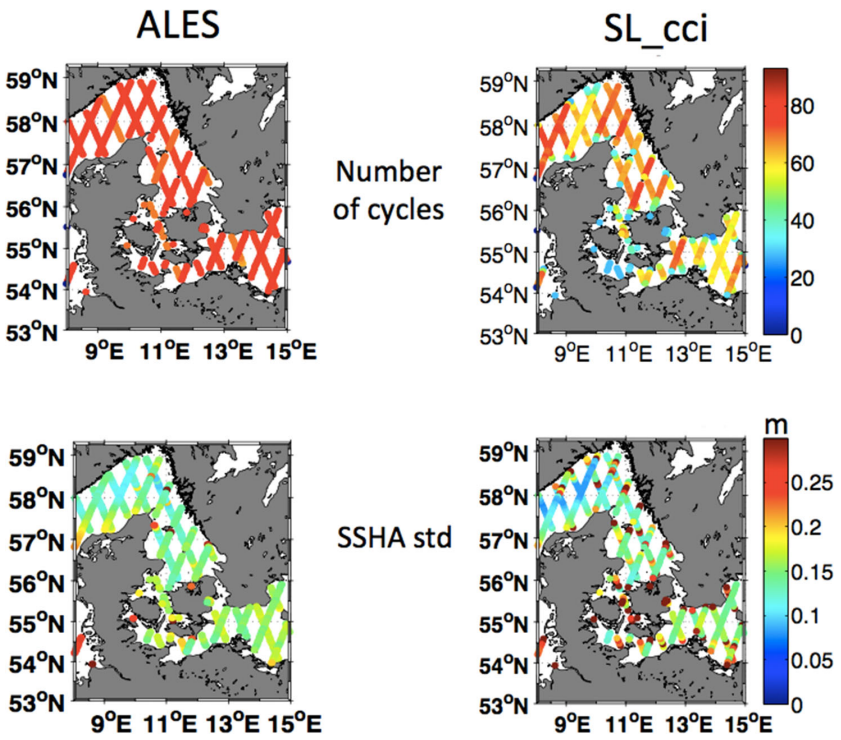

Figure A.1: North Sea/Baltic Sea transition area between Denmark and Finland: comparison between ALES reprocessed (left) and Envisat SL cci (right) datasets in terms of number of cycles available (upper plots) and standard deviation of the SSHA time series (lower plots) for each 1 Hz location (Passaro et al., 2015a).

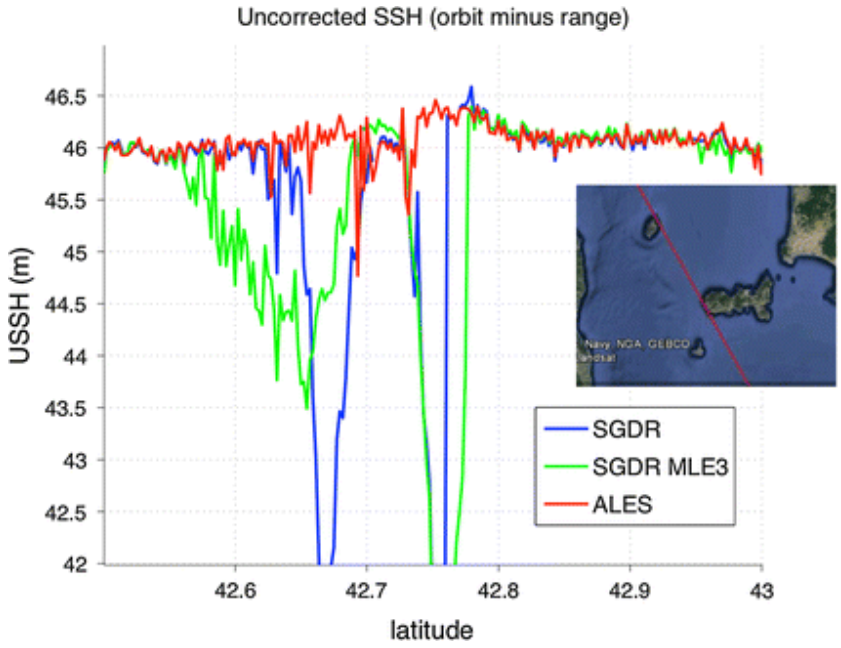

Figure A.2: Example shows the improved retrieval of SSH close to the coast by applying the ALES algorithm. The *inset* depicts Jason -2 satellite mission descending track 44 (red) near the Elba Islands (Passaro et al., 2014).

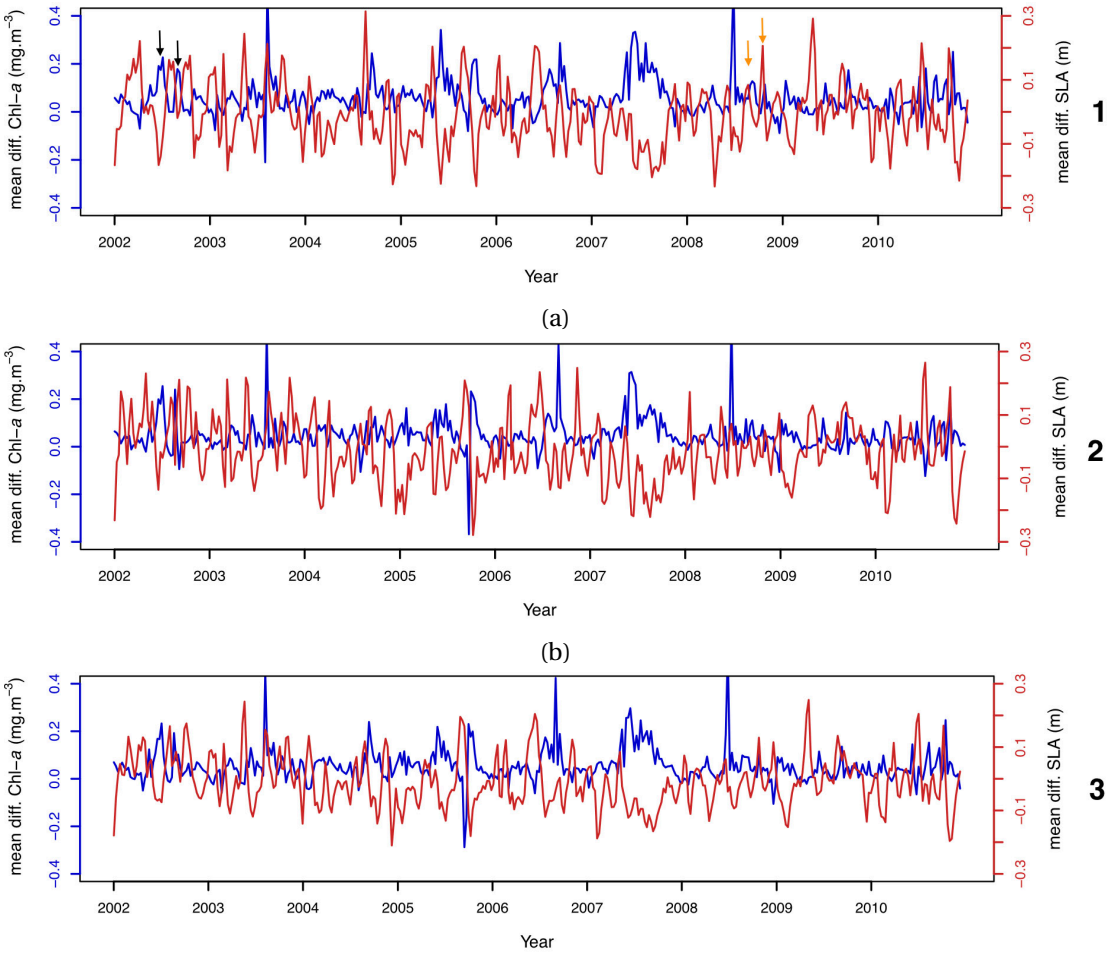

(a)

(b)

(c)

Figure A.3: Mean differences of chl-*a* and SLA between the eddy centre (A) and respective outside boxes: (a) 1, (b) 2 and (c) 3 (Fig. 3.4(b)) in the Delagoa Bight from 2002–2010.

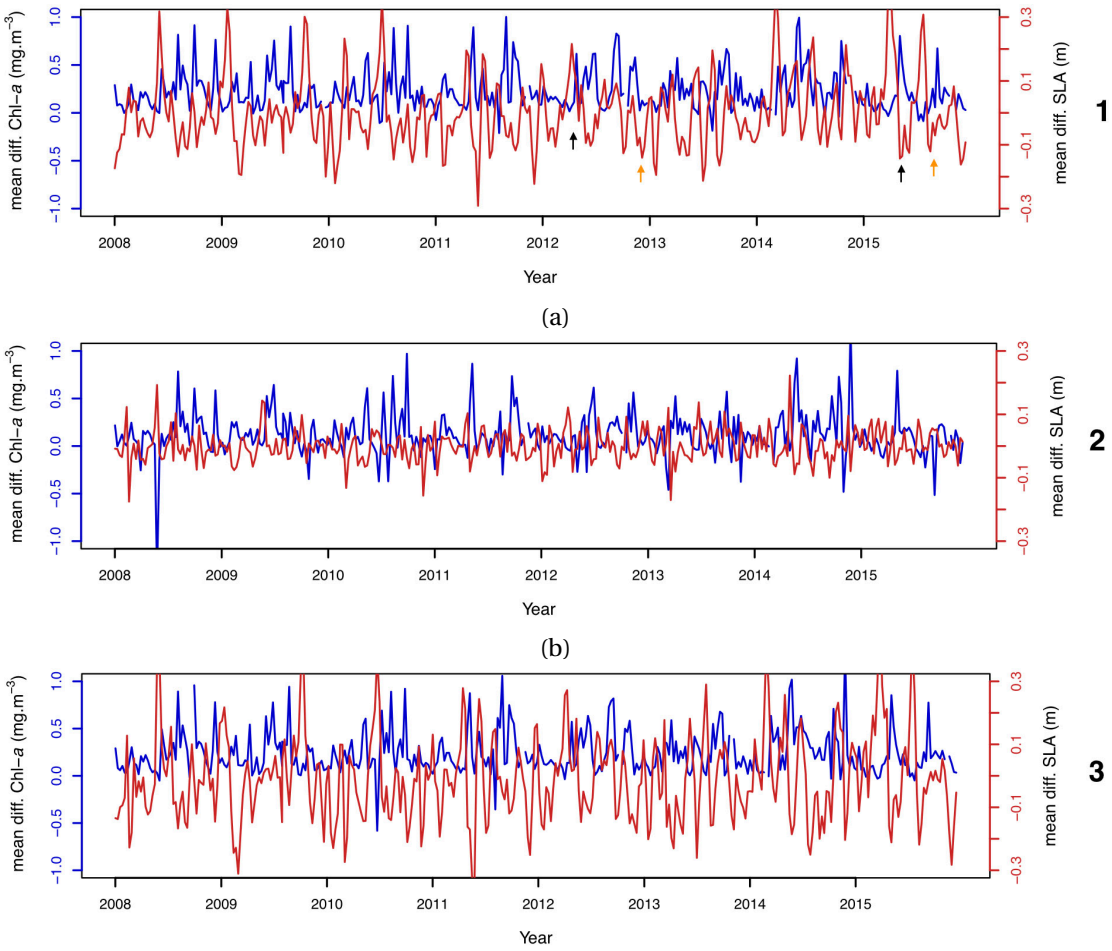

Figure A.4: Mean differences of chl-*a* and SLA between the eddy centre (A) and respective outside boxes: (a) 1, (b) 2 and (c) 3 (Fig. 3.4(a)) in the Natal Bight from 2008–2016.

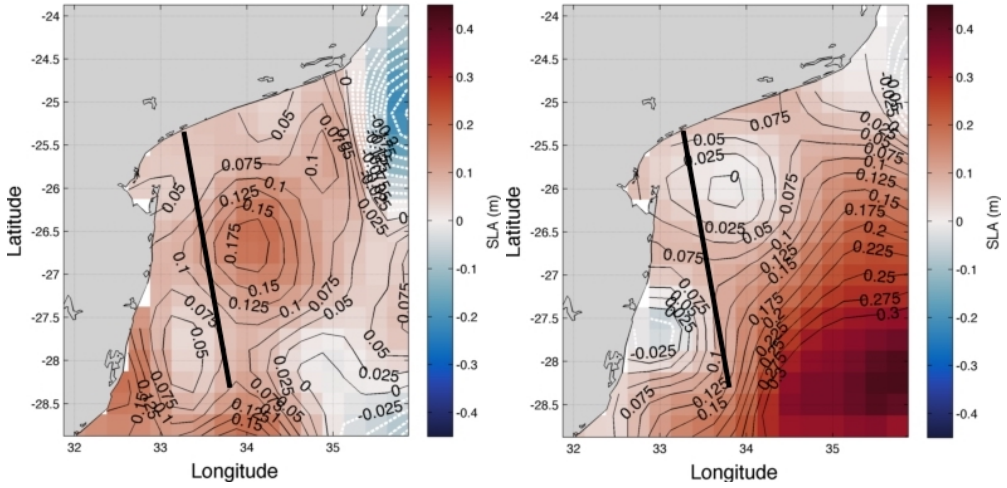

Figure A.5: Delagoa Bight: AVISO SLA images for 8 June and 30 July, 2008. Showing the absence of SLA signal that corresponds to that shown in the along-track data. Bold black line indicates Envisat track (0371) analysed in this study.

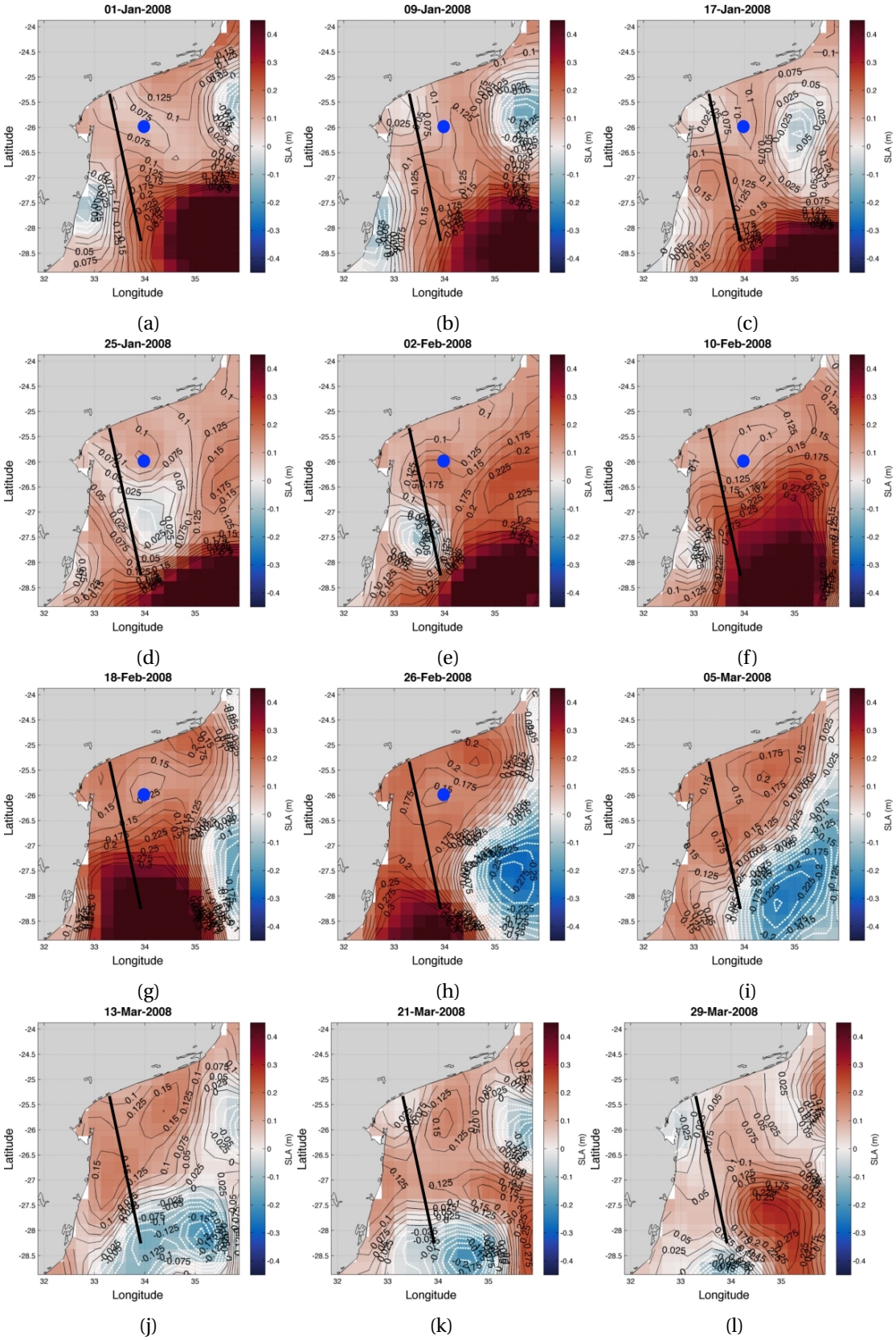

Figure A.6: Composite images of AVISO product of SLA taken at an 8 day interval shows the eddy movement in the Delagoa Bight during 1 January–29 March, 2008; superimposed by contours of SLA (m). Blue dot indicates where the 26°S point position is. Bold black line indicates Envisat track (0371) analysed in this study.

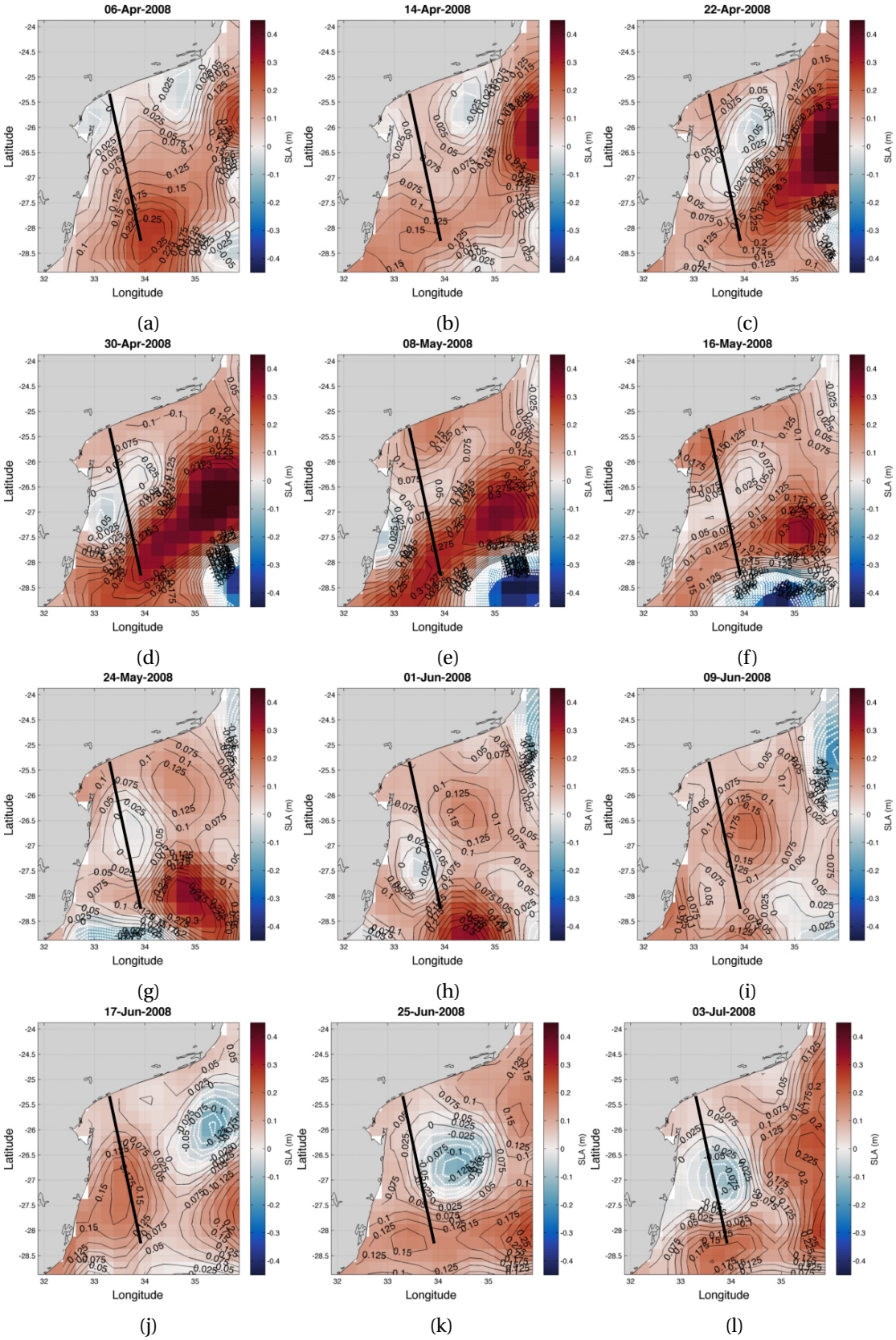

Figure A.7: Composite images of AVISO product of SLA taken at an 8 day interval shows the eddy movement in the Delagoa Bight during 6 April–3 July, 2008; superimposed by contours of SLA (m). Bold black line indicates Envisat track (0371) analysed in this study.

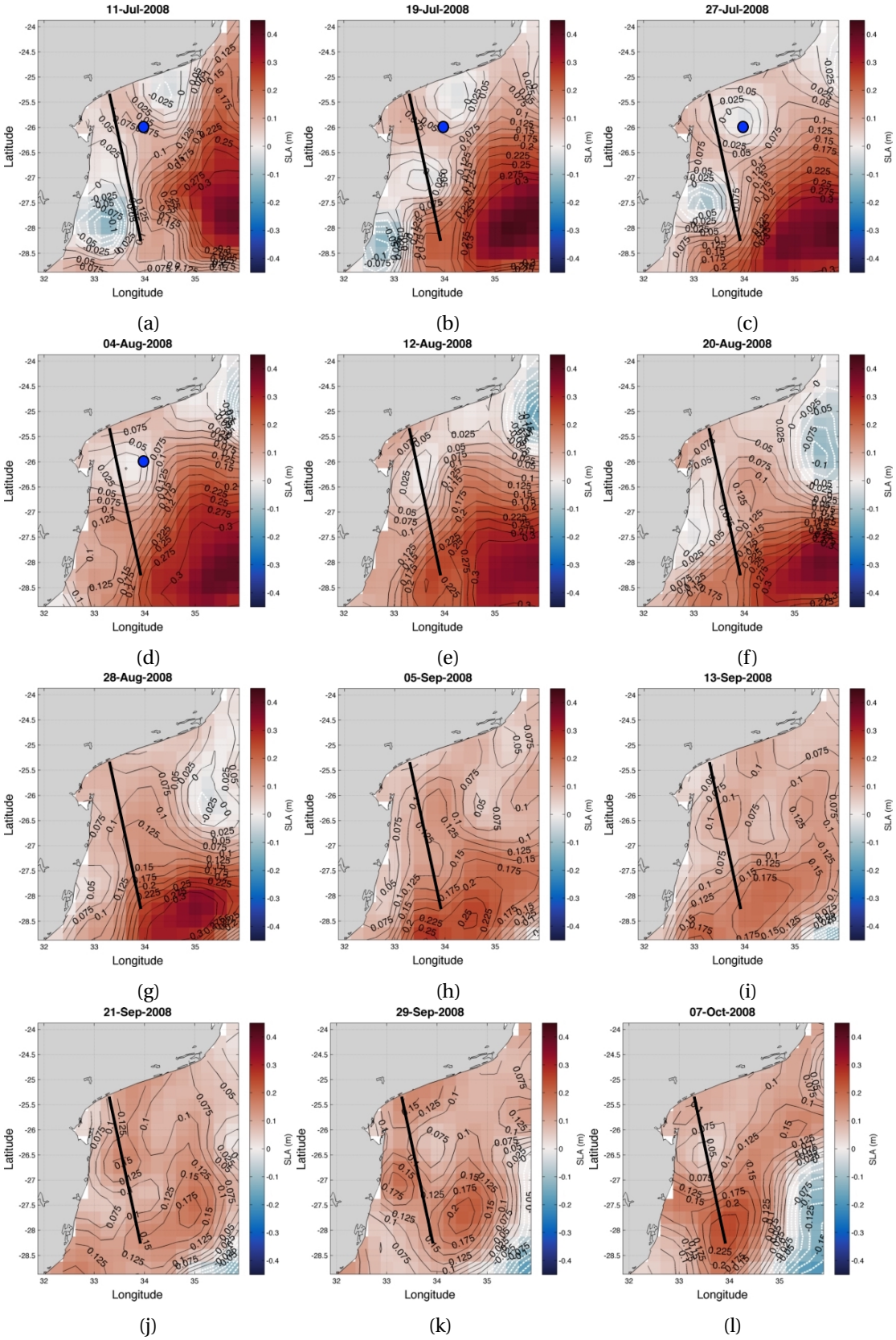

Figure A.8: Composite images of AVISO product of SLA taken at an 8 day interval shows the eddy movement in the Delagoa Bight during 11 July–7 October, 2008; superimposed by contours of SLA (m). Blue dot indicates where the 26°S point position is. Bold black line indicates Envisat track (0371) analysed in this study.

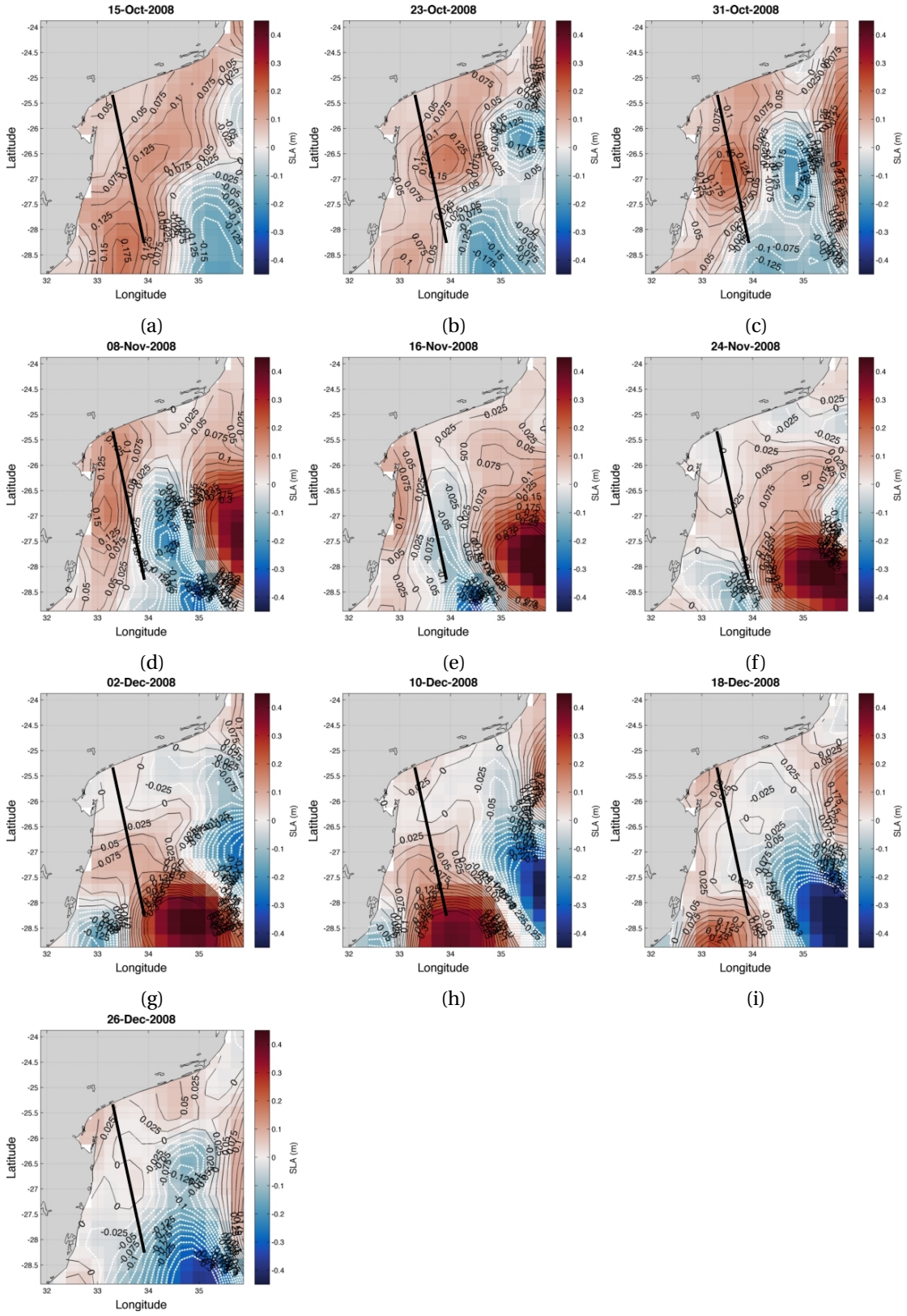

(a) (b) (c)

(d) (e) (f)

(g) (h) (i)

(j)

Figure A.9: Composite images AVISO product of SLA taken at an 8 day interval shows the eddy movement in the Delagoa Bight during 15 October–26 December, 2008; superimposed by contours of SLA (m). Bold black line indicates Envisat track (0371) analysed in this study.

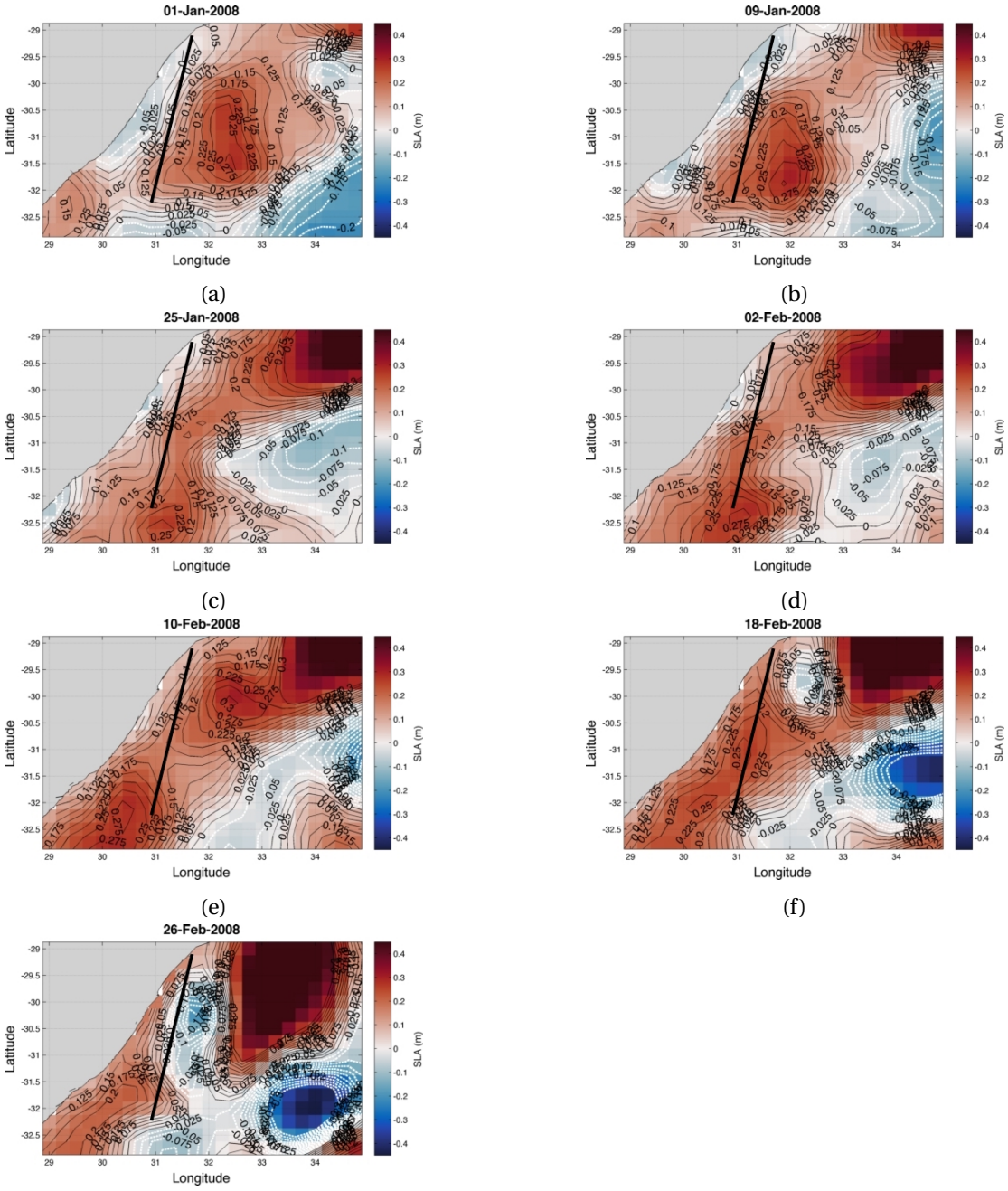

(a) (b) (c) (d) (e) (f) (g)

Figure A.10: Composite images AVISO product of SLA taken at an 8 day interval shows the eddy movement in the Natal Bight and further south of Durban during 1 January–26 February, 2008; superimposed by contours of SLA (m). Bold black line indicates Jason-2 track (0005) analysed in this study.

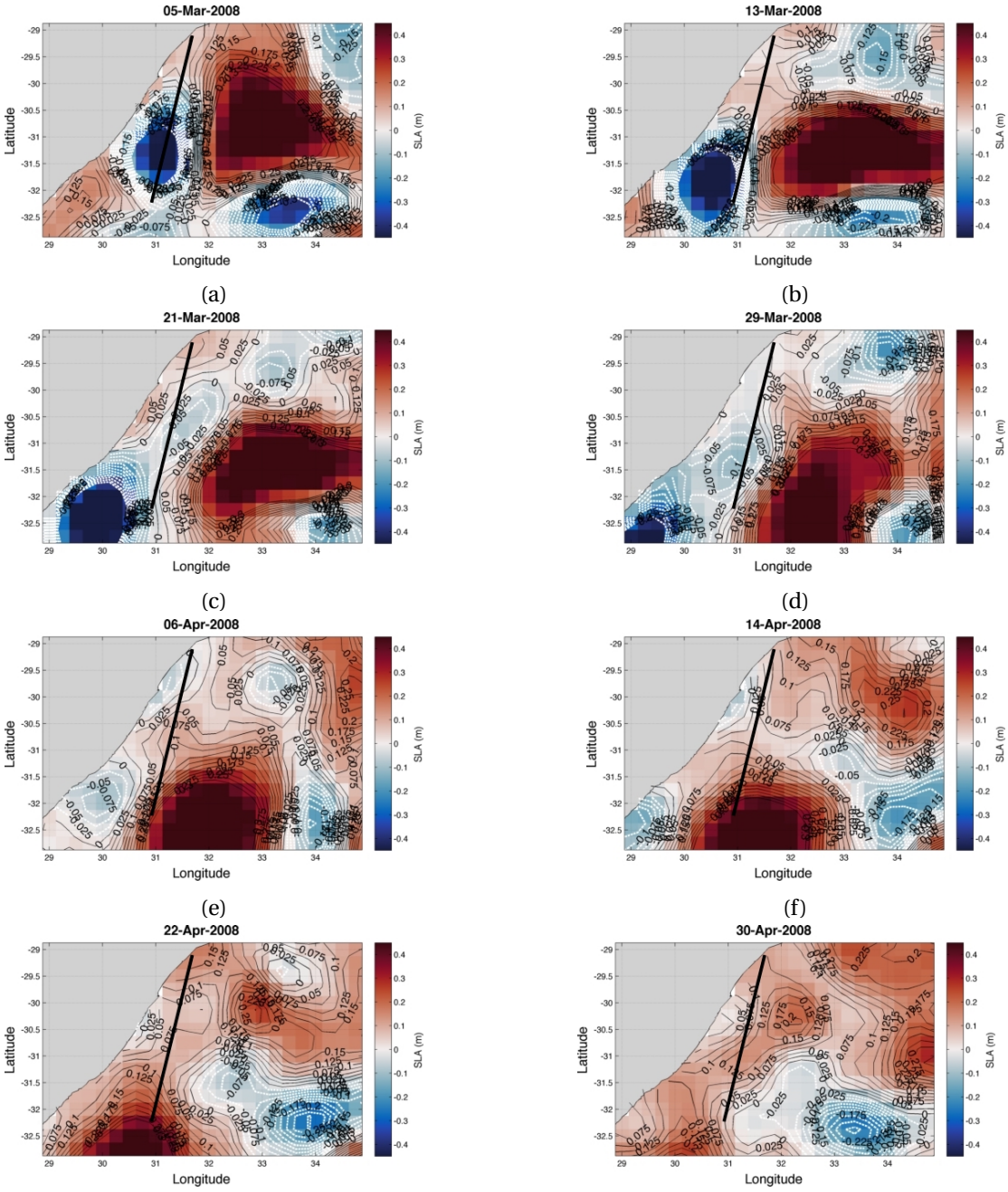

(a) (b) (c) (d) (e) (f) (g) (h)

Figure A.11: Composite images AVISO product of SLA taken at an 8 day interval shows the eddy movement in the Natal Bight and further south of Durban during 5 March–30 April, 2008; superimposed by contours of SLA (m). Bold black line indicates Jason-2 track (0005) analysed in this study.

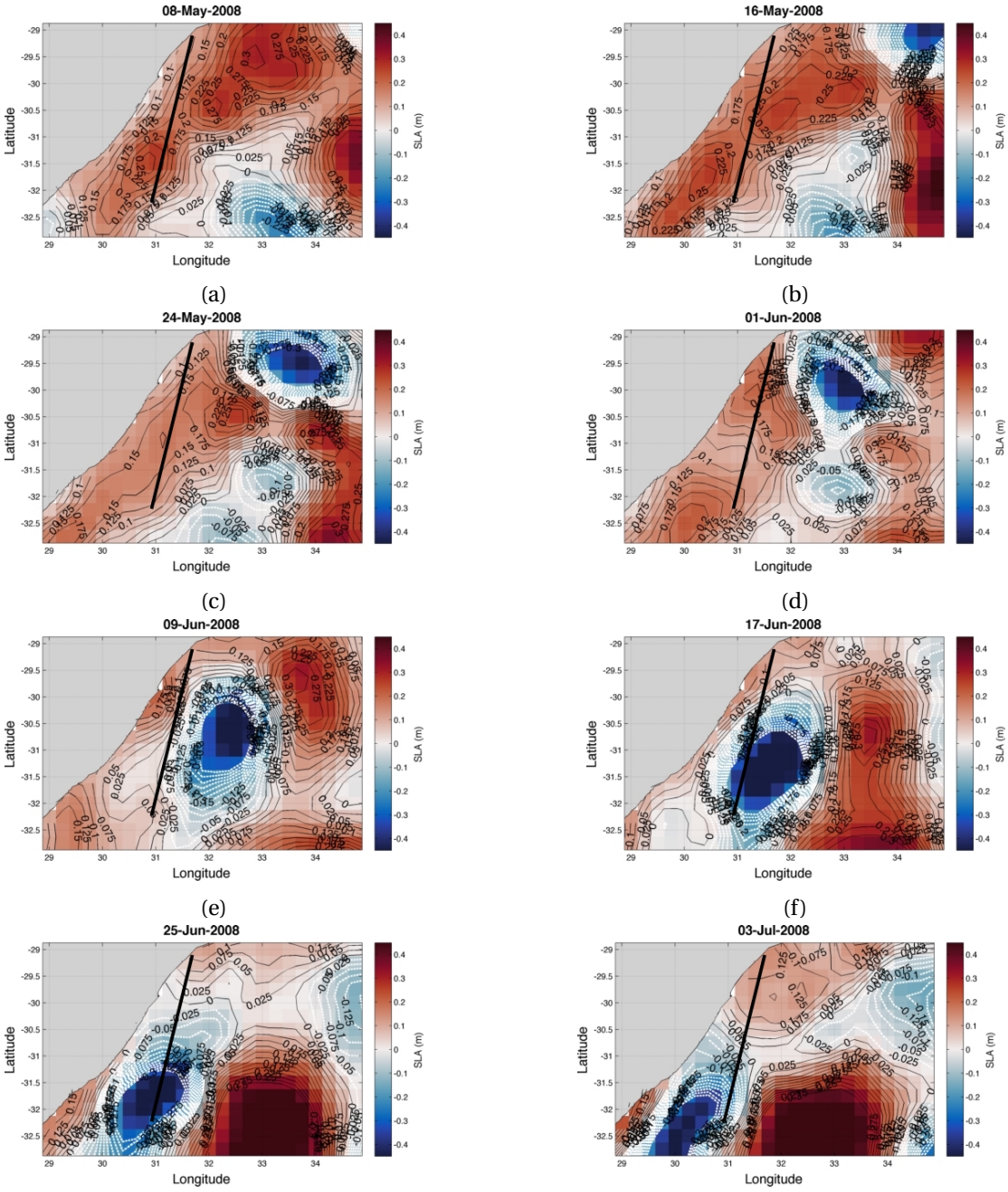

Figure A.12: Composite images AVISO product of SLA taken at an 8 day interval shows the eddy movement in the Natal Bight and further south of Durban during 8 May–3 July, 2008; superimposed by contours of SLA (m). Bold black line indicates Jason-2 track (0005) analysed in this study.

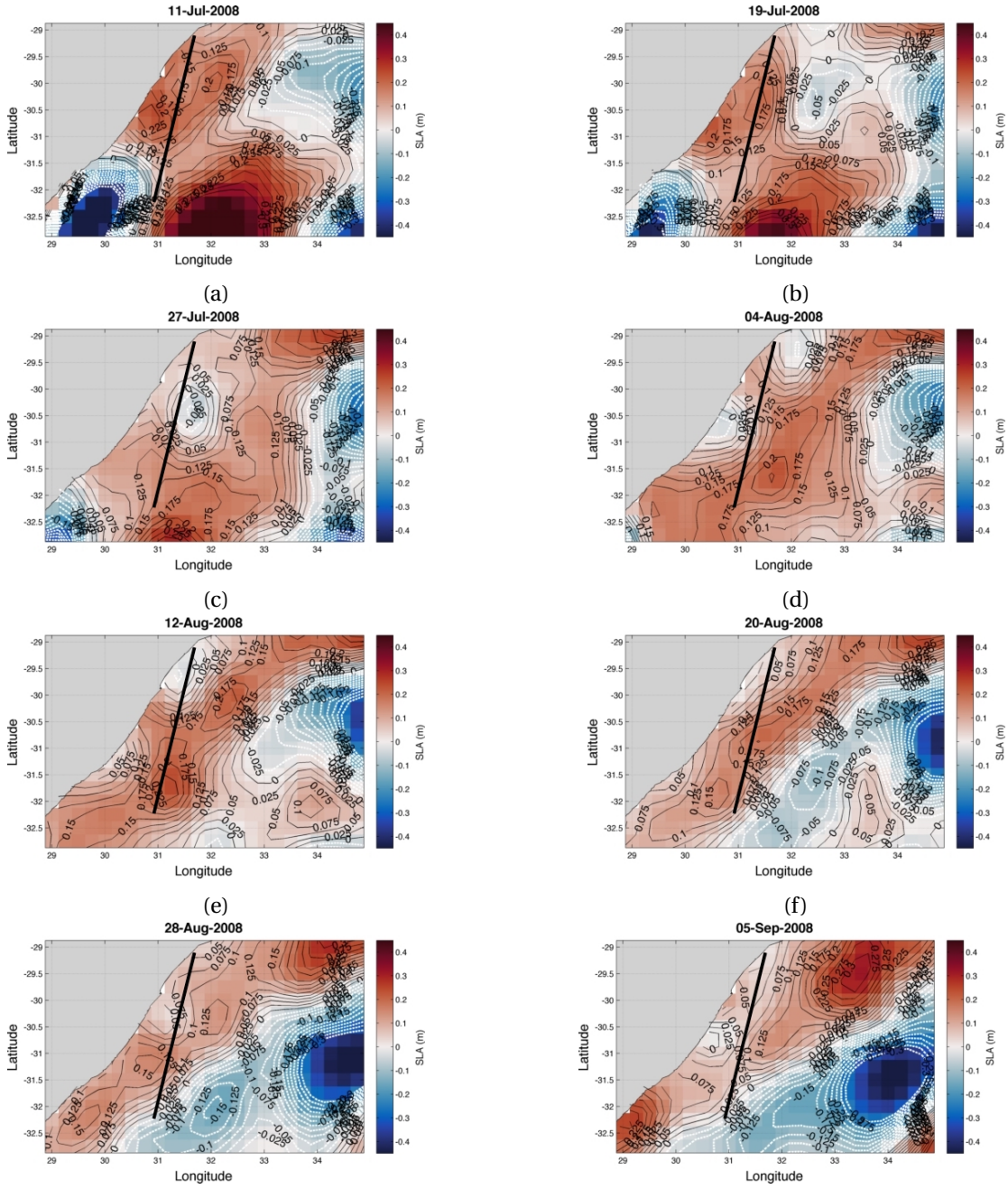

(a) (b) (c) (d) (e) (f) (g) (h)

Figure A.13: Composite images AVISO product of SLA taken at an 8 day interval shows the eddy movement in the Natal Bight and further south of Durban during 11 July–5 September, 2008; superimposed by contours of SLA (m). Bold black line indicates Jason-2 track (0005) analysed in this study.

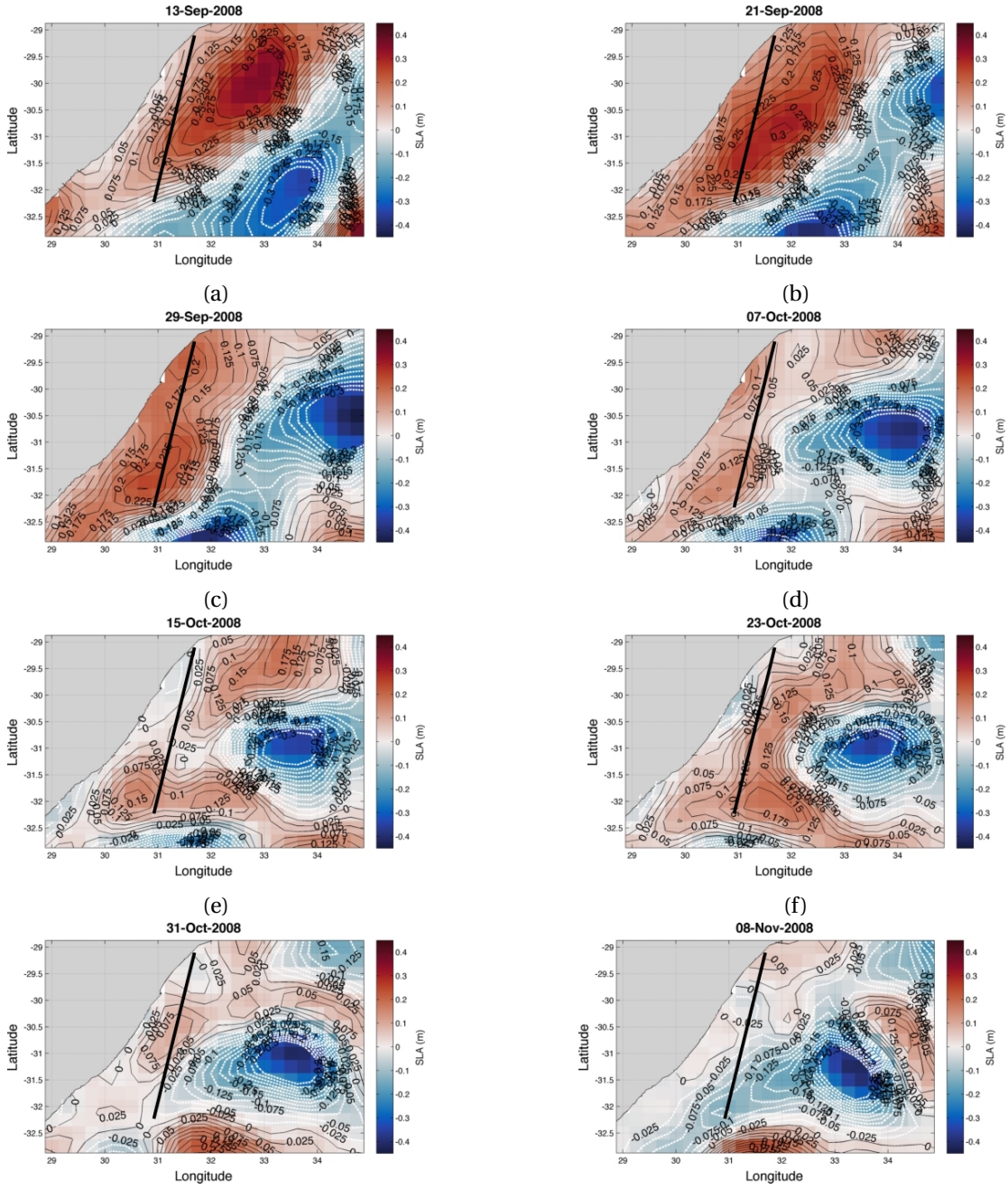

(a) (b) (c) (d) (e) (f) (g) (h)

Figure A.14: Composite images AVISO product of SLA taken at an 8 day interval shows the eddy movement in the Natal Bight and further south of Durban during 13 September–8 November, 2008; superimposed by contours of SLA (m). Bold black line indicates Jason-2 track (0005) analysed in this study.

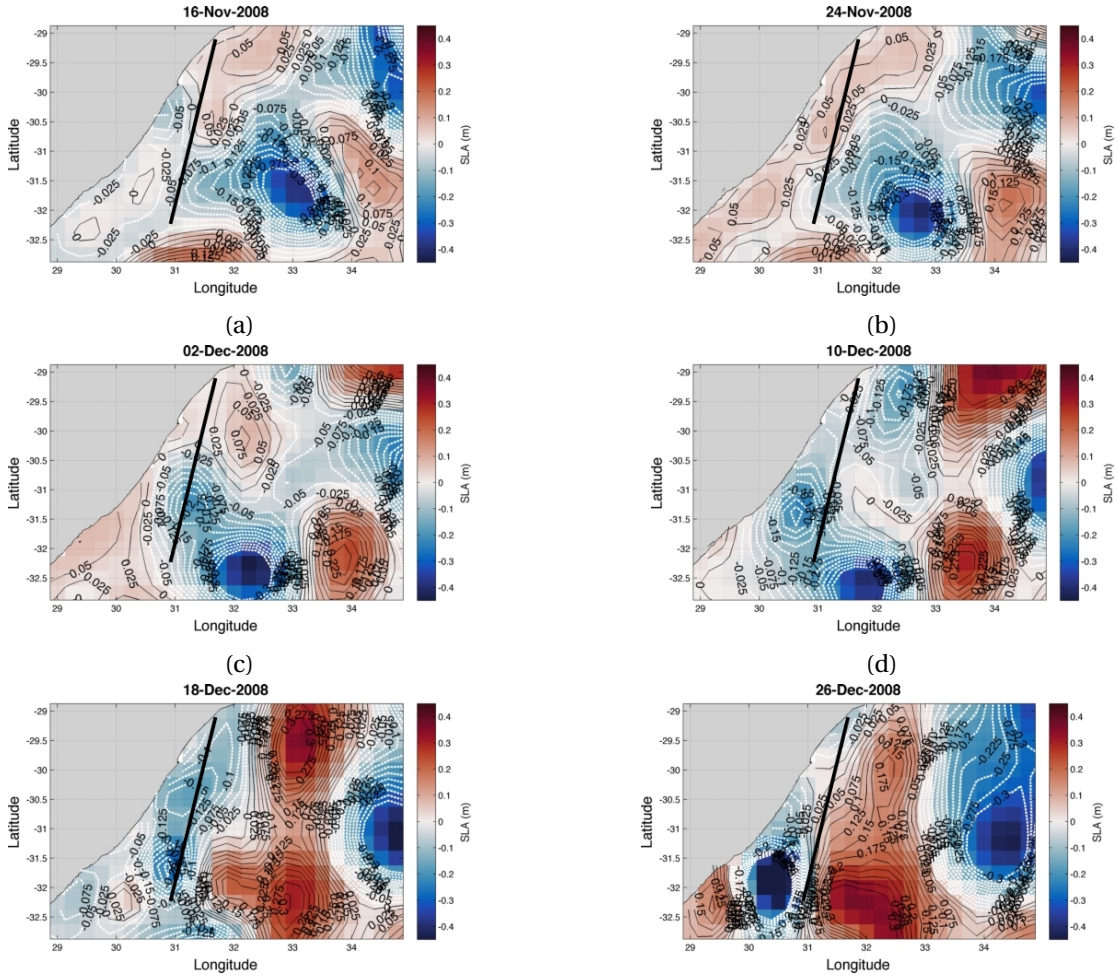

(a) (b) (c) (d) (e) (f)

Figure A.15: Composite images AVISO product of SLA taken at an 8 day interval shows the eddy movement in the Natal Bight and further south of Durban during 16 November–26 December, 2008; superimposed by contours of SLA (m). Bold black line indicates Jason-2 track (0005) analysed in this study.

Listing A.1: Variables extracted from Envisat and Jason-2 files using in Matlab

```
% extract variables needed to cal. ssha
% From Envisat (18 Hz) dataset
           orbit               = outvar.hz18_alt_cog_ellip;
           range               = outvar.hz18_ku_band_ocean;
           iono                = outvar.ion_corr_mod_ku;
           dry_tropo           = outvar.mod_dry_tropo_corr;
           wet_tropo           = outvar.mod_wet_tropo_corr;
           ssb                 = outvar.sea_bias_ku;
           solid_earth_tide    = outvar.solid_earth_tide_ht;
           ocean_tide          = outvar.tot_geocen_ocn_tide_ht_sol2;
           pole_tide           = outvar.geocen_pole_tide_ht;
           dynamic_atmosphere  = outvar.dib_hf;
           inverted_barometer  = outvar.inv_barom_corr;

% From Jason_2 (20 Hz) dataset

           orbit               = outvar.alt_20hz;
           range               = outvar.range_20hz_ku;
           range_ales          = outvar.Range_ALES;
           iono                = outvar.iono_corr_gim_20hz_ku;
           dry_tropo           = outvar.model_dry_tropo_corr_20hz;
           wet_tropo           = outvar.model_wet_tropo_corr_20hz;
           ssb                 = outvar.sea_state_bias_20hz_ku;
           solid_earth_tide    = outvar.solid_earth_tide_20hz;
           ocean_tide          = outvar.ocean_tide_sol1_20hz;
           pole_tide           = outvar.pole_tide_20hz;
           dynamic_atmosphere  = outvar.hf_fluctuations_corr_20hz;
           inverted_barometer  = outvar.inv_bar_corr_20hz;
```

BIBLIOGRAPHY

Adcroft, A., Griffies, S., Hallberg, R., 2016. Ocean Mesoscale Eddies. Accessed on 15 October 2016.
URL http://www.gfdl.noaa.gov/ocean-mesoscale-eddies

Andersen, O., 2010. The dtu10 gravity field and mean sea surface. In: Second international symposium of the gravity field of the Earth (IGFS2), Fairbanks, Alaska. pp. 20–22.

Bakun, A., 2006. Fronts and eddies as key structures in the habitat of marine fish larvae: opportunity, adaptive response and competitive advantage. Scientia Marina 70 (S2), 105–122.

Barlow, R., Kyewalyanga, M., Sessions, H., Van den Berg, M., Morris, T., 2008. Phytoplankton pigments, functional types, and absorption properties in the Delagoa and Natal Bights of the Agulhas ecosystem. Estuarine, Coastal and Shelf Science 80 (2), 201–211.

Beckley, L., Hewitson, J., 1994. Distribution and abundance of clupeoid larvae along the east coast of South Africa in 1990/91. South African Journal of Marine Science 14 (1), 205–212.

Beckley, L., Van Ballegooyen, R., 1992. Oceanographic conditions during three ichthyoplankton surveys of the Agulhas Current in 1990/91. South African Journal of Marine Science 12 (1), 83–93.

Bouffard, J., Roblou, L., Birol, F., Pascual, A., Fenoglio-Marc, L., Cancet, M., Morrow, R., Menard, Y., 2011. Introduction and assessment of improved coastal altimetry strategies: Case study over the northwestern Mediterranean Sea. In: Coastal altimetry. Springer, pp. 297–330.

Bowman, M. J., 1985. On the β-induced coastal trapping of a baroclinic eddy. Journal of Physical Oceanography 15 (6), 817–822.

Brandini, F., Lopes, R., L. Spach, H., Gutseit, K., Sassi, R., 1997. In: Planctolonologia na plataforma continental do Brasil: diagnose e revisao bibliografica. MMA.

Brooks, R., Lockwood, D., Lee, J., Hancock, D. I., Hayne, G., 1997. Land effects on TOPEX radar altimeter measurements on Pacific Rim coastal zones.

Brown, G., 1977. The average impulse response of a rough surface and its applications. IEEE Transactions on antennas and Propagation 25 (1), 67–74.

Burchall, J., 1968. An Evaluation of Primary Productivity Studies in the Continental Shelf Region of the Agulhas Current Near Durban (1961-1966). Oceanographic Research Institute Investigational Report 21, Durban, South Africa.

Campos, E. J., Velhote, D., da Silveira, I. C., 2000. Shelf break upwelling driven by Brazil Current cyclonic meanders. Geophysical Research Letters 27 (6), 751–754.

Castelao, R. M., Mavor, T. P., Barth, J. A., Breaker, L. C., 2006. Sea surface temperature fronts in the California Current System from geostationary satellite observations. Journal of Geophysical Research: Oceans 111, c09026.

Chelton, D. B., Ries, J. C., Haines, B. J., Fu, L.-L., Callahan, P. S., 2001. Satellite altimetry. International Geophysics 69, 1–131.

Church, J., Craig, P., 1998. Australiaś shelf seas: diversity and complexity coastal segment (30, W–S). In: Robinson, A.R., Brink, K.H. (Eds). The Sea: ideas and observations on progress in the study of the seas. Wiley and Sons Inc., New York, 933–963.

Ciotti, A., Kampel, M., 2001. Concurrent observations of ocean color and sea surface temperature between Cabo Frio e Cabo São Tomé In: SIMPÓSIO BRASILEIRO DE. Simpósio Brasileiro de Sensoriamento Remoto 10, 785–791.

Cipollini, P., Benveniste, J., Donlon, C., 2012. Coastal Altimetry: recent progress and application to storm surge research. In: IGARSS 2012, Munich, Germany, 24-29 Jul 2012. Richardson, Texas, IEEE, Ext Abstract-4240.

Cipollini, P., Calafat, F. M., Jevrejeva, S., Melet, A., Prandi, P., 2017. Monitoring Sea Level in the Coastal Zone with Satellite Altimetry and Tide Gauges. Surveys in Geophysics 38, 33–57.

Cipollini, P., Co-Authors, 2010. The role of altimetry in coastal observing systems. In Proceedings of OceanObś09: Sustained Ocean Observations and Information for Society (Vol. 2), Venice, Italy, 21–25 September 2009, Hall, J., Harrison, D.E., and Stammer, D. (Eds). ESA Publication WPP-306, 181–191.

Cipollini, P., Snaith, H., 2015. Altimetry 2 — Altimeter data processing (from satellite height to sea surface height). Accessed on 24 June 2016.
URL http://seom.esa.int/oceantrainingcourse2015/files/Cipollini_Altimetry_2.pdf

Cipollini, P., Vignudelli, S., Lyard, F., Roblou, L., 2008. 15 years of altimetry at various scales over the Mediterranean. In: Barale V., Gade M. (Eds). Remote Sensing of the European Seas. Springer, Dordrecht, pp. 295–306.

Condie, S., Condie, R., 2016. Retention of plankton within ocean eddies. Global Ecology and Biogeography 25 (10), 1264–1277.

Condie, S., Dunn, J., 2006. Seasonal characteristics of the surface mixed layer in the Australasian region: implications for primary production regimes and biogeography. Marine and Freshwater Research 57, 569–590.

Cossa, O., Pous, S., Penven, P., Capet, X., Reason, C. J. C., 2016. Modelling cyclonic eddies in the Delagoa Bight region. Continental Shelf Research 119, 14–29.

Deng, X., Featherstone, W., 2006. A coastal retracking system for satellite radar altimeter waveforms: Application to ers-2 around australia. Journal of Geophysical Research: Oceans 111, C06012.

Deng, X., Featherstone, W., Hwang, C., Berry, P., 2002. Estimation of contamination of ERS-2 and Poseidon satellite radar altimetry close to the coasts of Australia. Marine Geodesy 25 (4), 249–271.

Doney, S. C., Glover, D. M., McCue, S. J., Fuentes, M., 2003. Mesoscale variability of Sea-viewing Wide Field-of-view Sensor (SeaWiFS) satellite ocean color: Global patterns and spatial scales. Journal of Geophysical Research: Oceans 108, C3024.

Dove, V. F., 2015. Seasonal and interannual variability of surface chlorophyll-a and sea surface temperature in the Delgoa Bight, southern Mozambique. Ph.D. thesis, University of Cape Town.

Eden, C., Dietze, H., 2009. Effects of mesoscale eddy/wind interactions on biological new production and eddy kinetic energy. Journal of Geophysical Research 114, C05023.

Escudier, R., Mourre, B., Juza, M., Tintoré, J., 2016. Subsurface circulation and mesoscale variability in the Algerian subbasin from altimeter-derived eddy trajectories. Journal of Geophysical Research: Oceans 121 (8), 6310–6322.

Fennessy, S., Roberts, M., Paterson, A., 2016. A brief overview of the ACEP project: ecosystem processes in the KwaZulu-Natal Bight. African Journal of Marine Science 38, 1–6.

Fenoglio-Marc, L., Fehlau, M., Ferri, L., Becker, M., Gao, Y., Vignudelli, S., 2010. Coastal sea surface heights from improved altimeter data in the mediterranean sea. In: In: Mertikas S. (Eds). Gravity, geoid and Earth observation. International Association of Geodesy Symposia. Vol. 135. Springer, Berlin, Heidelberg, pp. 253–261.

Fréon, P., Coetzee, J., Van der Lingen, C., Connell, A., ODonoghue, S., Roberts, M., Demarcq, H., Attwood, C., Lamberth, S., Hutchings, L., 2010. A review and tests of hypotheses about

causes of the KwaZulu-Natal sardine run. African Journal of Marine Science 32 (2), 449–479.

Fu, L.-L., Chelton, D. B., Le Traon, P.-Y., Morrow, R., 2010. Eddy dynamics from satellite altimetry. Oceanography 23 (4), 14–25.

Fua, L. L., Le Traon, P.-Y., 2006. Satellite altimetry and ocean dynamics. Comptes Rendus Geosciences 338 (14-15), 1063–1076.

Gill, A., Schumann, E., 1979. Topographically induced changes in the structure of an inertial coastal jet: application to the Agulhas Current. Journal of Physical Oceanography 9 (5), 975–991.

Godø, O. R., Samuelsen, A., Macaulay, G. J., Patel, R., Hjøllo, S. S., Horne, J., Kaartvedt, S., Johannessen, J. A., 2012. Mesoscale eddies are oases for higher trophic marine life. PLoS One 7 (1), e30161.

Gómez-Enri, J., Cipollini, P., Passaro, M., Vignudelli, S., Tejedor, B., Coca, J., 2016. Coastal Altimetry products in the Strait of Gibraltar. IEEE Transactions on Geoscience and Remote Sensing 54 (9), 5455–5466.

Gründlingh, M. L., 1983. On the course of the Agulhas Current. South African Geographical Journal 65 (1), 49–57.

Gründlingh, M. L., Pearce, A. F., 1990. Frontal features of the Agulhas Current in the Natal Bight. South African Geographical Journal 72 (1), 11–14.

Guastella, L. A., Roberts, M. J., 2016. Dynamics and role of the Durban cyclonic eddy in the KwaZulu-Natal Bight ecosystem. African Journal of Marine Science 38 (sup1), S23–S42.

Harris, T., 1972. Sources of the Agulhas Current in the spring of 1964. Deep Sea Research and Oceanographic Abstracts 19, 633–650.

Hewitt, R., 1981. Eddies and speciation in the California Current. California Cooperative Oceanic Fisheries Investigations Reports 22, 96–98.

Hoguane, A., 2007. Diagnosis of Mozambique coastal zone. Journal of Integrated Coastal Zone Management 7, 69–82.

Hutchings, L., Beckley, L., Griffiths, M., Roberts, M., Sundby, S., Van der Lingen, C., 2002. Spawning on the edge: spawning grounds and nursery areas around the southern African coastline. Marine and Freshwater Research 53 (2), 307–318.

Hwang, C., Guo, J., Deng, X., Hsu, H.-Y., Liu, Y., 2006. Coastal gravity anomalies from retracked geosat/gm altimetry: improvement, limitation and the role of airborne gravity data. Journal of Geodesy 80 (4), 204–216.

Ito, T., Kaneko, A., Furukawa, H., Gohda, N., Koterayama, W., 1995. A structure of the Kuroshio and its related upwelling on the East China Sea shelf slope. Journal of Oceanography 51 (3), 267–278.

Jordi, A., Basterretxea, G., 2012. Using SVD Analysis of Combined Altimetry and Ocean Color Satellite Data for Assessing Basin Scale Physical-Biological Coupling in the Mediterranean Sea, Remote Sensing of Biomass - Principles and Applications, Dr. Lola Fatoyinbo (Ed.), ISBN: 978-953-51-0313-4, InTech, Available from:.
URL http://www.intechopen.com/books/remote-sensing-of-biomass-principles-and-applications/using-svd-analysis-of-combined-altimetry-and-ocean-color-satellite-data-for-assessing-basin-scale-ph

Jose, Y. S., Aumont, O., Machu, E., Penven, P., Moloney, C., Maury, O., 2014. Influence of mesoscale eddies on biological production in the Mozambique Channel: Several contrasted examples from a coupled ocean-biogeochemistry model. Deep Sea Research Part II: Topical Studies in Oceanography 100, 79–93.

Kahru, M., Gille, S., Murtugudde, R., Strutton, P., Manzano-Sarabia, M., Wang, H., Mitchell, B., 2010. Global correlations between winds and ocean chlorophyll. Journal of Geophysical Research: Oceans 115, C12040.

Kasai, A., Kimura, S., Nakata, H., Okazaki, Y., 2002. Entrainment of coastal water into a frontal eddy of the kuroshio and its biological significance. Journal of Marine Systems 37 (1), 185–198.

Kyewalyanga, M. S., Naik, R., Hegde, S., Raman, M., Barlow, R., Roberts, M., 2007. Phytoplankton biomass and primary production in Delagoa Bight Mozambique: Application of remote sensing. Estuarine, Coastal and Shelf Science 74 (3), 429–436.

Laiolo, L., McInnes, A. S., Matear, R., Doblin, M. A., 2016. Key drivers of seasonal plankton dynamics in cyclonic and anticyclonic eddies off East Australia. Frontiers in Marine Science 3, 155.

Lamont, T., Barlow, R. G., 2015. Environmental influence on phytoplankton production during summer on the KwaZulu-Natal shelf of the Agulhas ecosystem. African Journal of Marine Science 37 (4), 485–501.

Lamont, T., Roberts, M. J., Barlow, R. G., Morris, T., van den Berg, M. A., 2010. Circulation patterns in the Delagoa Bight, Mozambique, and the influence of deep ocean eddies. African Journal of Marine Science 32 (3), 553–562.

Lee, H., Shum, C., Emery, W., Calmant, S., Deng, X., Kuo, C.-Y., Roesler, C., Yi, Y., 2010. Validation of Jason-2 altimeter data by waveform retracking over California coastal ocean. Marine Geodesy 33, 304–316.

Lee, T. N., Atkinson, L. P., Legeckis, R., 1981. Observations of a Gulf Stream frontal eddy on the Georgia continental shelf, April 1977. Deep Sea Research Part A. Oceanographic Research Papers 28 (4), 347–378.

Lee, T. N., Yoder, J. A., Atkinson, L. P., 1991. Gulf Stream frontal eddy influence on productivity. Journal of Geophysical Research 96, 22–191.

Liang, X., Thurnherr, A. M., 2012. Eddy-modulated internal waves and mixing on a midocean ridge. Journal of Physical Oceanography 42 (7), 1242–1248.

Lima, I. D., Garcia, C. A., Möller, O. O., 1996. Ocean surface processes on the southern Brazilian shelf: characterization and seasonal variability. Continental Shelf Research 16, 1307–1317.

Longhurst, A., 2001. A major seasonal phytoplankton bloom in the Madagascar Basin. Deep Sea Research Part I: Oceanographic Research Papers 48 (11), 2413–2422.

Lutjeharms, J., 1976. The Agulhas Current system during the northeast monsoon season. Journal of Physical Oceanography 6 (5), 665–670.

Lutjeharms, J., 1981. Features of the southern Agulhas Current circulation from satellite remote sensing. South African Journal of Science 77 (5), 231–236.

Lutjeharms, J., 2006a. The coastal oceans of south-eastern Africa (15,W). The Sea, 14B, editors: Robinson, A.R. and Brink, K.H., Harvard University Press, Cambridge, 1–54.

Lutjeharms, J., Boebel, O., Rossby, H., 2003. Agulhas cyclones. Deep Sea Research Part II: Topical Studies in Oceanography 50 (1), 13–34.

Lutjeharms, J., Connell, A., 1989. The Natal pulse and inshore counter-currents off the South-African east coast. South African Journal of Science 85 (8), 533–535.

Lutjeharms, J., Machu, E., 2000. An upwelling cell inshore of the East Madagascar Current. Deep Sea Research Part I: Oceanographic Research Papers 47 (12), 2405–2411.

Lutjeharms, J., Valentine, H., Van Ballegooyen, R., 2000. The hydrography and water masses of the natal bight, south africa. Continental Shelf Research 20 (14), 1907–1939.

Lutjeharms, J. R., 2006b. The Agulhas Current. Springer, Berlin.

Lutjeharms, J. R. E., 2007. Three decades of research on the greater Agulhas Current. Ocean Science 3 (1), 129–147.

Lutjeharms, J. R. E., Da Silva, A. J., 1988. The Delagoa Bight eddy. Deep Sea Research Part A. Oceanographic Research Papers 35 (4), 619–634.

Malan, O., Schumann, E., 1979. Natal Shelf circulation revealed by landsat imagery. South African Journal of Science 75, 136–137.

Malauene, B., Shillington, F., Roberts, M., Moloney, C., 2014. Cool, elevated chlorophyll-a waters off northern Mozambique. Deep Sea Research Part II: Topical Studies in Oceanography 100, 68–78.

Martin, A., 1981a. Evolution of the agulhas current and its palaeo-ecological implications. South African Journal of Science 77 (12), 547–554.

Martin, A., 1981b. The influence of the agulhas current on the physiographic development of the northernmost natal valley (sw indian ocean). Marine Geology 39 (3-4), 259–276.

Martin, A., Flemming, B., 1988. Physiography, structure add geological evolution of the Natal continental shelf. In: Coastal Ocean Studies off Natal, South Africa (ed E. H. Schumann), Springer-Verlag, New York, 11–46.

Martin, A. K., 1984. Plate tectonic status and sedimentary basin in-fill of the Natal Valley (SW Indian Ocean). No. 14. Marine Geoscience Unit, Department of Geology, University of Cape Town.

Mathers, L., Berry, P., Freeman, J., 2004. Gravity, geoid and space missions. ggsm 2004. in: Proceeding international association of geodesy symposia, jekeli, c., bastos, l., fernandes, l. (eds), porto.

McGillicuddy, D. J., Robinson, A. R., 1997. Eddy-induced nutrient supply and new production in the Sargasso Sea. Deep Sea Research Part I: Oceanographic Research Papers 44 (8), 1427–1450.

Meyer, A., Lutjeharms, J., De Villiers, S., 2002. The nutrient characteristics of the Natal Bight, South Africa. Journal of Marine Systems 35 (1), 11–37.

Michaelis, G., 1923. Die Wasserbewegung an der Oberfläche des Indischen Ozeans im Januar und Juli: mit 2 abb. im Text u. 4 Karten. ES Mittler & Sohn.

Morel, A., Prieur, L., 1977. Analysis of variations in ocean color. Limnology and Oceanography 22 (4), 709–722.

Nilsson, C., Cresswell, G., 1980. The formation and evolution of East Australian Current warm-core eddies. Progress in Oceanography 9 (3), 133–183.

Oke, P. R., Griffin, D. A., 2011. The cold-core eddy and strong upwelling off the coast of New South Wales in early 2007. Deep Sea Research Part II: Topical Studies in Oceanography 58 (5), 574–591.

Oke, P. R., Middleton, J. H., 2000. Topographically induced upwelling off eastern Australia. Journal of Physical Oceanography 30 (3), 512–531.

Oke, P. R., Middleton, J. H., 2001. Nutrient enrichment off Port Stephens: the role of the East Australian Current. Continental Shelf Research 21 (6), 587–606.

O'Reilly, B., 2012. Phytoplankton associated with mesoscale eddies in the Mozambique channel. Ph.D. thesis, Nelson Mandela Metropolitan University.

Owen, R. W., 1981. Fronts and eddies in the sea: mechanisms, interactions and biological effects. Analysis of Marine Ecosystems 7, 197–233.

Passaro, M., Cipollini, P., Benveniste, J., 2015a. Annual sea level variability of the coastal ocean: The Baltic Sea-North Sea transition zone. Journal of Geophysical Research: Oceans 120 (4), 3061–3078.

Passaro, M., Cipollini, P., Vignudelli, S., Quartly, G. D., Snaith, H. M., 2014. ALES: A multi-mission adaptive subwaveform retracker for coastal and open ocean altimetry. Remote Sensing of Environment 145, 173–189.

Passaro, M., Dinardo, S., Quartly, G. D., Snaith, H. M., Benveniste, J., Cipollini, P., Lucas, B., 2016. Cross-calibrating ALES Envisat and CryoSat-2 Delay–Doppler: a coastal altimetry study in the Indonesian Seas. Advances in Space Research 58 (3), 289–303.

Passaro, M., Fenoglio-Marc, L., Cipollini, P., 2015b. Validation of significant wave height from improved satellite altimetry in the German Bight. IEEE Transactions on Geoscience and Remote Sensing 53 (4), 2146–2156.

Pearce, A. F., 1977. The shelf circulation off the east coast of South Africa. CSIR.

Peterson, R. G., Stramma, L., 1991. Upper-level circulation in the South Atlantic Ocean. Progress in oceanography 26 (1), 1–73.

Pond, S., Pickard, G. L., 2013. Introductory dynamical oceanography. Elsevier.

Quartly, G., Srokosz, M., 2004. Eddies in the southern Mozambique Channel. Deep Sea Research Part II: Topical Studies in Oceanography 51 (1), 69–83.

Reid, J. L., Roden, G. I., Wyllie, J. G., 1958. Studies of the California Current System. California Cooperative Oceanic Fisheries Investigations 6, 21–56.

Roberts, M. J., Nieuwenhuys, C., Guastella, L. A., 2016. Circulation of shelf waters in the KwaZulu-Natal Bight, South Africa. African Journal of Marine Science 38 (sup1), S7–S21.

Roberts, M. J., van der Lingen, C. D., Whittle, C., van den Berg, M., 2010. Shelf currents, lee-trapped and transient eddies on the inshore boundary of the Agulhas Current, South Africa: their relevance to the KwaZulu-Natal sardine run. African Journal of Marine Science 32 (2), 423–447.

Roblou, L., Lyard, F., Le Henaff, M., Maraldi, C., 2007. X-track, a new processing tool for altimetry in coastal oceans. In: Geoscience and Remote Sensing Symposium, 2007. IGARSS 2007. IEEE International. IEEE, pp. 5129–5133.

Roughan, M., Middleton, J. H., 2002. A comparison of observed upwelling mechanisms off the east coast of Australia. Continental Shelf Research 22, 2551–2572.

Sætre, R., Da Silva, A. J., 1984. The circulation of the Mozambique Channel. Deep Sea Research Part A. Oceanographic Research Papers 31 (5), 485–508.

Salmon, R., 1998. Lectures on Geophysical Fluid Dynamics. Oxford University Press.

Sarmiento, J. L., 2013. Ocean Biogeochemical Dynamics. Princeton University Press.

Schumann, E. H., 1988. Physical Oceanography Off Natal, in Coastal Ocean Studies off Natal, South Africa (ed Schumann, E.H.), Springer-Verlag, New York, 101–130.

Shum, C., Yi, Y., Cheng, K., Kuo, C., Braun, A., Calmant, S., Chambers, D., 2003. Calibration of Jason-1 altimeter over Lake Erie special issue: Jason-1 calibration/validation. Marine Geodesy 26 (3-4), 335–354.

Siegel, D. A., McGillicuddy, D. J., Fields, E. A., 1999. Mesoscale eddies, satellite altimetry, and new production in the Sargasso Sea. Journal of Geophysical Research: Oceans 104, 13359–13379.

Simpson, J., Dickey, T., Koblinsky, C., 1984. An offshore eddy in the California current system Part I: Interior dynamics. Progress in Oceanography 13 (1), 5–49.

Smith, D. C., Morison, J., Johannessen, J., Untersteiner, N., 1984. Topographic generation of an eddy at the edge of the East Greenland Current. Journal of Geophysical Research: Oceans 89 (C5), 8205–8208.

Speich, S., Blanke, B., De Vries, P., Drijfhout, S., Döös, K., Ganachaud, A., Marsh, R., 2002. Tasman leakage: A new route in the global ocean conveyor belt. Geophysical Research Letters 29 (10), 1–15.

Srokosz, M., 2000. Biological oceanography by remote sensing. in: Meyers, r.a., (ed.). encyclopedia of analytical chemistry. wiley and sons, chichester, 85068533.

Stewart, R. H., 2008. Introduction to Physical Oceanography. Orange Grove Text Plus.

Stramma, L., Bange, H. W., Czeschel, R., Lorenzo, A., Frank, M., 2013. On the role of mesoscale eddies for the biological productivity and biogeochemistry in the eastern tropical Pacific Ocean off Peru. Biogeosciences (BG) 10 (11), 7293–7306.

Stramma, L., England, M., 1999. On the water masses and mean circulation of the South Atlantic Ocean. Journal of Geophysical Research-Oceans 104, 20863–20833.

Tilburg, C. E., Hurlburt, H. E., O'Brien, J. J., Shriver, J. F., 2001. The dynamics of the East Australian current system: the Tasman front, the East Auckland current, and the East Cape current. Journal of Physical Oceanography 31 (10), 2917–2943.

Tsugawa, M., Hasumi, H., 2010. Generation and growth mechanism of the Natal Pulse. Journal of Physical Oceanography 40 (7), 1597–1612.

Vignudelli, S., Kostianoy, A. G., Cipollini, P., Benveniste, J., 2011. Coastal altimetry. Springer Science & Business Media.

WHOI, 2015. Currents, Gyres, & Eddies. Accessed on 25 March 2017.
URL https://www.whoi.edu/main/topic/currents--gyres-eddies

Yoder, J. A., Kennelly, M. A., 2006. Ocean variability. Oceanography 19 (1), 152.